Arabidopsis thaliana's metallothioneins involvement in iron and silver exposure and their vacuolar targeting to increase plant tolerance to heavy metals

Gonçalo Octávio Fraga Rodrigues Agodinho Vasques
Master in Applications in Biotechnology and Synthetic Biology
Departments of Biology and Chemistry and Biochemistry
Faculty of Sciences of the University of Porto
2024

Arabidopsis thaliana's metallothioneins involvement in iron and silver exposure and their vacuolar targeting to increase plant tolerance to heavy metals

Gonçalo Octávio Fraga Rodrigues Agodinho Vasques

Dissertation carried out as part of the Master in Applications in Biotechnology and Synthetic Biology

Departments of Biology and Chemistry and Biochemistry

2024

Supervisor
Jorge Teixeira, Auxiliar Professor, GreenUPorto (Centro de Investigação em Produção Agroalimentar Sustentável) & FCUP

Co-supervisor
Claúdia Pereira, PhD Researcher at GreenUPorto (Centro de Investigação em Produção Agroalimentar Sustentável)

Aknowledgements

Achieving this work was nothing but easy. Many obstacles almost made this goal impossible, but alas here we are. However, achieving this goal could have never been possible without the help of many people that stood with me with along this way. And to all of them I am truly grateful.

I would like to leave a special thanks to my supervisor Professor Jorge Teixeira, and my co-supervisor Cláudia Pereira for giving me the opportunity to achieve yet another step in my career. This work has truly been challenging, and you were always able to find an open door in situations where apparently, none could be found. I can say for certain that I could not have done this without your help and guidance. I truly admire your knowledge and hope to achieve the same level one day.

To Leonel, my companion throughout this hard work! I hope you have learned from me as much as I have learned from you. We have been through a lot but in the end we prevailed. Thank you for making part of the journey.

To the Plant stress Lab family, where my career in investigation began, thank you for all your friendship, and support. I cherish you all deeply.

To all the present and past members of PSI, thank you for taking me in, and letting me be part of the family. I am truly grateful for everything you have done to help me throughout this year, and it has been a pleasure get to know you and to work with you all.

Last, but not least, I would like to give a special thanks to my friends and family. You truly are the foundations that sustained my journey and made me get this far. None of this would be possible without your help and support. This work is yours as much as it is mine. I am eternally thankful to you.

Resumo

A contaminação de solos por metais pesados (MP) é uma consequência direta da elevada atividade antropogénica. O ferro (Fe) e a prata (Ag) pertencem ao grupo desses metais pesados, considerados como essenciais, ou não essenciais, respetivamente, no que toca à sua função no metabolismo das plantas. Contudo, ambos possuem a capacidade de induzir toxicidade em plantas quando em elevadas concentrações, pondo em risco a sua sobrevivência. As plantas, no entanto, possuem uma série de mecanismos que atuam em resposta ao risco de toxicidade por metais pesados. Nomeadamente, o uso de metalotioninas (MTs), que englobam uma família de pequenas proteínas ricas em cisteína capazes de quelatar metais pesados e intervir no controlo de stress oxidativo causado por espécies reativas de oxigénio. Elas estão divididas em quatro grupos (I a IV) cuja expressão difere de órgão para órgão da planta e também no tipo de MP. O sequestro de metais pesados para vacúolo é outra das estratégias das plantas no combate ao stress por MP. A capacidade de armazenamento deste organelo permite a acumulação de vários compostos tóxicos, incluindo os metais pesados. Ao longo dos anos, o nosso laboratório tem-se focado no estudo do sistema endomembranar, com especial atenção na função dos domínios *plant-specific insert* (PSI) das proteinases aspárticas Cardosinas A e B, isoladas de*Cynara cardunculus*, no endereçamento para o vacúolo. Recentemente, foi mostrado que o domínio PSI A, pertencente à Cardosina A, possui a função de sinal de endereçamento vacuolar (VSD) sendo capaz de induzir o transporte para o vacúolo de uma forma independente. Este trabalho teve como objetivo a avaliação bioquímica da tolerância de *Arabidopsis thaliana* à toxicidade de Fe e Ag, através da análise de diversos indicadores de stress, quando exposta a concentrações crescentes de cada metal durante 21 dias pós-germinação. Foi também determinado os níveis de bioacumulação de ambos os metais na parte aérea e nas raízes. A análise da expressão por RT-qPCR de MTs dos tipos I, II e III foi feita em folhas e raízes de modo a verificar o seu papel em resposta a MPs. Além disso, foi realizada uma tentativa de direcionar MTs para o vacúolo com a ajuda do PSI A como estratégia viável ao sequestro de MPs. Para tal, procedeu-se à fusão da MT2b de *A. thaliana* com o domínio PSI A procedendo-se à sua visualização *in vivo*, através de microscopia confocal, em folhas de *Nicotiana tabacum*. A expressão heteróloga *in vivo* do gene AtMT2b sozinho em folhas de N. tabacum também foi realizada. Em relação ao Fe, os níveis de MDA aumentaram na parte aérea, mas não foram encontrados resultados significativos nas raízes, enquanto para a Ag foi verificada uma redução nas raízes, e um aumento na parte aérea. Os níveis de H2O2 não apresentaram resultados

significativos para o Fe, em ambos os órgãos, enquanto na Ag houve um aumento na parte aérea, e diminuição nas raízes. Os níveis de GSH aumentaram tanto na parte aérea, como nas raízes, no tratamento com Fe, mas com Ag apenas aumentaram na parte aérea. Os níveis de tióis totais aumentaram na parte aérea e nas raízes após a exposição ao Fe, com um aumento dos tióis não proteicos e tióis proteicos nas folhas. Com a Ag, não foram encontradas alterações significativas nas raízes, mas na parte aérea os níveis de tióis totais e de tióis proteicos aumentaram. A acumulação de prolina teve uma diminuição geral em ambos os órgãos com Fe, no entanto, com Ag ocorreu um aumento na parte aérea, sem resultados significativos nas raízes. Os pigmentos fotossintéticos tiveram uma diminuição geral na sua acumulação, principalmente os β-carotenos, que diminuíram significativamente em todas as concentrações de Fe. Quanto à prata, os níveis de clorofila a e b e luteína, diminuíram significativamente, já os β-carotenos diminuíram significativamente com a menor concentração utilizada. Os resultados da bioacumulação mostraram que *A. thaliana* acumulou Fe de forma dependente da dose tanto na parte aérea quanto nas raízes. Para Ag, isto só aconteceu nas raízes, uma vez que a parte aérea só a acumulou aquando da maior concentração utilizada. Não foram encontrados resultados significativos com Fe na expressão de MTs para a maioria dos casos, tanto na parte aérea quanto nas raízes. No entanto, uma diminuição significativa na expressão de *AtMT1c* foi detetada com a menor concentração de Fe utilizada, e para *AtMT2a*, no tratamento de 6 mg/L de Fe. A maior concentração de Ag induziu a expressão de todos os MTs na parte aérea, enquanto nas raízes, apenas as expressões da *AtMT1a* e *AtMT1c* aumentaram significativamente. Relativamente ao endereçamento vacuolar da AtMT2b mediado pelo PSI A, esta não foi verificada. O rastreamento *in vivo* da AtMt2b sozinha revelou uma localização preferencial no citosol. Estes resultados mostraram que o Fe e Ag são capazes de induzir stress oxidativo em A. Thaliana, e que a resposta da planta difere tanto para órgãos e para MPs. Os níveis de expressão das AtMTs mostraram também ser especificos para órgãos e HM, uma vez que, no geral, não ocorreram variações significativas com Fe, mas foram todas altamente induzidas por Ag na parte aérea e apenas as MT tipo I nas raízes. Embora não tenha sido possível o endereçamento da AtMT2b para o vacúolo estes resultados revelam novas informações relativamente à função do PSI A como um VSD, uma vez que outros fatores podem estar em jogo.

Palavras-chave

Metais pesados, ferro, prata, metalotioninas, stress oxidativo, vacúolo, PSI A, *Arabidopsis thaliana*, microscopia confocal

Abstract

Pollution of soils by heavy metals (HM) is a concerning result of anthropogenic activities. The HM iron (Fe) and silver (Ag) are deemed essential and non-essential, respectively, regarding their function in plant metabolism. However, both can induce toxicity that risks the overall plant's fitness when in excess. Plants possess many strategies to deal with HM toxicity, one being metallothioneins (MTs) - small Cys-rich proteins encoded by a multigenic family, capable of binding HMs and scavage Reactive Oxygen Species - that are divided into 4 types (I to IV) with distinct expression levels throughout the plant and in response to different HM. Sequestration and accumulation of HM into the vacuole is another strategy plants use to mitigate HM toxicity. The plant-specific insert (PSI) domain of the aspartic proteinases cardosin A and B from *Cynara cardunculus* possess vacuolar targeting functions. This work focused on the biochemical assessment of *Arabidopsis thaliana* tolerance to Fe and Ag toxicity by analysing several stress indicators when exposed to increasing concentrations of each metal for 21 days post-germination. A bioaccumulation determination of both metals in shoots and roots was also performed. RT-qPCR expression analyses of types I, II and III MTs were done for shoots and roots to address their involvement in response to these HM. Also, an attempt was made to target MTs to the vacuole with the help of PSI A as a strategy for HM sequestration. For this, MT2b from *A. thaliana* was fused with PSI A and visualised *in vivo* through confocal microscopy in *Nicotiana tabacum* leaves. The *in vivo* heterologous expression of AtMT2b alone in *N. tabacum* leaves was also performed. Regarding Fe, the levels of MDA increased in shoots, but no significant results were found in roots, while for Ag, a reduction in roots and an increase in shoots were detected. H_2O_2 levels showed no significant results for Fe for both organs, while for Ag, an increase in the shoots and a decrease in the roots occurred. GSH increased for both shoots and roots with Fe treatments, but with Ag, it only increased in the shoots. Total thiol levels increased in shoots and roots upon Fe exposure, with non-protein thiols and protein thiols increasing in shoots. With Ag, no significant changes were found in roots, but in shoots, the total thiols and the protein thiols levels increased. Proline levels had a general decrease in both organs with Fe; however, with Ag, an increase occurred in shoots, with no significant results in roots. The photosynthetic pigments had a general decrease, especially the β – carotenes, which significantly decreased in all concentrations of Fe. As for Ag, chlorophyll a and b and lutein levels significantly decreased, while β – carotenes significantly decreased with the lowest concentration used. The bioaccumulation results showed that *A. thaliana* accumulated Fe dose-dependently in both shoots and roots. This

only happened for Ag in roots, as shoots only accumulated it with the highest concentration used. No significant results with Fe were found in the expression of MTs for most cases, both in shoots and roots. A significant decrease in *AtMT1c* expression was detected with the lowest concentration of Fe used, and for *AtMT2a*, it was with the 6 mg/L Fe treatment. The highest concentration of Ag induced the expression of all MTs in the shoots, whereas, in roots, only *AtMT1a* and *AtMT1c* expressions significantly increased. The AtMT2b PSI A-mediated vacuolar targeting procedure led to no accumulation of this MT in the vacuole. The *in vivo* tracking of AtMt2b alone revealed a preferential location in the cytosol. These results showed that Fe and Ag induced oxidative stress in *A. thaliana* and that the plants' responses differed for both organs and HM. The *AtMTs* expression levels revealed organ and HM specificities since, in general, no variations occurred with Fe but were highly induced by Ag in shoots and type I MTs in roots. Although no endorsement of the AtMT2b to the vacuole was possible, these results reveal new insights regarding the PSI A function as a VSD, as other factors may be at play.

Keywords

Heavy metals, iron, silver, metallothioneins, oxidative stress, vacuole, PSI A, *Arabidopsis thaliana*, confocal microscopy

Index

List of tables

List of figures

Lists of abbreviatures and acronyms

Ag	**Silver**
$AgNO_3$	Silver Nitrate
AgNPs	Silver Nanoparticles
AP	Aspartic proteinase
As	Arsenic
At	*Arabidopsis thaliana*
CAT	Catalase
Cd	Cadmium
Co	Cobalt
$CoSO_4 \cdot 7H_2O$	Cobaltous sulphate heptahydrate
Cu	Copper
Cys	Cystein
dw	Dry weight
ETC	Electron transport chain
Fe	Iron
FW	Primer forward
fw	Fresh weight
GAPDH	Glyceraldehyde-3-phosphate dehydrogenase
GS	Glutathione
GSH	Reduced glutathione
GSR	Glutathione reductase
His6x-tag	Hexa histidine tag
HM	Heavy metals
IRT-1	Iron regulated transporter 1
KOH	Potassium hydroxide
LV	Lytic vacuoles
MAs	Phytosiderophores
Mg	Mercury
Mn	Manganese
MS	Murashige and skoog
MT	Metalothionein
NASC	The European Arabidopsis Stock Center

$(NH_4)2SO_4 \cdot FeSO_4,6H_2O$	Ammonium ferrous sulphate hexahydrate
Ni	Nickel
NPT	Non-protein thiols
OL	Overlapping regions
Pb	Lead
PC	Phytochelatin
POD	Peroxidase
PSI	Plan specific insert
PSV	Protein storage vacuoles
PT	Protein thiol
Rev	Primer reverse
ROS	Reactive oxygen species
SOD	Superoxide dismutase
SP	Signal peptide
TAIR	The arabidopsis information resource
T-DNA	Transfer DNA
TT	Total thiols
UBQ10	Ubiquitin gene 10
VSD	Vacuole sorting determinant
Ct-VSD	C-terminal Vacuole sorting determinant
psVSD	Physical structure Vacuole sorting determinant
ssVSD	Sequence specific Vacuole sorting determinant
YS1	Iron-phytosiderophore transporter yellow stripe 1
YSL	Iron-phytosiderophore transporter yellow stripe
YLS8	Yellow leaf specific gene 8
Zn	Zinc

1. Introduction

1.1. Environmental pollution

During the last decades, humanity has witnessed a significant growth of the world's total population, followed by a rapid depletion of many essential resources and increasing environmental pressures to keep up with our everyday necessities [1, 2]. Consequently, several sectors, such as agriculture, livestock production, fossil-fuel energies, and other industrial areas, have adopted mass-scale production policies over the years to cope with the increasing global population [3]. Adding to the expansion of urban areas, this has unlocked a severe chain reaction of environmental changes, which negatively impact many ecosystems, mainly due to the over-accumulation of pollutants into the water, the air, and the soil [4, 5].

These environmental pollutants are toxic substances introduced into the environment via anthropogenic and/or natural means [4]. They are usually found in the form of heavy metals (HM), such as cadmium (Cd), copper (Cu) and lead (Pb), or other chemical substances present in many pesticides, fungicides and insecticides that are a result of, and used by, many anthropogenic activities mentioned above (Figure 1) [4, 6].

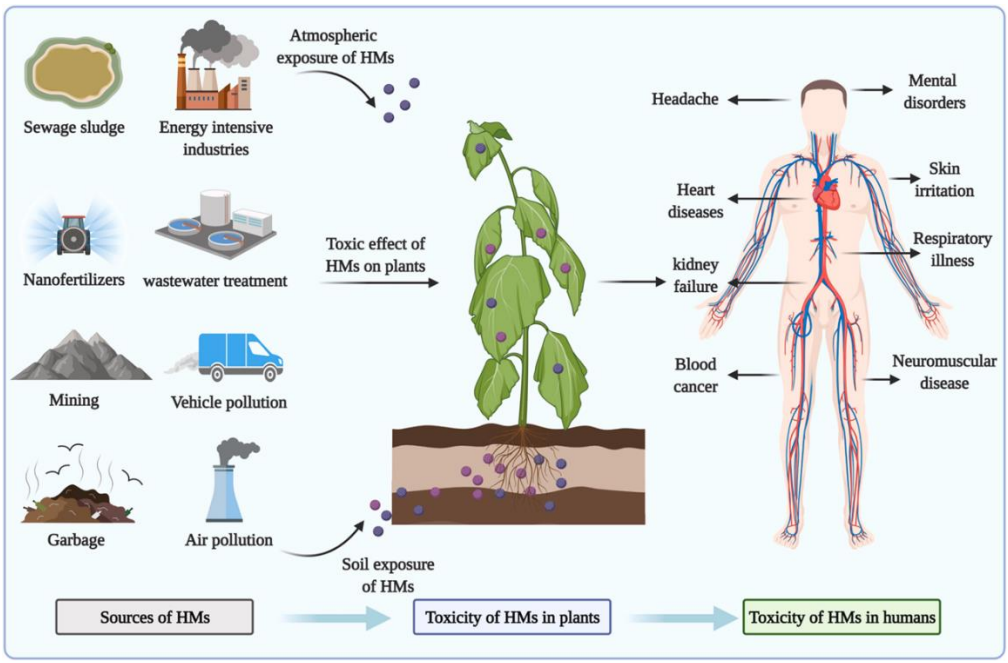

Figure 1| Visual representation of soil and plant contamination by heavy metals (HM) and subsequent health problems in humans. Adapted from [7].

Over the years, environmental and human overexposure to these contaminants has significantly increased, being the leading cause of most food chain deterioration of agricultural systems and many human diseases [4, 8]. Heavy metals (HM), amongst pollutants, pose a significant threat given their low biodegradation rate and high solubility, allowing them to persist in the environment for long periods [7, 9].

In this matter, soils have been negatively impacted since HM are known to alter their properties and sometimes reduce the bioavailability of essential elements, worsening the quality and productivity of soils. This is a major issue for agricultural soils, which often turn barren, posing an alarming threat to the environment and food safety [4, 7]. As such, there has been a necessity worldwide, amongst researchers and several organisations, to address this issue and find ways to improve soil quality and even, through biotechnological approaches, increase crop fitness in polluted soils [10].

1.1.1. Heavy metals' negative impact

Heavy metals comprehend a heterogeneous group of elements that possess various chemical properties and are known for weighing more than 5g/mL [11, 12]. This group of high-density metals can be found naturally throughout the Earth's crust, although in trace amounts [7, 13]. Most of these HMs are deemed essential, like iron (Fe), zinc (Zn), nickel (Ni), copper (Cu) and manganese (Mn), as they play an important role in homeostasis and co-factoring many proteins and enzymes, involved in DNA synthesis and cellular activity [7, 14, 15]. Others, because they have no known biological activity, such as cadmium (Cd), arsenic (As) and mercury (Mg), are considered "non-essential" [7, 14, 16].

Heavy metal presence in the environment ranges from a variety of natural sources. Usually, igneous and sedimentary rocks are the most common since they are known to contain HM traces in their chemical composition [4]. Even so, natural causes such as soil erosion, flooding, volcanic activity, and others also increase their accumulation, specifically in agricultural soils [7, 17]. However, in modern days, anthropogenic activities that include mining, automobile industries, sewage and agriculture are now the primary sources of HM contamination in the ecosystems [7]. For instance, agricultural activities have become the second leading source of HM pollutants due to the high usage of pesticides, fertilisers and others [17, 18]. This poses a major issue because, when in higher concentrations, HMs, either essential or non-essential, have nefarious effects on crops and, consequently, on human health [4, 9].

Plant crops exposed to high concentrations of HMs can easily be contaminated. Due to the non-biodegradability and water solubility of HMs, as mentioned earlier, plants

quickly absorb them along with other nutrients in the soil [7]. As HMs incorporate the plant systems, they contaminate the food chain, compromising food quality and human health safety [4, 7]. In some cases, HMs can accumulate in the edible part of the plant, resulting in the over-ingestion of the pollutants by animals and humans [19]. Previous studies have revealed that the intake of HMs by humans can cause a reduction of essential minerals, resulting in malnutrition and several types of cancer and diseases [8, 19].

Soil-plant relation is essential for the plant's survival. However, HM toxicity interferes with this relationship, starting by exerting its influence on the uptake of essential nutrients from the soil [4]. Cadmium (Cd), for example, affects the mineral uptake potential of plants [4, 20]. Additionally, copper (Cu) and zinc (Zn) can affect the bioavailability of nutrients present in the soil [4, 21, 22]. Once HMs are absorbed, they can disrupt many biochemical and physiological functions, including the photosynthetic apparatus, by decreasing chlorophyll content and enzymatic activities [19]. Furthermore, HMs induce the production of free radicals that increase the intercellular levels of reactive oxygen species (ROS). Subsequently, these cause oxidative stress in the plant that damages DNA, cellular structures, and other biological molecules, ultimately leading to the death of the entire plant [4, 19].

1.1.2 Iron

Iron (Fe) is one of the most abundant micronutrients on Earth's crust, and it is essential for the development of plants and several other organisms. It is associated with many cellular functions, including respiration, and as a cofactor for many enzymes participating in electron or oxygen transfers [23]. Moreover, in plants, Fe is involved in chlorophyll biosynthesis and photosynthesis [23, 24].

Higher plants obtain Fe from the soil; however, despite its abundance in mineral soils, Fe has very low bioavailability. Well–aerated soils, at physiological pH, contain less than 10-15 mM of Fe^{2+} and Fe^{3+}, which is far below the amount of Fe required for plant growth [25]. In addition, Fe^{3+} is the most found form of iron (ferric form) and has very low solubility at physiological pH and aerobic conditions [23]. This heavily hinders Fe uptake for plants that, in turn, have developed at least two strategies (I and II) to improve it: Strategy I – performed mainly by non-gramineous plants – which involves the release of protons and phenolic compounds to the rhizosphere, that reduce Fe^{3+} to Fe^{2+} (a more soluble form of Fe) by lowering soil's pH, and then transport it with the help of a membrane-localized high-affinity Fe transporter, IRT1 [26, 27]; and Strategy II – utilised by gramineous plants, usually when in Fe deficiency – characterised by the chelation of

Fe^{3+} (Fe(III)), using phytosiderophores (MAs) that are released to the soil [28], forming Fe(III) – MAs complexes that are then taken up using the YS1 and YSL transporters [29].

Plants heavily rely on Fe for their survival [30]. Because it is an essential micronutrient, Fe deficiency can cause severe consequences to the plant. These include the disruption of the photosynthetic machinery [31] and interveinal chlorosis in younger leaves [32] as the most prominent. Other effects include poor root development [33], reduction in photosynthetic pigments [34] and reduction of the activity and efficiency of the photosystem II [32, 35]. Overall, the disturbances that Fe deficiency causes in the photosynthetic activity negatively impact the plant's growth and development [30].

On the other hand, excess Fe causes toxicity inside the plant, and the most common symptoms include crop yield reduction and small reddish-brown spots on the leaves [36]. Naturally, this phenomenon does not pose a common problem for crops since Fe has low bioavailability in most soils. However, in waterlogged soils, it is considered one of the most problematic crop yield factors [36]. Because access to oxygen (O_2) is more difficult in these conditions, the formation of Fe^{3+} is considerably low, increasing the pool of Fe^{2+}, which is more soluble and therefore has a higher toxicity potential [37]. Nonetheless, Fe toxicity can also occur in drylands since drought induces Fe-catalysed ROS production in the chloroplasts [38, 39] and aerobic conditions due to the precipitation of Fe(III) hydroxides and phosphates that increase the Fe pool in the root apoplast [40].

The main issue regarding Fe toxicity is related to the excessive production of ROS [36]. To counteract this, plants have established several defence mechanisms composed of antioxidant enzymes, such as superoxide dismutase (SOD), catalase (CAT) and peroxidase (POD), and antioxidant metabolites that include glutathione, carotenoids, ascorbate, uric acid, amongst others [36, 37]. Moreover, plants also possess Fe detoxification strategies, including sequestration to the vacuole, using proteins with ferroxidase activity, such as ferritins [41] and binding Fe to the cell wall [42].

1.1.3. Silver

The inevitable growth and development of new technologies have increased the demand for silver usage over the last half-century [43]. Silver (Ag) has been an essential resource for many industrial applications and electronics that humanity uses daily. This includes circuit boards, silver nanoparticles in paints, textiles, medical applications, cosmetics, bandages and more [44]. When looking at non-polluted soils, silver can only be found in almost trace amounts, ranging from 0.01 to 1 mg/kg. However, increasing anthropogenic activity affects the accumulation of Ag in soils, which has been found to

rise severely, varying from 8 to 35.9 mg/kg in polluted soils. Even more alarming, Ag concentration can reach 7000 mg/kg in soils that contain ore deposits [43]. Most of the excess Ag that is being released to the environment, especially soils, is the result of emissions produced from anthropogenic activities such as coal-burning thermal power plants, metallurgy enterprises, solid waste landfills, cement plants and sewage sludges that are used as fertiliser that may contain Ag. On the other hand, excessive use of pesticides containing Ag, a known metal with antibacterial and antifungal properties [45, 46], can also contaminate the soils.

Since Ag is an HM, it can increase its bioaccumulation in the environment, affecting several organisms through the food chain. Indeed, as shown in previous studies, Ag interacts with proteins like other HMs do and induces enzyme inhibition, metabolic disturbance, DNA damage, necrosis and decreased permeability of biological membranes [47-49]. Moreover, Ag^+ ions have been reported to possess genotoxic properties [50].

Silver is expected to follow a similar pattern to other HMs regarding its behaviour in plants, mostly by inducing oxidative or physiological stress and affecting the overall development of the plant. Studies performed to assess the toxicity of Ag^+ and Ag nanoparticles (AgNPs) in *Arabidopsis thaliana* have shown that they did not only cause changes in gene expression but also a reduction in root elongation and leaf expansion, which in turn led to diminished photosynthesis and accumulation of high amounts of Ag^+ [44, 51]. However, the effects of silver toxicity still need to be further explored.

1.2. Plant strategies to deal with HMs toxicity

Toxicity by essential elements is one of the leading causes of the overall reduction of plant fitness. As such, they employ strategies to cope with this excess [52]. Plants' response acts following the physical and chemical properties of the metal, and it can range from ROS production - by Fenton-like reactions or auto-oxidation – impairment of essential functional groups in molecules, and the removal of essential metal ions from biomolecules [53]. For most, sequestration and neutralisation of free metal ions are vital in ensuring cellular homeostasis [52].

During HMs toxicity stress, plants activate a network of interconnected biochemical pathways that set in motion the biosynthesis and accumulation of several metabolites to counteract the accumulation of metals. These compounds include organic acids, like malate and citrate, phenylpropanoids, amino acids, and low-molecular-weight proteins such as metallochaperones (e.g., nicotinamide, glutathione (GSH), metallothioneins (MTs) and phytochelatins (PCs)) [52]. MTs and PCs are well known for

their metal chelation ability, which consists of the sequestration of free metal radicals by capturing and binding them, decreasing their reactivity and solubility [54, 55]. Higher plants use both peptides, and their production is usually triggered when HMs enter the cell [56, 57]. The first, MTs, belong to a gene-encoded protein family; the second, PCs, are enzymatically formed from glutathione by Phytochelatin Synthase [52].

1.2.1. Metallothioneins

Metallothioneins (MTs) comprehend a multigenic family of low-molecular-weight (4-14 kDa), cysteine-rich, metal-binding proteins. Their affinity to metals is related to the formation of mercaptide bonds with the thiol group of their cysteine residues [58]. MTs were first discovered in animals more than 50 years ago, whereas MTs in plants were only known 25 years later (approximately). Since its discovery in the horse kidney, this protein and its functions have taken an interest within the scientific community and have been broadly studied.

Despite its long-time discovery, the plant MTs research field is still in its earliest days [59]. Their protective function against HM toxicity and oxidative stress in animals through metal chelation, regulation of cellular metal homeostasis and detoxification processes (ROS scavenging) is widely recognised [57, 60-62]. Moreover, in mammalian genomes, these genes were found to have different regulations that, most likely, have overlapping but distinct functions [60]. In plants, MTs involvement in seed germination and the response to abiotic stresses was also noted [57, 63]. Additionally, MTs were found to participate in some vital development processes, such as fruit ripeness, root development, suberisation and pathogenic defence [64, 65].

Metallothionein proteins are commonly classified according to the arrangement of their cysteine (Cys) residues. Henceforth, all of the known plant MTs are divided into four groups [66]: type I (MT1), whose gene expression is higher in roots than shoots; type II (MT2), in which gene expression occurs mainly in shoots; type III (MT3), being transcribed in shoots mainly in fleshy ripening fruits [67, 68]; and type IV (MT4), having its transcription essentially confined to developing seeds [66, 69, 70].

Regarding general characteristics, MT1, MT2 and MT3 are structurally similar. They have two Cys-rich domains flanking a linker region: one at the C-terminal, which is conserved and follows the arrangement CXCXXCXCXXCXC (C stands for cysteine and X for any other amino acid), and another at the N-terminal region, that is specific for each MT subfamily. Type IV MTs contain three Cys-rich domains, with two aromatic amino acids, tyrosine (Tyr) and phenylalanine (Phe), on the linker regions (Cys-free regions that separate the Cys-rich domains). Additionally, for types I, II and III MTs, the linker

region has approximately 40 amino acids, while the one belonging to MT4 has 10-15 amino acids [66] (Figure 2).

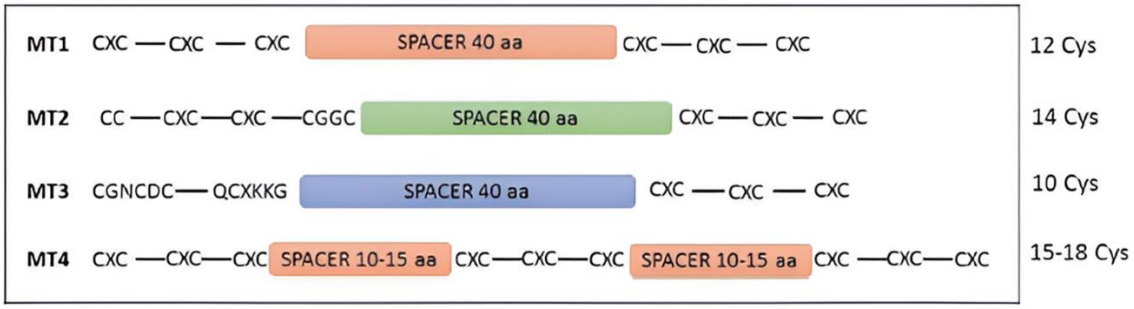

Figure 2| Structural representation of the four metallothionein (MT) types according to [66].

Looking into more specific details, MT1 has a total of 12 Cys in the peptide structure, consisting of six motifs Cys-X-Cys, evenly distributed by the two domains; MT2 contains 14 Cys, with a characteristic N-terminal pattern that has a pair of cysteines (C-C) in positions 3 and 4 of the Cys-rich region, and a motif Cys-Glycine-Glycine-Cys, at the C-terminal region; type III MTs are the smallest type, with 10 Cys in their amino acid sequence, with an N-terminal region characterised by the motif Cys-Glycine-Asparagine-Cys-Asparagine-Cys at the N-terminal and Glutamine-Cysteine-X-Lysine-Lysine-Glycine at the C-terminal region; MT4 has the highest number of thiolate groups, with 15-18 Cys residues, with an amino acidic pattern that consists of 5 or 6 Cys organised on C-X-C motifs in each of the three Cys-rich domains [59, 66, 71].

Determining the intracellular functions and roles of the different MT types has been the goal of several research studies over the years. Many plant species, including soybeans, tomato, wheat and Arabidopsis, have been reported to encode MTs. Just in *A. thaliana*, 8 different and active MT-encoding genes (*AtMTs*) that represent the four types have been annotated: three genes for the type I family (*AtMT1a*, *AtMT1b* and *AtMT1c*); two for the type II (*AtMT2a* and *AtMT2b*); one for type III (*AtMT3*); and two for the type IV (*AtMT4a*, and *AtMT4b*) [66, 72]. Despite mainly being known for its metal chelation properties, previous research has suggested that MTs can act as ROS scavengers [68]. In fact, studies have shown that, during senescence, MT induction prioritises ROS signalling and scavenging rather than metal chelation and remobilisation [73]. As for their metal chelation activity, type I MTs have been reported to increase plants' tolerance to Cd [63, 74] and Cu [75, 76] and regulate Zn homeostasis [67]. More recently, it was found that overexpression of this type of MT also increases As and Cu

tolerance [57]. Type II MTs have also been reported to play an important role in Cd and Cu tolerance [77, 78] and are induced by Cu in seedlings [79].

Regarding type III MTs, reports have highlighted their function in abiotic stresses [80]. However, other studies noted that MT3 also confer tolerance to Cd and Cu in rice [81]. Similar results were found when the overexpression of *A. thaliana* MT2a and MT3 genes conferred Cd resistance in plant cells [82]. Type IV MTs have a more prominent role in seeds, which makes it challenging to study the impact of these MTs during HM stress. However, researchers have found that MT4 confers Zn tolerance when expressed in a heterologous system [76]. Moreover, they could also be involved in Zinc homeostasis in seeds [69, 83].

1.2.2. Plant antioxidant system

Oxidative stress is one of the major causes of cell death. It is characterised by the over-production of ROS – like hydrogen peroxide (H_2O_2), hydroxyl radical (•OH) or superoxide anion ($•O_2^-$) [84, 85] – that cause damage at a molecular level through protein oxidation, lipid peroxidation and DNA damage that ultimately leads to cell death [85].

Production of ROS can occur naturally during an organism's normal cellular metabolism. For example, mitochondria produce $•O_2^-$ during the electron transport chain (ETC) [86]. In plants, more specifically, chloroplasts produce ROS when the photosynthetic machinery is affected, and peroxisomes, through photorespiration, also increase ROS accumulation [56, 86, 87]. As such, cells employ an antioxidant system composed of several enzymatic and non-enzymatic antioxidants that tightly regulate their production and abundance [88]. However, intense ROS formation can occur, commonly due to exposure to certain environmental conditions, like biotic or abiotic stresses, nutrient excess or deficiency, wounding and others. Usually, a balance exists between ROS production and the antioxidant defence inside the cell. However, when in excess, these ROS cause a disturbance in this balance, favouring the overproduction of free radicals. Thus, oxidative stress occurs [88].

Regarding HM, their ability to induce oxidative stress is well known. Their toxicity and how they produce ROS vary depending on several factors, such as accumulation, pattern of exposure, or even the metabolic activity of the HM itself in the cell [88]. Some metals, like Fe and Cu, possess redox activity and can catalyse Fenton/Haber-Weiss reactions that convert H_2O_2 and $•O_2^-$ into •OH, using their metals ions Fe^{2+} and Cu^+, respectively [56, 87]. Other metals like Zn, Ni and Cd, which are redox-inactive and cannot directly produce ROS, disturb the normal function of enzymatic activities, ultimately leading to ROS accumulation [56, 89].

Plants have developed a set of defensive mechanisms to counteract the adverse effects of oxidative stress. They protect the plant by reducing the levels of ROS and maintaining, at the same time, the antioxidant defence compounds [56]. These defence mechanisms include enzymatic antioxidants, such as superoxide dismutase (SOD), catalase (CAT) and peroxidase, mentioned above, glutathione reductase (GSR), amongst others; and non-enzymatic metabolites, such as reduced glutathione (GSH) and carotenoids [90]. Additional research has shown that proline is another metabolite with antioxidant properties in response to oxidative stress [91].

Considering glutathione (GS), this non-enzymatic antioxidant is one of the most relevant metabolites in plants' intercellular defence mechanisms against ROS activity. Its reduced form, GSH, is abundant throughout plant compartments (e.g., in chloroplasts, mitochondria, cytosol, endoplasmic reticulum and peroxisomes). It is involved in a wide range of physiological pathways, such as xenobiotics detoxification, regulation of sulphate transport, synthesis of proteins, nucleotides and phytochelatins and the expression of stress-related genes [90, 92]. Moreover, it was also noted that GSH plays an important role in growth-related mechanisms, such as cell division, differentiation and death [90].

Carotenoids comprehend a group of pigments that are synthesised in large quantities in chloroplasts and chromoplasts and are known for their light-harvesting capabilities, as well as a potent antioxidant activity against oxidative damage caused in the photosynthetic apparatus due to light excess conditions [93]. Their efficiency, however, as an antioxidant not only requires their interaction with other co-antioxidants but is also strongly dependent on the nature of the ROS itself [94].

As for proline, this metabolite is essentially an osmolyte with an important role in osmotic regulations and protein stabilisation. Nonetheless, studies have found that it also has potent antioxidant and metal chelation properties [92, 95].

1.3. The vacuole

Vacuoles represent the largest organelle inside the plant cell, known to be part of the endomembrane system [96-99]. It is actively involved in many functions within the cell, such as homeostasis maintenance, cell growth and development, turgor pressure control, and cellular responses to abiotic and biotic stress [97, 98]. They also possess storage compartment functions and are usually responsible for storing water, nutrients, ions, hormones, secondary metabolites, and proteins [97], amongst other compounds that include toxic cell residues, waste products, excess solutes and even HMs [100, 101].

Moreover, there is evidence that vacuoles partake in the programmed death of the cell [102].

Plant vacuoles are divided into two types, not only in size but also in content [99]. These are the protein storage vacuoles (PSV) and the lytic vacuole (LV). The first one (PSV) has a higher pH but lower hydraulic activity than the LV. As such, it can withstand protein accumulation and is usually found in storage tissues, like cotyledons, endosperm and tubers, but also in vegetative tissues, such as bark, leaves or pods, often associated with mature plant features [103-105]. On the contrary, LVs' lower pH and higher hydrolytic activity allow them to function as a degradative station for multiple macromolecules and other compounds [106, 107], which is a major asset for the detoxification processes of damaging products [108]. Furthermore, they participate in programmed cell death and play a role during senescence [97, 99]. As the equivalent of animal lysosomes or yeast vacuoles, LVs also function as deposit and storage sites for waste compounds [96], mostly occurring in vegetative tissues [99].

1.3.1 Vacuolar sorting motifs

The secretory and endocytic pathways are among the most important trafficking routes that compose the intricate network of the endomembrane system. Numerous results over the past years have undoubtedly contributed to expanding the knowledge regarding protein sorting and its primary mechanisms [109]. They are essential for plant cell homeostasis, and therefore, there has been extensive research on the proteins involved in vacuolar targeting, their pathways and sorting methods. So far, many signal and protein effectors have already been described [110]. However, some of the data collected suggests the existence of alternative routes that might shed a different view on protein delivery to the vacuole [111, 112]. Proteins involved in vacuolar targeting require a signal-receptor system to perform their function. Additionally, they possess sorting motifs, also known as vacuolar sorting determinants (VSDs), that can be arranged into three types: sequence-specific VSDs (ssVSDs), C-terminal VSDs (Ct-VSDs) and VSDs dependent on the physical structure of proteins (psVSDs) [104, 110]. Some of these motifs have already been localised in plant proteins [99], such as the case of a Ct-VSD in barley lectin and tobacco chitinase C-terminal domain [113, 114] and a psVSD in legumins of field bean [115]. Commonly, these motifs are recognised at the late or post-Golgi level and then redirected from the secretory pathway to the vacuole. However, this process is not always linear and, in most cases, depends on the type of cell/tissue and the organ's metabolic activity [110, 112].

1.4. Aspartic proteinases (AP) and the plant-specific insert (PSI) domain

Over the years, our laboratory has focused on understanding the biogenesis and sorting mechanisms of aspartic proteinases (APs), from which a good amount of new information has been collected [112, 116-123]. Accumulation of different types of APs can occur in different cell compartments, and the same protein can be secreted to the apoplast or directed to the vacuole. However, this depends on the cell type and its developmental stage [121, 122, 124]. Therefore, the hypothesis that different APs had different sorting motifs that provided this flexibility depending on the cell's conditions came to light. Cardosin A and cardosin B are well-characterized APs from *Cynara candunculus* that our laboratory has used as working models [116, 124]. They possess many similarities in their protein sequence but tend to accumulate in different cell compartments during the plant's development [116, 119]. While Cardosin A tends to accumulate in PSVs or LVs, depending on the cell's needs [117, 118, 121, 124], cardosin B mainly accumulates in the cell wall or the apoplast [116]. Additionally, cardosin A was found in both PSV and LV vacuoles during heterologous expression in *A. thaliana* and *Nicotiana tabacum* [119, 120], while cardosin B, on the other hand, only appeared in the LVs in the same heterologous expression conditions [122]. All this information makes cardosins an interesting subject for studying vacuolar trafficking and VSDs in plants.

Another characteristic of some APs, which includes cardosins A and B, is the presence of a plant-specific insert (PSI) domain. They consist of small peptides with about 100 amino acids that, despite being an enzyme's domain, appear to have independent enzymatic activity, unrelated to its "parent" proenzyme, when isolated *in vitro* [125-127]. Despite its functions in the cell still needing further clarification, some have suggested its involvement in pathogenic defence through membrane modulation and, interestingly, in vacuolar targeting of the APs [119, 128-130]. Moreover, Pereira et.al. (2013) showed that PSI A functions as a VSD. Nevertheless, the understanding of PSI roles in the vacuolar trafficking system is still to be revealed, and therefore, further research is necessary.

1.5. *Arabidopsis thaliana* as a model organism

Arabidopsis thaliana is a small eudicot plant species from the Brassicaceae family (which also includes mustard and cabbage). It is a native species from Eurasia that, over the years, has become the leading model organism for studying plants' physiological and molecular aspects. The fact that it was the first flowering plant to have its genome

completely sequenced has enabled significant advances in understanding the molecular principles underlying plant development, cell biology, metabolism, physiology, genetics, and epigenetics [131]. As it grew in popularity, the widespread use of *A. thaliana* became evident, as did the increasing knowledge about its biology. This then led to the creation of the Arabidopsis Information Resource (TAIR) (https://www.arabidopsis.org/) database [132], a comprehensive database containing information regarding *A. thaliana*'s molecular biology and genetic portfolio.

Apart from that, many other attributes render *A. thaliana* an ideal model organism for research, as it allows for faster, cost-effective experimentation. It is a small, higher plant with a short life cycle (about 6-8 weeks); despite being unable to produce fleshy fruits, it requires minimal maintenance and can thrive in confined spaces under fluorescent lighting. Additionally, its fully sequenced and annotated genome has led to the development of extensive biochemical, molecular, and bioinformatic tools that further support its widespread use in research [131, 133].

Taking advantage of these qualities of *A. thaliana* as a biological model, numerous studies, with the help of biotechnological approaches, have been performed to develop solutions for practical challenges in agriculture, environmental management, and other fields. This model organism has also been used in research to evaluate abiotic stress in plants, such as climate change and excessive use of fertilisers and pesticides [134].

1.6. Objectives

Looking at the nefarious effects that HM toxicity have over the many ecosystems, including the overall reduction of plant fitness and risk to human health, this work aimed primarily to evaluate the response of Arabidopsis plants when exposed to increasing concentrations of Ag and Fe by biochemically evaluating several oxidative stress-related parameters and the expression of the MT-encoding genes in an organ-specific way. Also, targeting large amounts of *At*MT2b to the vacuole, using the PSI domain of the cardosin A AP, was attempted as a strategy for future applications in the phytoremediation of HM-contaminated soils.

2. Materials and methods

2.1. Heavy metal viability test

To assert the HM selection for this project, a viability test was conducted by submitting *A. thaliana*'s wild-type seeds to 3 different HMs to see if they could germinate and grow so that enough biological material could be collected for further testing. The HMs tested in this preliminary study were Silver (Ag), Iron (Fe) and Cobalt (Co). A stock solution was prepared for each HM to add to the MS medium mentioned below at a final concentration of 12.5 mg/L. The silver solution was made with Silver Nitrate ($AgNO_3$), the iron solution with Ammonium Ferrous Sulphate Hexahydrate ($(NH_4)2SO_4{\cdot}FeSO_4,6H_2O$) and the cobalt solution with Cobaltous Sulphate Heptahydrate ($CoSO_4{\cdot}7H_2O$). These salts were selected due to the presence of NH_4^+, SO_4^{2-} and NO_3^-, which are plant macronutrients and thus do not induce stress if supplied in large quantities. This would not happen with the alternative salts containing Cl^-.

2.2. Medium preparation and seed germination

Murashige and Skoog (MS) medium, with vitamins included (4.4 g/L; Duchefa), was prepared with 1.5 % (w/v) sucrose and 0.7% (w/v) micro agar (Duchefa). The medium's pH was set to 5.7 using KOH before the final volume was adjusted. Finally, the solution was poured into Erlenmeyer flasks and then autoclaved at 121 ºC for a time according to its volume.

In a laminar flow chamber, 25 mL of autoclaved MS medium was measured in sterile conic tubes and then supplemented with the amount of Iron (Fe^{2+}) or Silver (Ag^+) from a stock solution of 87.7 mg/mL of Ammonium Ferrous sulphate Hexahydrate ($(NH_4)_2SO_4{\cdot}FeSO_4$, $6H_2O$) and 12.8 mg/mL of Silver Nitrate ($AgNO_3$), respectively, to a final concentration of 0, 3, 6 and 12.5 mg/L of Fe, and 0, 6.1 and 25.6 mg/L of Silver. These solutions were then poured into Petri dishes, previously identified for each Fe and Ag concentration, and left to set.

Additionally, seeds of wild-type *A. thaliana*, Col-0 ecotype, were surface disinfected for 3 minutes in 70 % (v/v) ethanol by agitation and then left to dry in the laminar flow chamber. Once the medium was ready, the seeds were scattered in all petri dishes with the help of a sterile toothpick. Afterwards, the Petri dishes were closed and sealed using micropore tape. To break seed dormancy and ensure seed stratification (gemination synchronised), the Petri dishes were left for 48 hours at 4 ºC before they were transferred to a growth chamber with a long day photoperiod (16 h light and 8 h

dark), at 24 ºC, with 50-60% relative humidity and light intensity at 180 µmole m^{-2} s^{-1} and left to grow for approximately 21 days.

2.3. Preparation and harvest of biological samples for biochemical analysis, RNA extraction and metal quantification

Twenty-one days after germination, the *A. thaliana* plants were collected from each treatment and separated into shoots and roots. For the biochemical analysis,150-200 milligrams of both organs were collected separately into 1.5 mL tubes, previously labelled with a one-letter and two-digit code: the letter indicating the organ (Shoot (S) or Root (R)) and the two digits indicating the treatment and the biological replicate number, as represented in the table below (Table 1). In addition, an indication of the corresponding metal treatment (Fe or Ag) was added. Furthermore, 50-100 mg of shoots and roots were collected in aliquots for RNA extraction. The samples were then stored at -80 ºC until further use.

Table 1| One letter and two-digit code system utilised to identify samples from treatments and biological replicates. In the "Organs" column, the "S" and "R" stand for "Shoots" and "Roots", respectively.

Heavy Metal	Treatment	Concentration	Replicate #	Organ	Final code
Iron (Fe)	0 mg/L	0	1	S/R	Fe S/R 0-1
			2		Fe S/R 0-2
			3		Fe S/R 0-3
	3 mg/L	1	1	S/R	Fe S/R 1-1
			2		Fe S/R 1-2
			3		Fe S/R 1-3
	6 mg/L	2	1	S/R	Fe S/R 2-1
			2		Fe S/R 2-2
			3		Fe S/R 2-3
	12.5 mg/L	3	1	S/R	Fe S/R 3-1
			2		Fe S/R 3-2
			3		Fe S/R 3-3
Silver (Ag)	0 mg/L	0	1	S/R	Ag S/R 0-1
			2		Ag S/R 0-2
			3		Ag S/R 0-3

6.1 mg/L	1	1	S/R	Ag S/R 1-1
		2		Ag S/R 1-2
		3		Ag S/R 1-3
25.6 mg/L	2	1	S/R	Ag S/R 2-1
		2		Ag S/R 2-2
		3		Ag S/R 2-3

Shoots and roots were also harvested from each treatment for the metal quantification analysis. These samples were collected and wrapped in aluminium foil. After that, they were dried in an oven at 60 °C to evaporate all the water in the tissue. The weight was registered periodically until no variations were detected, meaning the water had fully evaporated. This procedure lasted until 0.1-0.5 g of completely dried shoots and roots from each treatment were obtained. Finally, the samples were stored inside an oven at 37 ºC to prevent rehydration until the metal quantification analysis.

2.4. *Arabidopsis thaliana* MT1a and MT2b mutant genotyping

*At*MT1a and *At*MT2b mutant *A. thaliana* (Col-0 ecotype) seeds, received initially from NASC (https://arabidopsis.info/) were germinated, and the resulting plants were previously genotyped. The seeds from the heterozygous plants were collected using a sieve and stored at 4 °C until they were used for this study.

The heterozygous seeds were germinated in soil, and gibberellic acid (100 µM) was sprayed to stimulate germination. The resulting plants were left to grow until they reached a reasonable size so that a piece of leaf could be harvested for DNA extraction without compromising the plants' survival. The obtained DNA was then used for genotyping to confirm the homozygous presence of the T-DNA fragment - an insert that blocks gene expression when inserted into its sequence, in this case, the MT types 1a and 2b.

2.4.1. Genomic DNA extraction

Genomic DNA extraction was adapted from Edwards et al. (1991). For this, 100 to 200 mg of leaf biomass were collected in aliquots in 1.5 mL tubes and homogenised with 400 µL of extraction buffer, aided with quartz sand. Extraction buffer was made with 10 mL of 1 M Tris-HCl, 3.125 mL of 4 M NaCl, 2.5 mL of 0.5 M EDTA, 2.5 mL of 10% (w/v) SDS and water to complete a final volume of 50 mL. Afterwards, the tubes were vortexed for 5 seconds and then centrifuged for 1 minute at maximum velocity. The

supernatant (SN) was transferred to a new tube and mixed by inversion with 350 µL of isopropanol. The samples were then left to incubate at room temperature for 2 minutes. Next, the tubes were centrifuged at maximum velocity for 5 minutes to eliminate the SN. To wash the pellet for traces of isopropanol, 350 µL of 70% (v/v) ethanol was added to each tube, and the centrifugation was repeated at maximum velocity for 1 minute. The supernatant was eliminated again, and the tubes were left to dry at 37 ºC until no smell of ethanol could be detected. Finally, the DNA pellet was dissolved in 50 µL of sterilised deionised H_2O and quantified spectrophotometrically.

2.4.2. Genotyping PCR for *A. thaliana* MT1a and MT2b mutants

The presence of homozygous T-DNA mutants for *AtMT1a* and *AtMT2b* genes in *A. thaliana* plants was checked by PCR. Each reaction was made using three combinations of primers: one using the forward and reverse primers specific for the MT of interest; a second one using the MT's primer forward and a specific primer for the T-DNA insert; and a third reaction in which the MT's primer reverse and the T-DNA specific primer. These last two reactions were made to assess the forward or reverse function of the T-DNA primer. Additionally, each primer specific to the MTs was designed to be able to flank the T-DNA insert [137]. PCR reactions were prepared using X µL of previously extracted and quantified DNA, where "X" was calculated for 50 ng of DNA, 0.5 µL of each primer (forward and reverse) from a 10 µM working solution, 5 µL of 2x GRS Taq Master Mix Hotstart (Grisp) and sterilised H_2O to a final volume of 10 µL. The primers used for each reaction and their respective annealing temperatures are in the table below (Table 2).

All PCR reactions were performed using the same settings (Table 3) since the primer pairs' annealing temperatures were very similar (see Table 2).

Table 2| Selected primers for the genotyping PCR reactions and their respective sequences and annealing temperatures. The "Fw" and "Rev" annotations stand for "Forward" and "Reverse", respectively.

Gene	Primer	Sequence (5'-3')	T_a (ºC)
AtMT1a	MT1A_Fw_GNT	CCT GCA AAT GTG GTG ACT CT	57
	MT1A_Rev_GNT	ACC CAC AGC TGC AGT TTG AT	
AtMT2b	MT2b_Fw_GNT	GTG GAA GCT GTG GTT GTG G	58
	MT2b_GNT_Rev	AAC GAA AGT CTC GCC GGA AG	
T-DNA	T-DNA SALK	CGC AAG CTT GTC GAC ACA GGA TAA GTG TTC ACA CG	58

Table 3| Settings for the PCR genotyping reactions.

PCR steps	3-step protocol		Cycles
	Temperature	Time	
Initial denaturation	95 ºC	5 min	1
Denaturation	95 ºC	30 s	35
Annealing temperature	60 ºC	30 s	
Extension	72 ºC	1:30 min	
Final Extension	72 ºC	5 min	1
End/Hold	16 ºC	∞	-

PCR results for each sample were observed and interpreted by electrophoresis in a 0.8% (w/v) agarose gel in 1x Sodium borate (SB) buffer.

2.5. Biometric analysis

For the biometric analysis, wild-type *A. thaliana* Col-0 strain seeds were germinated in square-shaped plates, one containing only MS culture medium and the others supplemented with the different concentrations of Fe and Ag previously mentioned. The seeds were evenly spread in two lines. Before being placed in the growth chamber, the plates were left for 48 hours at 4 ºC. The plates were placed at a 70º angle in the growth chamber to ensure the root could grow vertically.

Twenty-one days after germination, the plants were removed and photographed with the assistance of a dark chamber. The leaf area and root length were measured using the image analysis functionalities of the program Fiji from Image J [135].

2.6. RNA extraction and isolation

RNA extraction from Roots (R) and Shoots (S) was performed using the "TripleXtractor" (GRiSP) protocol following the manufacturer's instructions. For this, 50-100 mg of tissue were homogenised in 1 mL of TripleXtractor reagent with the help of a mortar and pestle and quartz sand. The homogenised was transferred to a 1.5 mL tube and incubated for 5 minutes at room temperature (RT). Afterwards, 200 µL of chloroform for each 1 mL of TripleXtractor used was added, and the tubes were vigorously shaken and incubated for 2-3 minutes at RT. Next, the samples were centrifuged at 15,000 xg for 15 minutes at 4 ºC. After the centrifugation, the aqueous phase was gently transferred to a new RNase-free tube using a micropipette, and 1 mL of isopropanol for each 1 mL of TripleXtractor used was added. The tubes were incubated for 10 minutes at RT before

centrifugation at 15,000 xg for 10 minutes at 4 ºC. The SN was discarded, and to wash the pellet, 1 mL of ethanol 70% (v/v) was added, and the tubes were gently inverted. Next, the samples were centrifuged at 15,000 xg for 5 minutes at 4 ºC, the SN was discarded, and the pellet was left to dry for 10-15 minutes at RT. The pellet was resuspended in 40 µL of RNase-free water, and the tubes were placed in a thermal block at 58 ºC for 10-15 minutes to induce the evaporation of the remaining ethanol and speed up the dissolution of the total RNA extracted. The RNA was kept on ice until it was spectrophotometrically quantified and stored at -80 °C until further use.

2.7. DNA and RNA quantification

Quantification and purity assessment of the DNA and RNA extracted was performed using the DS-11+Spectrophotometer (DeNovix) and the respective programmes included in the device. The absorbances (Abs) were read at 260, 230 and 280 nm, and the abs ratios of 260/230 and 260/280 were analysed. The results obtained were expressed in ng/µL.

An electrophoresis was performed in a 0.8% (w/v) agarose gel to assess the quality of the extracted total RNA. Before loading the RNA samples, 300 ng of total RNA were mixed with 1 µL of 10x xylenecyanol loading buffer and H_2O to a final volume of 15 µL in small droplets on a piece of parafilm over ice.

2.8. Synthesis of cDNA

The Xpert cDNA Synthesis Supermix (Grisp Research Solutions) was used following the manufacturer's instructions for the cDNA synthesis. A mixture was prepared with 1 µg of total RNA, previously extracted, 4 µL of the Master Mix and sterile and deionised H_2O to a final volume of 20 µL. Using a thermocycler, the reaction was then heated at 37 ºC for 30 min to induce the cDNA synthesis, after which it was submitted to 10 min at 60 ºC. The reaction tubes were heated for 3 min at 95 ºC to inactivate the reverse transcriptase. Finally, the cDNAs were stored at -20 ºC and thawed over ice when needed.

2.9. RT-qPCR

The RT-qPCR assay in this study was performed using Xpert Fast SYBR 2x Mastermix (GRISP) for both shoots and roots and for all Fe and Ag treatments. Additionally, to study the gene expression for each MT, 2 biological replicates were used, and 3 technical replicates were made for each biological replicate. Furthermore, the

cDNA samples were diluted to a ratio of 1:10, as previous studies verified that it was the most suitable concentration for this RT-qPCR [136]. In the end, each reaction was composed of 4 µL of diluted cDNA, 6 µL of a Master Mix composed of 5 µL of the 2x SYBR Mastermix, 0.3 µL of each 10 µM primer (Table 4) and 0.4 µL of sterile and deionised H_2O.

Table 4| Primers used in RT-qPCR assay for each MTs expression, their respective sequence, final T_a for optimal results and reference found in literature.

Gene	Primer	Sequence (5'→3')	Amplicon size (bp)	T_a (ºC)
AtMT1a	Forward	CCTGCAAATGTGGTGACTCT	90	57
	Reverse	ACCCACAGCTGCAGTTTGAT		
AtMT1b	Forward	AGAGATGTGTGTTGTTGG	152	53
	Reverse	TTGGTGAGAGTGGGACTTG		
AtMT1c	Forward	CCTGCAAATGTGGTGATTCGT	104	59
	Reverse	ACAGTTACAGCTTGACCCGCA		
AtMT2a	Forward	GGTTGCAAAATGTACCCTGAC	127	51
	Reverse	TCTCAGCGTTGTTACTCTCC		
AtMT2b	Forward	GTGGAAGCTGTGGTTGTGG	158	58
	Reverse	AACGAAAGTCTCGCCGGAAG		
AtMT3	Forward	ACAAGACCCAGTGCGTAAAG	79	55
	Reverse	ATGGCCTCCTTGTAGCTCTC		

Both cDNA and Master mix were then loaded separately in the specified wells of a 96-well plate to avoid any possible reaction outside the PCR program. Then, the plate was sealed and spun to ensure the reaction mixtures would settle to the bottom of the wells. The Bio-Rad CFX96 thermocycler was used to run the RT-qPCR program. Once the plates were ready and placed in the thermocycler, the reaction would occur according to the recommended settings by the SYBR Mastermix manufacturer, apart from the number of cycles during the annealing/extension phase, which was set for 39 instead of 40 cycles. As such, the program included 3 minutes at 95 ºC, 39 cycles of 5 sec at 95 ºC, and 25 sec at 60 ºC. To establish the melting curve, a cycle of 5 sec at 65 ºC was added to the end of the reaction, followed by an increase of temperature until 95 ºC, increasing 0.5 ºC every 5 sec.

For this study, three reference genes were used (Table 5): the yellow-leaf-specific gene 8 (*YLS8*), the Ubiquitin 10 gene (*UBQ10*), and the Glyceraldehyde 3-phosphate dehydrogenase gene (*GAPDH*). In the case of Iron (Fe) treatments, *GAPDH* and *YLS8* genes were used for the shoots and the *UBQ10* and *GAPDH* for the roots. In the case of Silver (Ag) treatments, *UBQ10* and *GAPDH* genes were used for the shoots, and the *GAPDH* and *YLS8* genes were used for the roots.

Table 5| Reference genes used in the RT-qPCR and the respective primers 5' to 3' sequence, as well as the amplicon size and the reference from where the primers were obtained.

Locus	Genes	Primer	Sequence (5'→3')	Amplicon size (bp)	Reference
AT5G08290	*YLS8*	Forward	AAGATCAACTGGGCTCTCAAGG	141	[137]
		Reverse	TGGGAAGCTCGATTAGTAACGG		
AT4G05320	*UBQ10*	Forward	GGCCTTGTATAATCCCTGATGAATAAG	61	[138]
		Reverse	AAAGAGATAACAGGAACGGAAACATAGT		
AT3G26650	*GAPDH*	Forward	TTGGTGACAACAGGTCCAAGCA	62	[138]
		Reverse	AAACTTGTCGCTCAATGCAATC		

2.10. Biochemical parameters

2.10.1. Lipid peroxidation

The assessment of lipid peroxidation was determined according to Heath & Packer (1968) [139] via quantification of MDA levels. Since it is an end-product of polyunsaturated fatty acids peroxidation in the cells, it allows the evaluation of heavy metal-induced membrane damage. For this, 150-200 mg of fresh weight of both roots and shoots from *A. thaliana* was homogenised in 0.8 mL of 0.1% (w/v) trichloroacetic acid (TCA). Samples were then centrifuged for 5 minutes at 10,000 xg. Afterwards, 250 µL of recovered supernatant of each sample was added to 1 mL of 0.5% (w/v) Thiobarbituric acid (TBA) in 20% (w/v) TCA. Aliquots containing this mixture were heated at 95 ºC for 30 minutes and then incubated on ice for 15 minutes. Lastly, samples were subjected to an eight-minute centrifugation at 10,000 xg, followed by a reading of their absorbance values at 532 and 600 nm. The latter values were subtracted from the first to avoid the effects of non-specific turbidity. MDA content was expressed in nmol/g fresh weight (fw) using the extinction coefficient 155 mM^{-1} cm^{-1}. The homogenisation solution was used for the blank.

2.10.2. Quantification of H_2O_2

The methodology used to determine H_2O_2 levels in *A. thaliana* was in accordance with Sousa et al. (2013) [140]. Aliquots containing 150-200 mg of frozen biological material were homogenised at room temperature in 1.2 mL of potassium phosphate buffer (50 mM, pH 6.5). The samples were centrifuged at 6,000 xg for 25 min at 4 ºC. Five hundred µL of supernatant was recovered to fresh new tubes and added to 500 µL of a solution of 0.1% (w/v) Titanium sulphate ($TiSO_4$) in 20% (w/v) Sulphuric acid (H_2SO_4). Both were mixed by vortex for 15 seconds. Afterwards, centrifugation conditions were repeated, except this time for 15 minutes. Finally, the absorbance values of each sample were read at 410 nm. Results were expressed in mmol/g fw using 0.28 $\mu M^{-1}\,cm^{-1}$ as the extinction coefficient. A solution containing 500 µL of phosphate buffer and 500 µL of the $TiSO_4$/ H_2SO_4 solution was used for the blank.

2.10.3. Total thiols, non-protein thiols and proline quantification

To quantify total thiols, non-protein thiols and proline levels, 150-200 mg of plant material (shoots and roots) were homogenised in ice in 1.5 mL of a solution containing 20 mM EDTA and 20 mM Ascorbic acid. Each sample was centrifuged at 12,000 xg for 20 minutes, and the supernatant was recovered in a new tube. This first SN (SN1) would be used to determine the levels of the total thiols and to prepare a second SN (SN2) that would be used to assess both proline and non-protein thiols concentrations.

As such, for SN2, 700 µL of the previously collected SN1 and 700 µL of 10% (w/v) Sulfosalicylic acid were added to a new tube, mixed, and incubated at RT for 15 minutes. This solution was centrifuged at 3,000 xg for 15 minutes in refrigerated conditions (4 ºC). Finally, the resulting SN was collected in a new tube and stored in ice until further use.

2.10.3.1. Total thiols

In a new tube, 100 µL of the SN1 was mixed with 480 µL of Tris-HCl 200 mM (pH=8.2) and 20 µL of 10 mM 5,5'-dithiobis (2-nitrobenzoic acid) (DTNB). After mixing well, the tubes were incubated at RT for 15 minutes. Absorbances were read at 412 nm, and total thiols concentration was determined in µmol/g fw using 13,600 $M^{-1}\,cm^{-1}$ as extinction coefficient. For the blank, homogenisation solution was used instead of the SN1.

2.10.3.2. Proline quantification

Two hundred µL of the SN2 were added to a 1.5 mL tube with 200 µL of glacial acetic acid and 200 µL of acid ninhydrin and incubated at 96 ºC for one hour. After a colling on ice, 800 µL of Toluene was added to each sample and vortexed for 15 seconds. Absorbance values were determined at 520 nm using the resultant upper phase, and proline concentration was determined in µmol/g fw. Toluene was used as blank.

2.10.3.3. Non-protein thiols quantification

To quantify the levels of non-protein thiols, 250 µL of the SN2 was mixed with 237.5 µL of 400 mM Tris-HCl (pH=8.9) and 12.5 µL of 10 mM DTNB and incubated at RT for 5 minutes. Afterwards, absorbance levels were read at 412 nm, and the non-protein thiols concentration was determined in µmol/g fw using 13,600 M^{-1} cm^{-1} as the extinction coefficient. Protein thiols were determined by subtracting the values of the non-protein thiols concentration from the total thiols' concentration.

2.10.4. Reduced glutathione (GSH) determination

Reduce Glutathione (GSH) was determined using an adaptation of the glutathione Assay kit from Sigma-Aldrich, where the assessment of GSH levels resulted from the amount of DTNB directly reduced by GSH. To prepare the samples, 150-200 mg of plant tissue was homogenised in 500 µL of 3% (w/v) sulfosalicylic acid using a ratio of 3 mL per 1 g of tissue under ice-cold conditions to deproteinise the samples. Afterwards, 1.2 mL of 3% (w/v) sulfosalicylic acid was added to each sample, using a ratio of 7 mL per 1 g of tissue, followed by an incubation in ice for 10 minutes. The homogenates were then centrifuged at 10,000 xg for 10 minutes at 4 ºC, and the supernatant was collected into fresh tubes and maintained on ice until further use.

In this assay, a standard curve of GSH was necessary to determine the amount of GSH in each sample. To this end, GSH standard solutions of 10, 20, 30, 40 and 50 µM were prepared in 3 % (w/v) sulfosalicylic acid from a stock solution. Additionally, a working solution of 1 mM EDTA in 100 mM phosphate buffer, pH=7.0, was prepared, in which 400 µL of 1.5 mg/mL DTNB was added to 14 mL of this solution. Afterwards, the reaction tubes for extract samples and the standard curve were assembled using the volumes in the table below (Table 6).

Table 6| Reaction tubes composition and respective volumes.

Component	Volume
Working solution	750 µL
H_20	200 µL
Extract (or GSH standard)	50 µL
Final volume	1 mL

Each reaction was mixed and then incubated for 10 minutes in the dark. The absorbances were then registered at 412 nm, and the GSH levels were expressed in nmol/g fw. The blank was prepared using 3% (w/v) sulfosalicylic acid instead of extract (or GSH standard).

2.10.5. Extraction and quantification of photosynthetic pigments

One hundred and fifty to 200 mg of biological material were homogenised in 80% acetone to a final volume of 5 mL (2 mL + 2 mL + 1 mL), with the help of quartz sand. Between each homogenisation step, samples were transferred to a 15 mL tube protected from the light to void the photodegradation of the pigments. The tubes were centrifuged at 3,500 rpm for 10 minutes in a MEGA STAR 1.6R centrifuge (VWR), and the resultant supernatant was transferred to a new 15 mL tube, protected from the light as well. After adjusting the final volume to 10 mL with 80% acetone, absorbances were read in the following wavelengths: 480 nm, 495 nm, 645 nm, and 655 nm. To remove any influence from all photosynthetic pigments in the Abs values, two equations, (1) and (2), were used to perform the necessary corrections:

(1) Abs (480 nm) corrected = Absº (480 nm) – 0.566 × Abs (645 nm) + 0.121 × Abs (655 nm)
(2) Abs (495 nm) corrected = Absº (495 nm) – 0.112 × Abs (645 nm) – 0.0036 × Abs(655nm)

Afterwards, the contents of each photosynthetic pigment - chlorophyll A (Chla) (3), chlorophyll B (Chlb) (4), β-carotene (ß-car) (5) and lutein (Lut) (6) – were determined and expressed in mg/L, using the formulas below:

(3) [Chla] (mg/L) = 19.00 × Abs (655 nm) – 7.61 × Abs (645 nm)

(4) [Chlb] (mg/L) = 21.45 × Abs (645 nm) – 5.92 × Abs (655 nm)

(5) [ß-car] (mg/L) = 17.16 × Abs (495 nm) – 3.96 × Abs (480 nm)

(6) [Lut] (mg/L) = 11.51 × Abs (480 nm) – 20.61 × Abs (495 nm)

The final calculations for each pigment were determined and expressed in mg g^{-1} fw from these values [141].

2.11. Quantification of iron and silver

Dried samples weighing 0.1 to 0.5 g of shoots and roots from each Fe and Ag treatment were collected and ground using an ultra-centrifugal mill (ZM 200, RETSCH). The ground samples were then submitted to a microwave-assisted wet digestion (Multiwave, Anton Paar) with 4 mL of suprapure HNO_3 and 2 mL of suprapure H_2O_2. The digestion program was performed at 400 W for 2 minutes, 600 W for 2 minutes and 700 W for 20 minutes. The readings of iron and silver digested samples were done separately and using different equipment. Iron measurements were read using an Atomic Absorption Spectrometer with atomisation by flame (Model iCE™ 3300, Thermo Fisher Scientific). In the case of Ag, the values in each sample were read with the help of an Inductively Coupled Plasma Mass Spectrometer (ICP MS PlasmaQuant MS Elite S, Analytik Jena GmbH). Fe concentration was expressed in mg g^{-1} of dry weight, and Ag concentration in µg g^{-1} of dry weight.

2.12. Cloning strategy

This study analysed plant MTs' localisation and putative vacuolar sorting by confocal laser scanning microscopy. The main goal was to obtain fusions of AtMT1a and AtMT2b with a fluorescent protein – mNeonGreen – for localisation and with cardosin A Plant Specific Insert (PSI A) [119] for vacuolar targeting. Two final constructs were obtained for AtMT2b: pMDC83-MT2bΩ-6xHis-PSIA-mNeonGreen, containing a hexa histidine-tag (His) - for future pull-down assays, and pMDC83-MT2bΩ-mNeonGreen. Several steps were taken to achieve this, described in the sections below.

2.12.1. Amplification of *AtMT1a* and *AtMT2b* genes for plasmid insertion

Metallothionein types 1a and 2b coding sequences were amplified with the inclusion of *Xba*I and *Sal*I restriction sites as these restriction enzymes create sticky ends for further pSK insertion. For this, 1 µL of *A. thaliana* wild-type cDNA was used as the

template. The genes were amplified by PCR reaction in a Biometra $T_{ADVANCED}$ thermocycler (Analytic Jena), with 25 µL of NZY Proof 2X Green Master Mix (NZY tech) containing a proofreading *Taq* DNA polymerase, 1 µL of 0.4 µM primers forward and reverse, previously designed to include the restriction sites (Table 7), and deionised H_20 to a final volume of 50 µL. The PCR settings are presented in Table 8. PCR results were analysed in 1% (w/v) agarose gel electrophoresis and gel purified as described below.

Table 7| Primers used for *AtMT1a* and *AtMT2b* full cDNA amplification from a cDNA pool and their respective annealing temperatures (T_a).

Primers	Sequence (5'→3')
MT1a_Fw_XbaI	AATCTAGAATGGCAGATTCTAACTGTGG
MT1a_Rev_SalI_Stop	AAAGTCGACTCAACAGTTACAGTTTGACCCA
FW_MT2b_XbaI	AATCTAGAATGTCTTGCTGTGGTGGAAG
Rev_MT2b_SalI	AAAGTCGACTTTGCAGGTACAAGGGTTGC

Table 8| Settings for the *AtMT1a* and *AtMT2b* with XbaI and SalI restriction sites PCR reactions.

PCR steps	3-step protocol		Cycles
	Temperature	Time	
Initial denaturation	95 ºC	3 min	1
Denaturation	95 ºC	30 s	30
Annealing temperature	55 ºC	30 s	
Extension	72 ºC	30 s	
Final Extension	72 ºC	5 min	1
End/Hold	8 ºC	∞	-

The reverse primer for *AtMT2b*, Rev_MT2b_SalI, was also designed to remove the STOP codon of this MT gene and allow in-frame expression with a fluorescence protein. Therefore, the *AtMT2b* sequence in each construct is presented as "MT2bΩ", in which the "Ω" refers to the lack of the STOP codon.

2.12.2. DNA purification from gel

DNA purification from the gel was performed using the GFX PCR DNA and Gel Band Purification (Ilustra, Cytivia) kit following the protocol provided by the manufacturer. DNA bands of interest, separated through agarose gel electrophoresis, were cut using a

sterile surgical blade and placed into a 1.5 mL sterile microtube. The mass was determined, and for each 10 mg of agarose gel, 10 µL of buffer type 3 was added (when gel weight was lighter than 300 mg, a recommended minimum of 300 µL of buffer should be added). Afterwards, the agarose in the tubes was dissolved by incubation at 60 ºC in a thermoblock for 15-30 minutes with small inversions every 3 minutes. The mixture was centrifuged and transferred to the kit's assembled GFX MicroSpin column and Collector tube when dissolved. After a small incubation at RT (1 minute), another centrifugation followed for 30 seconds at 16,000 xg. The flowthrough was discarded, and 500 µL of the type 1 buffer was added to the column. The mixture was centrifuged at 16,000 xg for 30 seconds, and the collector tube was discarded afterwards. The GFX MicroSpin column was transferred to a new sterile micro tube, and 20 µL of buffer type 6 was added to the column. Finally, a 1-minute incubation at RT occurred before centrifuging the assembled column for 1 minute at 16,000 xg to collect the purified DNA. After quantification, the DNA was stored and conserved at -20ºC until further use.

2.12.3. Restriction and ligation of the *At*MT1a and *At*MT2b cDNAs in a vector backbone

Integration of the *AtMT2b* cDNA in the pbluescript SK- (pSK) vector was performed via restriction and ligation to obtain the pSK-MT2bΩ construct. The previously amplified and purified *AtMT2b* cDNA and pSK vector DNA were treated with FastDigest *Xba*I (Thermo Scientific) and FastDigest *Sal*I (Thermo Scientific) restriction enzymes to create sticky ends. The reaction was composed of 1 µL of both enzymes, 5 µL of DNA (either purified cDNA or vector DNA), 2 µL of 10x FastDigest Buffer (Thermo Scientific) and purified H_2O to a final volume of 20 µL. When assembled, each reaction tube was incubated at 37 ºC for 15 minutes in a thermoblock. All the reactions were loaded in 1 % (w/v) agarose gel for electrophoresis and then gel purified as previously described.

Additionally, to further increase the chances of ligation, the pSK vector was also treated with Anza™ Alkaline phosphatase (5 U/µL, Invitrogen) to remove the phosphate group in the 5' end that remained after restriction, preventing a subsequent re-ligation of the plasmid. This way, 17 µL of the purified pSK vector were loaded in a 0.2 mL sterile tube, and 2 µL of Anza™ 10X Buffer and 1 µL of Anza™ Alkaline phosphatase were added to a final volume of 20 µL. The new reaction was incubated for 15 minutes at 37 ºC, followed by a second incubation at 80 ºC for 5 minutes to inactivate the enzyme.

To perform the ligation of the *AtMT2b* insert into the vector, the T4 DNA ligase (5 U/µL, Invitrogen™) was used following the protocol provided by the manufacturer. As such, 50 ng of previously treated plasmid was used, along with a specific amount of

insert, calculated using the formula $insert\ (ng) = \frac{insert\ (ng) * insert\ (bp)}{insert\ (bp)}$. Since both *AtMT1a* and *AtMT2b* cDNAs are relatively small DNA sequences (100-200 bp), the volume of insert used in the reaction was 5 times higher than the calculated volume to increase the chances of ligation success further. This way, the ligation reaction for *AtMT2b* was composed of X µL of insert, Y µL of insert, 2 µL of 10X T4 DNA Ligase Buffer, 1 µL of T4 DNA Ligase and sterile H_2O to a final volume of 20 µL. A control reaction containing only vector DNA was also made to assess the alkaline phosphatase's success in preventing the plasmid's re-ligation. The reaction tubes were incubated at RT for 1 hour and then immediately transformed into chemically competent DH5α *Escherichia coli* cells as described below.

On the other hand, *AtMT1a* was integrated into the pMiniT 2.0 plasmid (NEB) to obtain the pMiniT2.0-*At*MT1a construct. Following the manufacturer's protocol, the ligation reaction was made using the "NEB PCR Cloning Kit" (NEB).

2.12.4. Gibson assembly cloning

Fusion of the PSI A sequence and the hexa histidine-tag (His) in the middle of the *AtMT2b* cDNA was performed using Gibson assembly. The synthesised insert MT2bΩ-6xHisPSIA would then be integrated into a pSK plasmid to obtain the intermediate construct pSK-MT2bΩ-6xHisPSIA (Figure 3). For this, purified pSK-MT2bΩ plasmid and the PSI A sequence were amplified by PCR reaction using specific primers to add the His-tag and overhang adapters with overlapping regions (OL): in the case of pSK-MT2bΩ, the primer forward would include an OL for PSI A, and the reverse primer an OL for the 6xHis-tag; the primers used to amplify the PSI A gene included an OL for the *AtMT2b* cDNA in the primer forward, and the primer reverse contained the 6xHis-tag and also an OL for *AtMT2b* (Table 9). Additionally, the restriction sites of *Xba*I and *Sal*I restriction enzymes were kept. The PCR results were verified by gel electrophoresis in 1% (w/v) agarose gel, and the amplicons were gel purified.

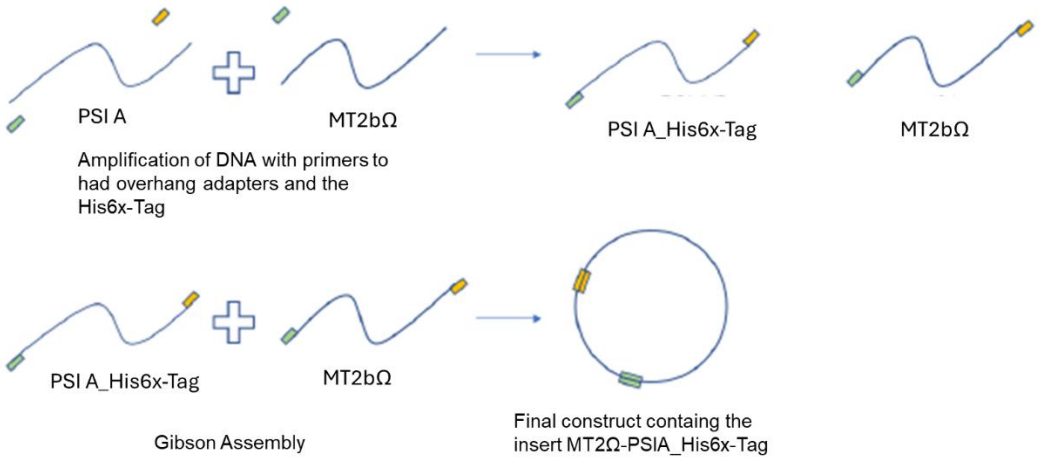

Figure 3| Visual representation of the Gibson Assembly process. The yellow and green blocks represent the DNA sequences that facilitate the recombination of the amplicons, resulting in a complete plasmid through DNA ligase, DNA polymerase, and exonuclease enzymes' actions.

Table 9| Primers used for the Gibson Assembly cloning, the corresponding templates, and their respective annealing temperatures (T_a). The 6xhexa histidine-tag is represented in **bold**.

Template	Primers	Sequence (5'→3')	T_a (ºC)
pSK_MT2bΩ	Mt2b_OL_His_Fw	TGATGATGATGAGCAACACCGAGGACAAGAG	58.6
	Rev_Mt2b_OLPSI	AACACTTATCCCCGGCGATGAACTCTCAGTA	
PSI A	Fw_PSI_OLmt2b	TTCATCGCCGGGGATAAGTGTTCACACAACT	51.9
	PSI_HIS_OLmt2b_Rev	CTCGGTGTTGCT**CATCATCATCATCATCAT**GTCA TGAACCAGCAATGCAA	

The Gibson Assembly reaction was prepared following an adapted protocol from Gibson et al., 2009 [142], described in Table 10, followed by a 1-hour incubation at 50 ºC. This reaction was then used to transform chemically competent TOP10 *E. coli* cells.

Table 10| Gibson Assembly reaction mix. "OL" stands for "Overlapping region".

Components	Volume (µL)
DNA	X equimolar OL DNA fragments
5xIRB	4
Taq DNA Ligase	2

Phusion HF DNA Polymerase	0.25
T5 Exonuclease (prediluted 1:30 in1xIRB)	0.25
Total	20

2.12.5. Assembly of the constructs for confocal microscopy

An enzymatic restriction cloning strategy, similar to the one described above, regarding the assembly of the pSK-MT2bΩ construct, was performed to obtain the final constructs for confocal microscopy: pMDC83-MT2bΩ-6xHisPSIA-mNeonGreen, and pMDC83-MT2bΩ-mNeonGreen (see supplementary figures 28 and 29). In this case, the MT2bΩ and MT2bΩ-6xHisPSIA fragments were inserted in a pMDC83 plasmid containing the mNeonGreen fluorescent protein. Both the plasmid and the previously obtained pSK-MT2b-6xHisPSIA and pSK-MT2b constructs were treated with FastDigest *Xba*I (Thermo Scientific) and FastDigest *Sal*I (Thermo Scientific) restriction enzymes. Each reaction was composed of 1 µL of both enzymes, 10 µL of DNA (corresponding to µg), 2 µL of 10x FastDigest Buffer (Thermo Scientific) and purified H_2O to a final volume of 20 µL. Each fragment was gel purified afterwards. A ligation reaction was performed using the T4 DNA ligase (5 U/µL, Invitrogen™) following the steps previously mentioned. In addition, purified pMDC83 was also treated with Anza™ Alkaline phosphatase (5 U/µL, Invitrogen™) after the digestion reaction. Both ligation reactions were transformed into chemically competent TOP10 *E. coli* cells.

2.12.6. Transformation of chemically competent *E. coli* cells

For this work, both DH5α and TOP10 *E. coli* strains were used. Aliquots of chemically competent *E. coli* cells stored at -80 ºC were thawed in ice. Once liquid, 100 µL of cells were carefully transferred to a 1.5 mL sterile tube, and 20 µL of ligation reaction was added. The tubes were left in ice for 30 minutes and then submitted to a thermal shock, being heated for 1 min at 42 ºC and then quickly transferred to ice and left there for another 1 to 2 min. Afterwards, 1 mL of LB (Luria Broth Base, Miller, Duchefa Biochemie) medium was added to the tubes, and these were incubated at 37 ºC for 1 hour under agitation to allow cell recovery. Next, the cells were centrifuged at 1,000 xg for 2 min, and about 1 mL of SN was discarded. Ultimately, the transformed cells were resuspended (about 100 µL) and plated in the appropriate selective media. When dried, the plates were placed in an incubator at 37 ºC and left overnight. Every step that required the exposure of the cells was performed near an open flame.

2.12.7. Selective medium preparation

Media containing sterile LB Medium, with 1.5 % (w/v) agar (Liofilmchem), and an antibiotic acting as a selective agent was prepared and poured into 9 cm ø Petri dishes. For both pSK and pMiniT 2.0, ampicillin at 100 µg/mL was used. Additionally, for pSK, X-GAL at 100 µg /mL was also used, as this plasmid allows the recognition of colonies carrying the recombinant plasmid through the loss of blue colour in the presence of X-GAL. For pMDC83, kanamycin at 50 µg/mL was used.

2.12.8. Positive colony screening

The transformation success of *E. coli* strains was confirmed via restriction analysis. For this, various single bacteria colonies from each construct were inoculated in 5 mL LB media with the specific selective agent and grown overnight, as described below. The next day, plasmid minipreps were prepared from the liquid cultures (as mentioned below), and the purified plasmids were digested using FastDigest *Xba*I (Thermo Scientific) and FastDigest *Sal*I (Thermo Scientific). The reaction was composed of 0.5 µL of both enzymes, 2.5 µL of purified plasmid DNA, 1 µL of 10x FastDigest Buffer (Thermo Scientific) and purified H_2O to a final volume of 10 µL. Restriction success and insert size were verified by gel electrophoresis in a 1% (w/v) agarose gel. When the clone was confirmed to be correct, the constructs were submitted for DNA sequencing (https://eurofinsgenomics.eu/), and the sequencing data was analysed using SnapGene software (https://www.snapgene.com/).

2.12.9. Culture of bacteria

Under sterile conditions, 5 mL of sterile liquid LB medium (Luria Broth Base, Miller, Duchefa Biochemie), supplemented with the appropriate antibiotic at the corresponding concentration for each plasmid, was transferred to a 15 mL sterile tube. A single colony was carefully picked using a sterile toothpick and inoculated into the LB medium. The culture was incubated overnight at 37°C with shaking at 200 rpm (GFL 3031, GFL).

2.12.10. Plasmid purification

To obtain a high-purity plasmid DNA from the transformed *E. coli* DH5α or Top10 liquid cultures, the NZYMiniprep kit (NZYtech) was used according to the manufacturer's instructions. As such, 1 mL from the overnight liquid cell culture was centrifuged for 30 sec at 13,000 rpm (Centrifuge 5418/5418R, Eppendorf), and the supernatant was

discarded. The pellet was then resuspended in 250 µL of A1 Buffer, followed by the addition of 250 µL of A2 Buffer. The mixture was incubated at RT for 4 minutes. Next, 300 µL of A3 Buffer was added, mixed by inversion and centrifuged for 3 minutes at 13,000 rpm. Afterwards, the supernatant was transferred to a column assembled in a 2 mL collector tube provided by the manufacturer and centrifuged for 30 sec at 13,000 rpm. The flow-through was removed, and 600 µL of the AS Buffer was added to the column. The column-collector tube assembly was centrifuged twice for 1 minute, with the flow-through being discarded each time. The column was then transferred to a new sterile 1.5 mL tube, and 30 µL of AE Buffer was added. After incubation at RT for 1 minute, the tube was centrifuged for 1 minute at 13,000 rpm to obtain the purified plasmids. The tube was kept at -20ºC until needed.

2.12.11. Stock preparation of transformed *E. coli*

The bacterial stocks were prepared in sterile conditions, mixing 300 µL of sterile 50 % (v/v) glycerol and 700 µL of the liquid cell culture containing the respective antibiotic in a 1.5 mL sterile microtube. Stocks were stored at -80 ºC until further use.

2.13. Cell imaging

2.13.1. *Agrobacterium tumefaciens* transformation by electroporation

Shots containing 50 µL of previously prepared electrocompetent *A. tumefaciens* cells were thawed on ice for 10 minutes. When liquid, 5 µL of each construct was gently added, and the solution was transferred to an electroporation cuvette. The cuvette was introduced in a MicroPulser ™ electroporator (Bio-Rad), and an electrical shock struck the cells. Immediately afterwards, 1 mL of liquid LB medium was added to allow cell recovery, followed by incubation for 4 h at 28 ºC. Finally, 100 µL of cells were plated in LB 1.5 % (w/v) agar with the appropriate antibiotics and supplements (see below) and left at 28 ºC for 48 h.

2.13.2. *A. tumefaciens* culture preparation for infiltration

Single aliquots of transformed *A. tumefaciens*, holding the constructs of interest, were inoculated in 10 mL of LB medium containing the appropriate antibiotics [Kanamycin (50 µg mL^{-1}) and Gentamicin (50 µg mL^{-1})]. The culture was then incubated for 24 h, under agitation at 28 ºC, until an approximate OD_{600nm} of 2.2 was reached.

2.13.3. Transient expression in *Nicotiana tabacum*

The transient expression of each construct was performed using *N. tabacum* leaves. For this study, *N. tabacum* plants were germinated directly on fertilised substrate (Universal substrate, SYRO PLANT) and grown under continuous light at 22 °C with 50-60 % relative humidity and light intensity at 180 µmole m^{-2} s^{-1}.

Confocal microscopy was used to assess the vacuolar targeting of plant MTs and the *in vivo* localisation of *At*MT2b. As such, six-week-old *N. tabacum* with fully expanded leaves were infiltrated with *A. tumefaciens* GV3101 holding each final construct. First, *A. tumefaciens* cells containing the construct of interest were inoculated in 5 mL of LB (supplemented as above) and left to grow overnight at 28 ºC under shacking conditions (200 rpm). The next day, 1 mL of the culture was collected and centrifuged at 1,000 xg for 15 minutes. The pellet was resuspended in infiltration medium [10 mM $MgCl_2$ (Sigma-Aldrich), 10 mM MES (Sigma-Aldrich) and 100 µM acetosyringone (Sigma-Aldrich)]. The centrifugation and washing steps were repeated three times to remove any residual antibiotic. The OD_{600nm} was measured using a 1:10 dilution of cells, and the final OD was obtained by multiplying by 10. The infiltration was performed using a culture absorbance of 0.3, and the volume needed was calculated using the formula $Initial\ volume = \frac{Final\ concentration * Final\ volume}{Initial\ concentration}$. Next, infiltration buffer was added to the estimated volume of cell suspension to a final volume of 1 mL and then transferred to a 1 mL syringe. The infiltration process involved pressing the syringe against the lower epidermis of the leaf and pressing down the plunger gently while holding the upper side of the leaf with a finger.

2.13.5. Confocal microscopy settings

The transiently transformed plants were examined using a Confocal Laser Scanning Microscope (CLSM, Leica SP5). Leaf portions were placed onto a slide with a drop of water, and the lower epidermis faced the coverslip. The green fluorescent protein (mNeonGreen) was detected within the short 505-530 nm wavelength range, assigning the green colour. An excitation wavelength of 507 nm was used.

2.14. Statistical analysis

The statistical analysis was performed using the program GraphPad Prism 8.0 (GraphPad Software Inc., USA), in which a one-way analysis of variance (One-way ANOVA), followed by Dunnett's multiple comparison tests, was used to assess the differences between the control situation and the results from the Fe and Ag treatments.

Results were considered significant when the *p*-value was lower than 0.05. RT-qPCR results analysis was first made in the Bio-Rad CFX Maestro 2.0 program before analysis with the GraphPad Prism 8.0 software.

All DNA and RNA quantification results, absorbances, and OD readings were performed in a DS-11 Spectrophotometer/Fluorometer (DeNovix).

Confocal Microscopy images were analysed and processed using the LAS X (Leica) software.

3. Results

3.1. *A. thaliana*'s growth viability test for heavy metal selection

To determine which HMs were to be used in this study, *A. thaliana*'s wild-type seeds were grown in 12.5 mg/L of three different heavy metals: Silver (Ag), Iron (Fe) and Cobalt (Co). Germination and growth rates were observed, ensuring that sufficient biomass could be harvested for biological samples for further testing. After 21 days post-germination, these plants were compared, and the results are shown in Figure 4 below.

Figure 4| Wild type *A. thaliana* plants when exposed to 12.5 mg/L of Silver (Ag^{+}), Iron (Fe^{2+}) and Cobalt (Co^{2+}) 21 days after germination, represented by the numbers 2, 3 and 4, respectively. The control situation is represented by the number 1.

Despite being able to germinate, *A. thaliana*'s wild-type seedlings exposed to Co were substantially more affected, in both shoot and root size, than the ones exposed to Fe and Ag. Additionally, leaves in these plants suffered high levels of chlorosis, as seen in Figure 4 – 4; therefore, the treatment with Co was excluded from this study.

Plants grown in Fe and Ag also differed from those grown in the control situation. However, they grew enough to extract biomass for the subsequent molecular and biochemical studies. This way Ag and Fe were selected for this study.

3.2. Biometric parameters in Fe and Ag treatments

Analysing the biometric parameters, specifically root size and total leaf area, it is possible to observe that increasing concentrations of Fe and Ag caused a significant impact in both organs.

Regarding root size, higher concentrations of Fe and Ag negatively impacted its growth and, thus, its size. As shown in Figure 5, both Fe (Figure 5 – A) and Ag (Figure 5 – B) treatments caused a significant decrease in root size for all tested concentrations. In the Fe treatments, a significant reduction of 26.1% occurred in the 3 mg/L treatment, 56.5% in the 6 mg/L and 90.8% in the 12.5 mg/L treatment. In the case of Ag treatments, roots had a significant reduction of 46.6% in the 6.1 mg/L treatment and 64.4% in the 25.6 mg/L treatment.

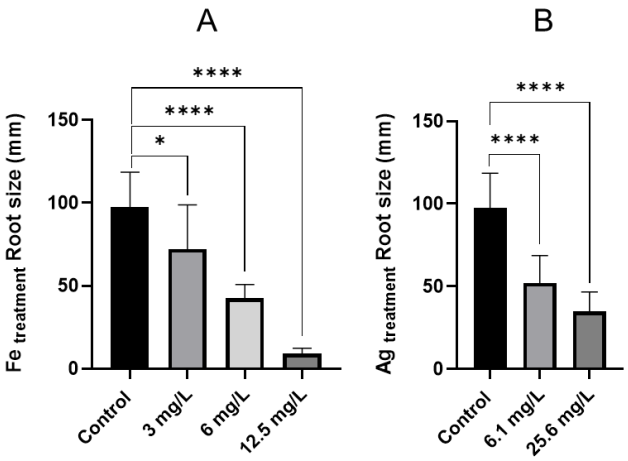

Figure 5| Biometric analysis of the effects of Fe and Ag in root size of *A. thaliana* with the increasing concentrations of Fe^{2+} (A): 3, 6 and 12. 5 mg/L; and Ag^{+} (B): 6.1 and 25.6 mg/L. Values presented are mean ± SD. The "*" on top of the connecting lines represent the significant differences from the control situation. * $p < 0.05$, ** $p < 0.01$, *** $p < 0.001$, **** $p < 0.0001$.

As for the shoots (Figure 6), exposure to Fe and Ag had similar effects to the ones observed in roots, in which a significant decrease can also be detected. However, treatment with Ag had a more substantial impact than Fe. Whereas the exposure to Fe only caused a significant reduction of 49% in the 12.5 mg/L treatment of the total leaf area (Figure 6 – A), treatment with Ag caused a significant reduction in all concentrations: 57.9% and 70.1% in the 6.1 mg/L and 25.6 mg/L treatments, respectively (Figure 6 – B).

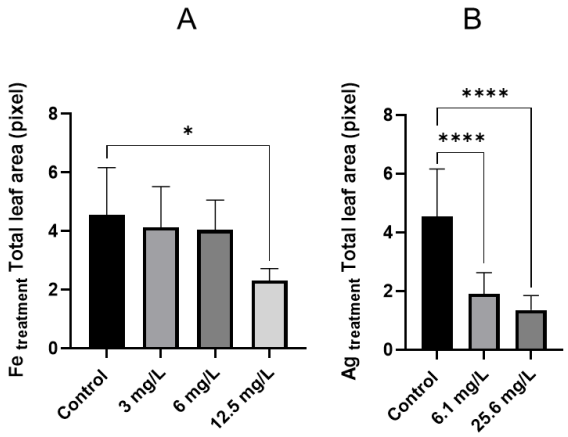

Figure 6| Biometric analysis of the effects of Fe and Ag in shoot size of *A. thaliana* with the increasing concentrations of Fe^{2+} (A): 3, 6 and 12. 5 mg/L; and Ag^{+} (B): 6.1 and 25.6 mg/L. Values presented are mean ± SD. The "*" on top of the connecting lines represent the significant differences from the control situation. * $p < 0.05$, ** $p < 0.01$, *** $p < 0.001$, **** $p < 0.0001$.

3.3. RNA quality assessment

Spectrophotometry analysis allowed the quantification of the RNA samples of Fe and Ag treatments and the quality assessment through the ratio between 260 nm and 280 nm readings. This would determine RNA purity when values fall between 1.50 and 2.00 for an acceptable purity degree (Supplementary Tables 1 and 2).

To verify the integrity and quality of RNA samples, gel electrophoresis was performed for both Ag and Fe treatments and thus to confirm the 2 bands corresponding to the subunits of the eukaryotic ribosomal RNA: the 28S and 18S, which was indicative of the RNA integrity.

3.4. Gene expression analysis for MTs under Fe and Ag treatments

*AtMT*s' gene expression was assessed by RT-qPCR. Exposure to Fe appears to have a small impact on MTs' expression. In the case of shoots, a significant decrease of 42.5% in *AtMT1c* expression occurred in the 3 mg/L treatment (Figure 7 – B), while a reduction of 52.1% in *AtMT2a* expression occurred in the in 6 mg/L, as it is observed in figure 7 - C. Although a higher relative expression can be verified in the 12.5 mg/L Fe treatment (indicative of a tendency to increase their expression), in every MT analysed, no statistical significance was detected for this treatment.

Regarding the analysis of MTs expressed in roots, it is possible to see some variation in their expression throughout every treatment and an increasing tendency in *AtMT3*'s expression, as seen in Figure 8 - E. However, no significant differences were found for any gene analysed (Figure 8).

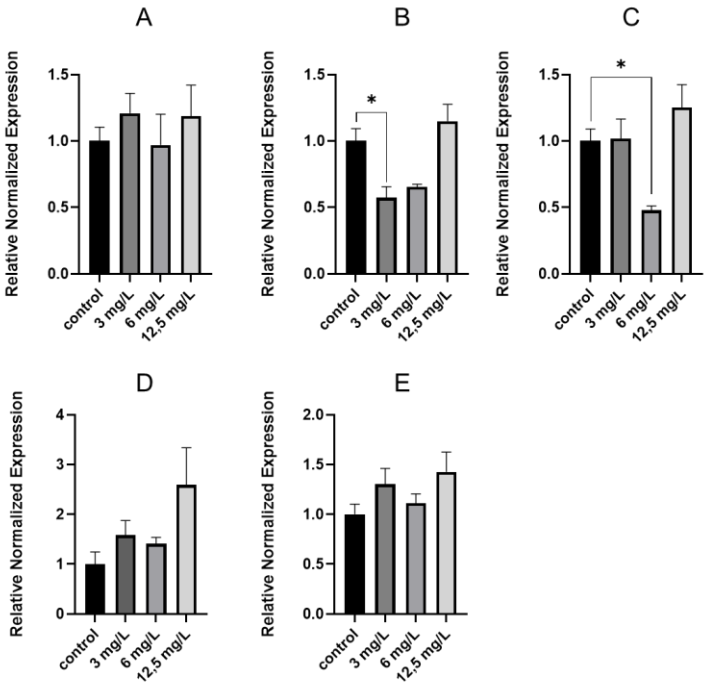

Figure 7| Relative normalised expression of the *AtMT1a* (A), *AtMT1c* (B), *AtMT2a* (C), *AtMT2*b (D), and *AtMT3* (E) in shoots of plants exposed to 3, 6 and 12.5 mg/L of Fe. The "*" on top of the connecting lines represent the significant differences from the control situation. * $p < 0.05$, ** $p < 0.01$, *** $p < 0.001$, **** $p < 0.0001$.

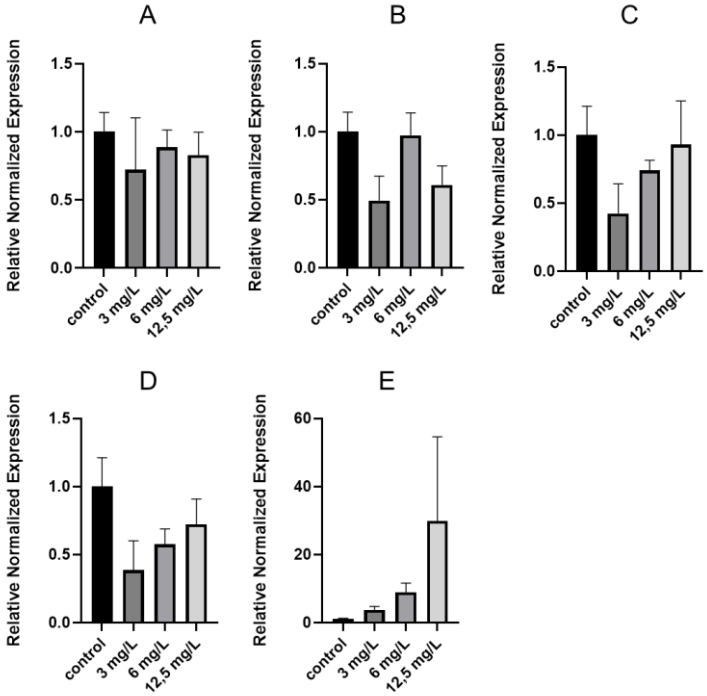

Figure 8| Relative normalised expression of the *AtMT1a* (A), *AtMT1c* (B), *AtMT2a* (C), *AtMT2b* (D), and *AtMT3* (E) in roots of plants exposed to 3, 6 and 12.5 mg/L of Fe. The "*" on top of the connecting lines

represent the significant differences from the control situation. * p < 0.05, ** p < 0.01, *** p < 0.001, **** p < 0.0001.

Unlike the treatment with Fe, exposure to Ag did have a significant impact on MTs' expression. When observing the expression of the MTs in shoots, a significant increase occurred for every MT analysed in the 25.6 mg/L Ag treatment (Figure 9) – 121.7% for *AtMT1a*, 84.3% for *AtMT1c*, 184% for *AtMT2a*, 226.7% for *AtMT2b* and 178.7% for *AtMT3*. Some minor variations can be seen between the control and the 6.1 mg/L situations for every MT; however, no significant differences were found.

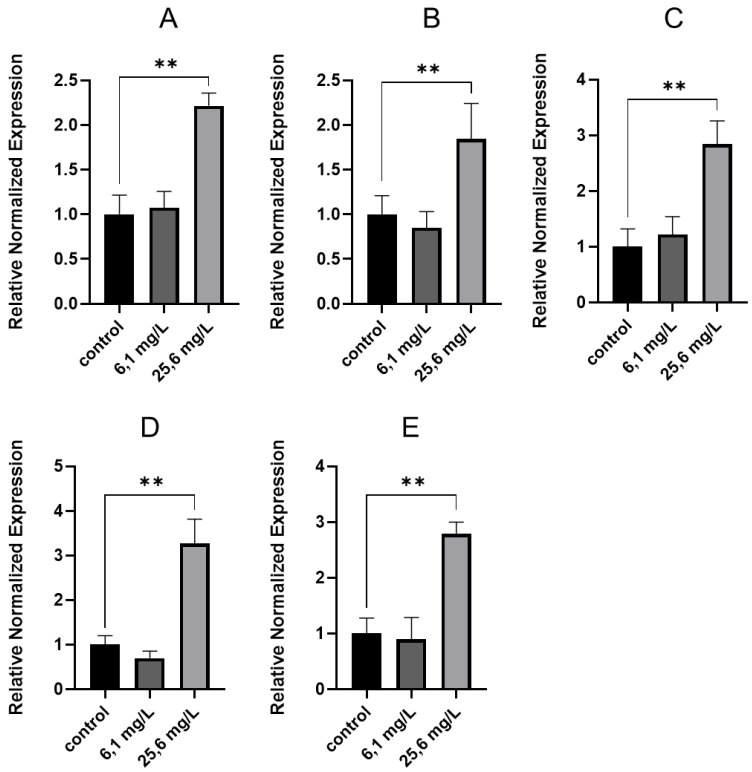

Figure 9| Relative normalized expression of the *AtMT1a* (A), *AtMT1c* (B), *AtMT2a* (C), *AtMT2b* (D), and *AtMT3* (E) in shoots of plants exposed to 6.1 and 25.6 mg/L of Ag. The "*" on top of the connecting lines represent the significant differences from the control situation. * p < 0.05, ** p < 0.01, *** p < 0.001, **** p < 0.0001.

In the case of the roots, type I MTs (*AtMT1a* and *AtMT1c*) seem to be the most affected when exposed to Ag (Figure 10 – A and B) since a significant increase in their expression also occurs with the highest concentration of Ag used in this study (25.6 mg/L). No significant differences were observed for the other MT types. However, an increasing tendency can be found in *AtMT2b* and *AtMT3*'s expressions (Figure 10 – D

and E) and a decreasing tendency of *AtMT2a* expression in the 25.6 mg/L treatment (Figure 10 – C).

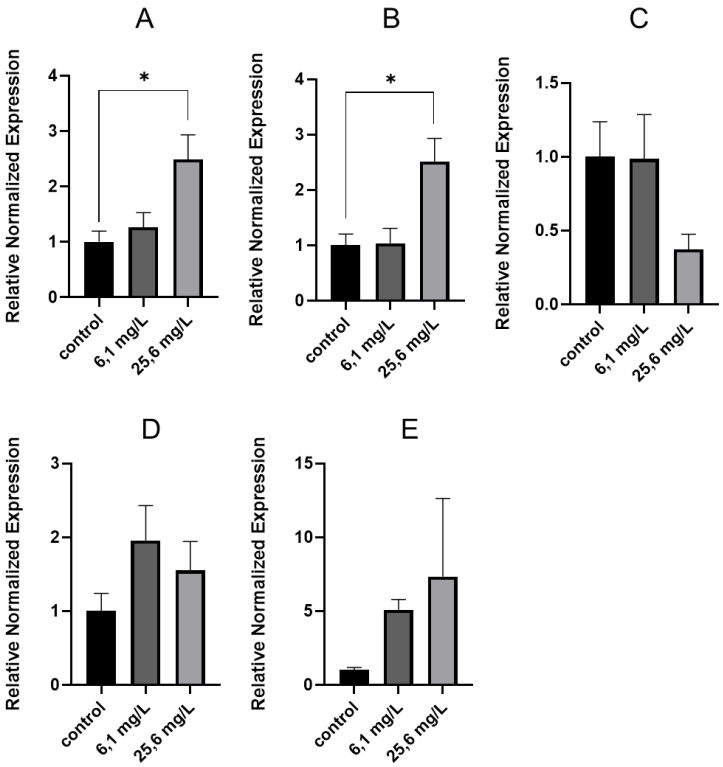

Figure 10| Relative expression of the *AtMT1a* (A), *AtMT1c* (B), *AtMT2a* (C), *AtMT2b* (D), and *AtMT3* (E) in roots of plants exposed to 6.1 and 25.6 mg/L of Ag. The "*" on top of the connecting lines represent the significant differences from the control situation. * $p < 0.05$, ** $p < 0.01$, *** $p < 0.001$, **** $p < 0.0001$.

AtMT1b analysis was excluded from this study since the results obtained in the RT-qPCR were inconsistent and, therefore, unsuitable for statistical analysis. This was also verified by previous work in the laboratory [136]. Additionally, no analysis was performed for MT type 4 A and B, as these types of MTs are mostly expressed in fruits and seeds [66], which were not addressed in this study.

Additionally, to ensure that the sample had no contamination and that the amplicons had the expected size, one triplicate of each biological sample was analysed by agarose gel electrophoresis, which validated these results. The NTC was also analysed to verify that the mixtures had no contamination (Figure 11).

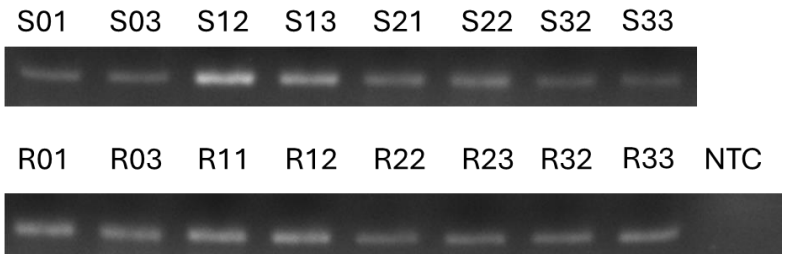

Figure 11| Example of a gel electrophoresis analysis of the RT-qPCR for *AtMT1c* shoot and root samples of the Fe treatment, using the cDNA from one of the technical replicates from each of the biological samples and NTC. Shoots: S01 and S03 – control; S12 and S13 – 3 mg/L Fe; S21 and S22 – 6 mg/L Fe; S32 and S33 – 12.5 mg/L Fe. Roots: R01 and R03 – control; R11 and R12 – 3 mg/L Fe; R22 and R23 – 6 mg/L Fe; R32 and R33 – 12.5 mg/L Fe.

3.5. Biochemical parameters

A biochemical study was conducted using shoots and roots to analyse the stress-induced effects of Fe and Ag in *A. thaliana* when exposed to increasing concentrations of these HMs individually. The results of each biochemical parameter evaluated are presented below.

3.5.1. Effects of the increasing concentration of Fe and Ag in lipid peroxidation

The concentration of MDA in both shoots and roots was measured to assess the level of lipid peroxidation due to the exposure to Iron (Fe) and Silver (Ag). Results are shown in Figure 12.

For both metals analysed, a significant increase in MDA was detected in the shoots at their highest concentration (27.7% in 12.5 mg/L Fe and 49.2% in 25.6 mg/L Ag), as we can see in Figure 12 – A and C. Whereas in roots, a significant effect could only be observed when plants were exposed to Ag (Figure 12 – D). Interestingly, in roots, as opposed to the situation in the shoots, MDA levels dropped in the lowest (58.6%) and highest (46.3%) concentrations of Ag utilised in this study. However, MDA concentration was slightly higher at 25.6 mg/L than at 6 mg/L. No significant changes were verified in roots when exposed to Fe despite its apparent tendency to increase (Figure 12 – B).

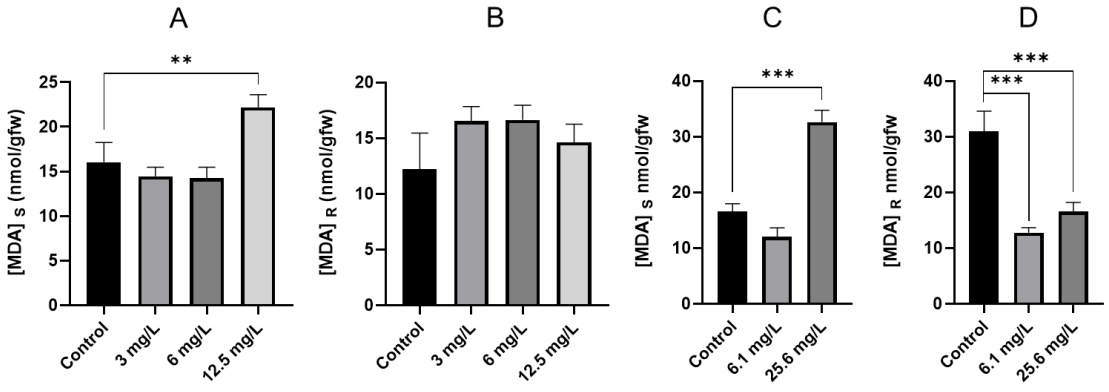

Figure 12| MDA levels in Shoots (S) and Roots (R) of *A. thaliana* exposed to increasing concentrations of Fe^{2+} (A and B): 3, 6 and 12. 5 mg/L; and Ag^{+} (C and D): 6.1 and 25.6 mg/L. Values presented are mean ± SD. The "*" on top of the connecting lines represent the significant differences from the control situation. * $p < 0.05$, ** $p < 0.01$, *** $p < 0.001$, **** $p < 0.0001$.

3.5.2. Effects of the increasing concentration of Fe and Ag in the H_2O_2 levels

When exposed to Fe, H_2O_2 levels had no significant changes in shoots and roots (Figure 13 – A and B). However, it is possible to observe a tendency to increase in both organs despite the smaller value detected in roots in the latter Fe treatment.

In the presence of Ag, the results reveal a significant effect in both organs. In shoots, the amount of H_2O_2 had a significant increase of 62.3% with the highest concentration of Ag (Figure 13 – C), whereas in the roots, it drops significantly, although gradually, to a total of 66.5% registered in the highest Ag concentration used (Figure 13 – D).

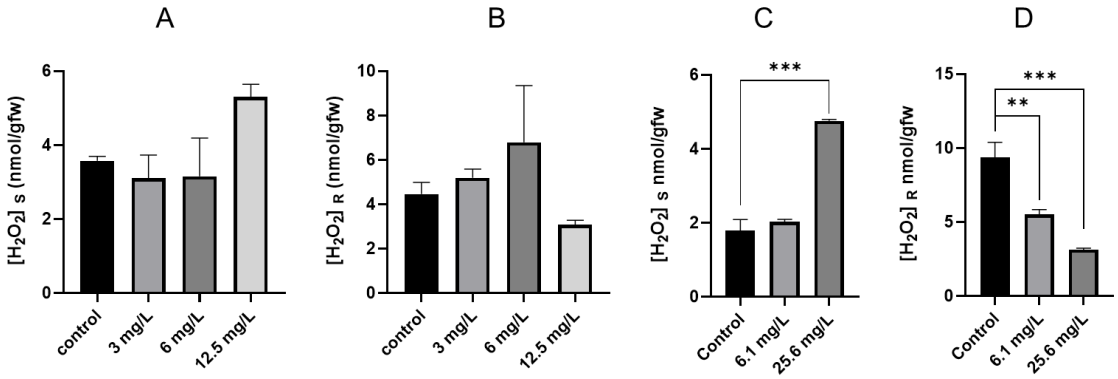

Figure 13| H_2O_2 levels in Shoots (S) and Roots (R) of *A. thaliana* with the increasing concentrations of Fe^{2+} (A and B): 3, 6 and 12. 5 mg/L; and Ag^{+} (C and D): 6.1 and 25.6 mg/L. Values presented are mean ± SD. The "*" on top of the connecting lines represent the significant differences from the control situation. * $p < 0.05$, ** $p < 0.01$, *** $p < 0.001$, **** $p < 0.0001$.

3.5.3. Effects of the increasing concentration of Fe and Ag in the proline levels

The levels of Proline measured significantly changed when exposed to either Fe or Ag, as seen in Figure 14.

Fe exposure generally decreased Proline accumulation in both organs (Figure 14– A and B). In shoots, a significant decrease occurs in the 6 mg/L and 12.5 mg/L Fe treatments (63.7% and 63.4%, respectively), whereas in roots, the highest decrease (48.8%) was detected in the first treatment, with the lowest Fe concentration (3 mg/L). In the 6 and 12.5 mg/L Fe treatment, a slight recovery in proline levels was detected for this organ.

As for the exposure to Ag, a significant increase in proline levels, to a maximum of 36.4%, is detected in shoots as the concentration of Ag increases - detected in the treatment with the highest Ag concentration (Figure 14 – C). However, no significant alteration was observed in roots despite a slight tendency to increase, as shown in Figure 14 – D.

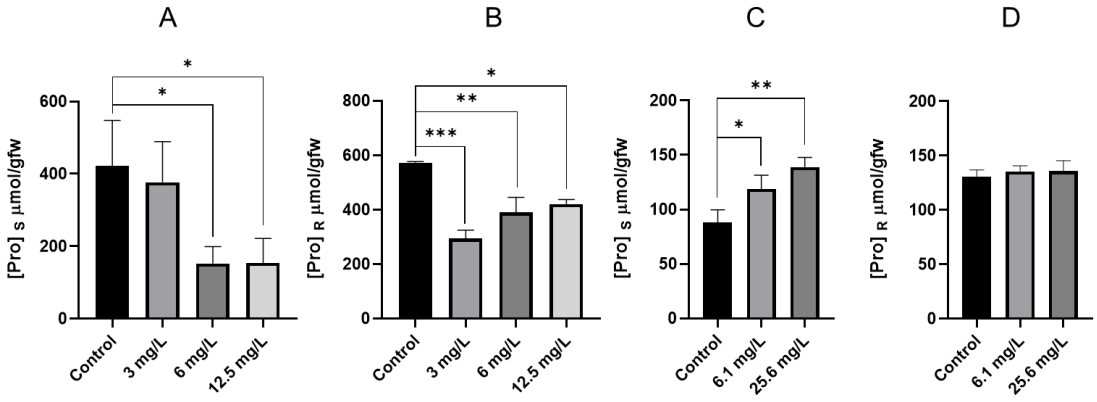

Figure 14 | Proline (Pro) levels in Shoots (S) and Roots (R) of *A. thaliana* with the increasing concentrations of Fe^{2+} (A and B): 3, 6 and 12. 5 mg/L; and Ag^{+} (C and D): 6.1 and 25.6 mg/L. Values presented are mean ± SD. The "*" on top of the connecting lines represent the significant differences from the control situation. * $p < 0.05$, ** $p < 0.01$, *** $p < 0.001$, **** $p < 0.0001$.

3.5.4. Effects of the increasing concentration of Fe and Ag in reduced glutathione levels

The measurement of Reduced Glutathione (GSH) levels revealed significant results in both Fe and Ag treatments, as presented in Figure 15.

In shoots and roots, the presence of Fe positively influenced the concentration of GSH, as an increase of 33.8% for shoots and 46.6% for roots was detected in the 12.5 mg/L Fe treatment, despite more statistically significant in roots (Figure 15 – A and B).

The influence of Ag primarily affected shoots, generating a significant increase of 49.8% in GSH levels in the 25.6 mg/L Ag treatment, as shown in Figure 15 – C. No significant changes were verified in roots (Figure 14 – D).

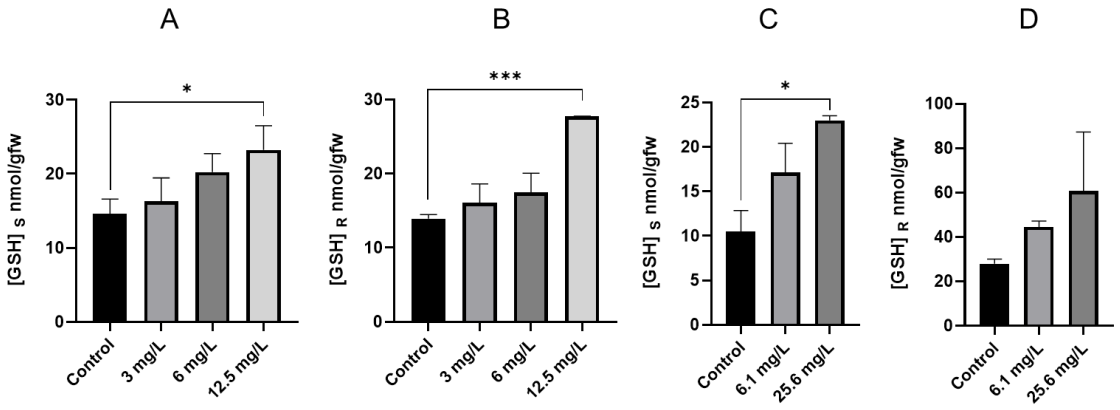

Figure 15| Reduced Glutathione (GSH) levels in Shoots (S) and Roots (R) of *A. thaliana* with the increasing concentrations of Fe^{2+} (A and B): 3, 6 and 12. 5 mg/L; and Ag^{+} (C and D): 6.1 and 25.6 mg/L. Values presented are mean ± SD. The "*" on top of the connecting lines represent the significant differences from the control situation. * $p < 0.05$, ** $p < 0.01$, *** $p < 0.001$, **** $p < 0.0001$.

3.5.5. Effects of the increasing concentration of Fe and Ag in the total thiols, non-protein thiols and protein thiols levels

Total thiols (TT), non-protein thiols (NPT) and protein thiols (PT) levels revealed statistically significant changes in both shoots and roots when exposed to Fe (Figure 16).

In the shoots, TT, NPT and PT increased with the 12.5 mg/L treatment in response to the presence of Fe, as can be seen in Figure 16 – A, B and C (34.5%, 46.8% and 31.5%, respectively). In roots, an increase in the latter treatment also occurs - 18.6% for TT and 23.1% for PT. On the other hand, NPT levels decrease significantly (36.8%) with the lowest treatment of Fe (Figure 16 – E).

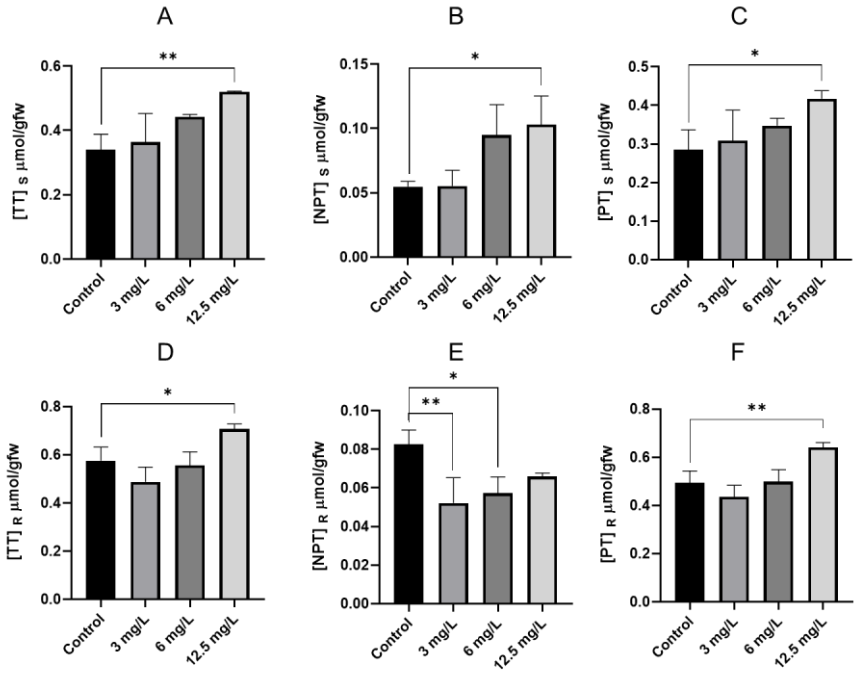

Figure 16| Total thiols (TT), Non-protein thiols (NPT) and Protein thiols (PT) levels in Shoots (A - C) and Roots (D - F) of A. thaliana with the increasing concentrations of Fe^{2+}: 3, 6 and 12. 5 mg/L. Values presented are mean ± SD. The "*" on top of the connecting lines represent the significant differences from the control situation. * $p < 0.05$, ** $p < 0.01$, *** $p < 0.001$, **** $p < 0.0001$.

Exposure to Ag only affected shoots' TT and PT, causing a significant increase (27.2% and 28.4%, respectively) in the highest Ag concentration treatment (Figure 17 – A and C). No significant changes occurred in the roots (Figure 17 – D, E and F).

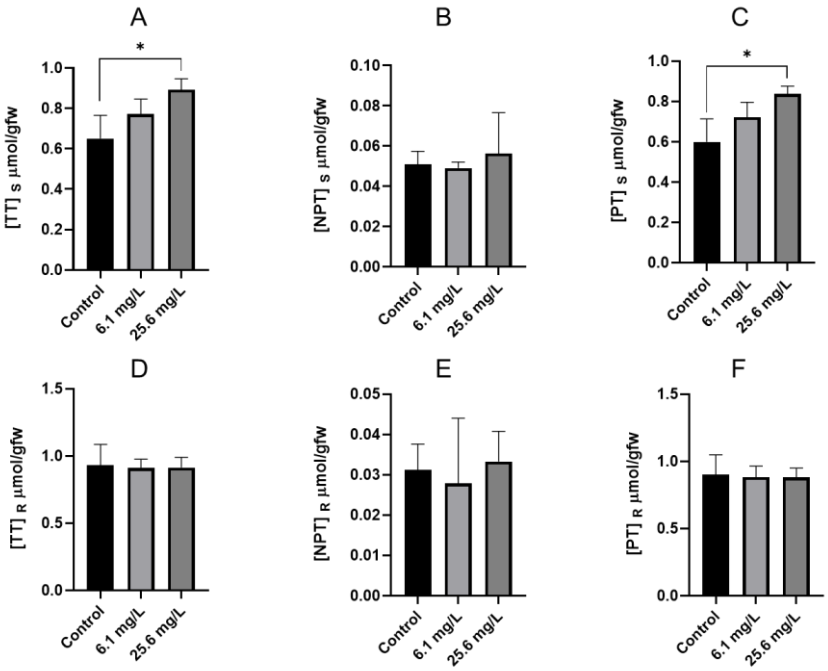

Figure 17| Total thiols (TT), Non-protein thiols (NPT) and Protein thiols (PT) levels in Shoots (A - C) and Roots (D - F) of A. thaliana with the increasing concentrations of Ag^{+}: 6.1 and 25.6 mg/L. Values presented are mean ± SD. The "*" on top of the connecting lines represent the significant differences from the control situation. * p < 0.05, ** p < 0.01, *** p < 0.001, **** p < 0.0001.

3.5.6. Effects of the increasing concentrations of Fe and Ag in the photosynthetic pigment's levels

The presence of Fe negatively impacted the levels of photosynthetic pigments, as observed in Figure 18.

Both chlorophyll a (Chla) and b (Chlb) significantly decreased by 46.5% and 44.5%, respectively, in the treatment with 6 mg/L Fe concentration (Figure 18 – A and B). Despite an increased value of their concentration registered in the 12.5 mg/L Fe treatment, no statistical significance was observed. However, a general decrease in these photosynthetic pigments can be verified.

B-Carotenes (β-Car), on the other hand, show a significant decrease in all treatments – 44.9% at 3 mg/L Fe, 57.8% at 6 mg/L Fe and 40.4% at 12.5 mg/L Fe - (Figure 18 – C). It is also possible to see a slight recovery in the 12.5 mg/L Fe treatment. However, a general decrease can be verified compared to the control situation.

No significant changes were observed in Lutein (Lut) levels, as shown in Figure 18– D.

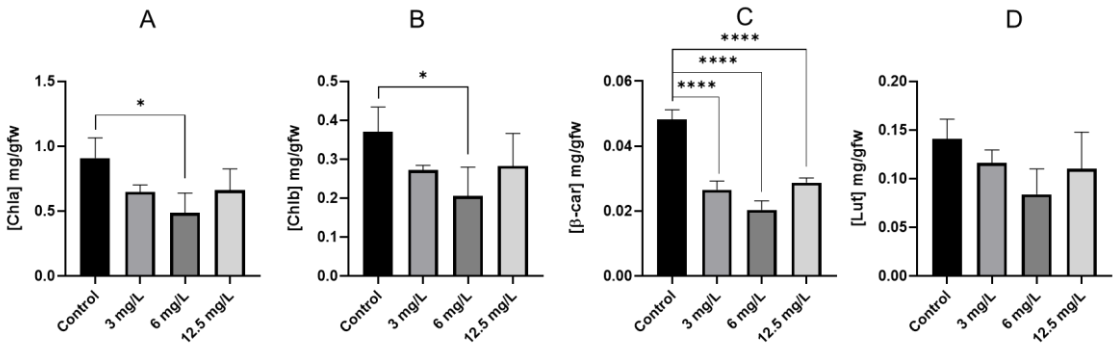

Figure 18| Chlorophyll A (A), Chlorophyll B (B), β – Carotenes (C) and Lutein (D) levels in Shoots of *A. thaliana* with the increasing concentrations of Fe^{2+}: 3, 6 and 12.5 mg/L. Values presented are mean ± SD. The "*" on top of the connecting lines represent the significant differences from the control situation. * p < 0.05, ** p < 0.01, *** p < 0.001, **** p < 0.0001.

Similar to Fe, Ag negatively impacted photosynthetic pigments, although with some slight differences (Figure 19).

Regarding Chlorophyll A and B, a significant decrease of 34.1% and 31.4% was detected in the 6.1 mg/L Ag treatment (Figure 19 – A and B). However, unlike the results

with the Fe treatment, a statistically significant decrease in the highest Ag concentration could also be detected (25.3% for Chla and 29.8% for Chlb).

Like Chlorophyll a and b, Lut levels have also significantly decreased in every Ag treatment– 27.5% for 6.1 mg/L Ag and 26.6% for 25.6% (Figure 19 – D).

Unlike the Fe treatment, ß-Carotenes were not affected with the same intensity. However, a significant decrease of 36.2% in their levels was observed in the 6.1 mg/L Ag treatment (Figure 19 – C).

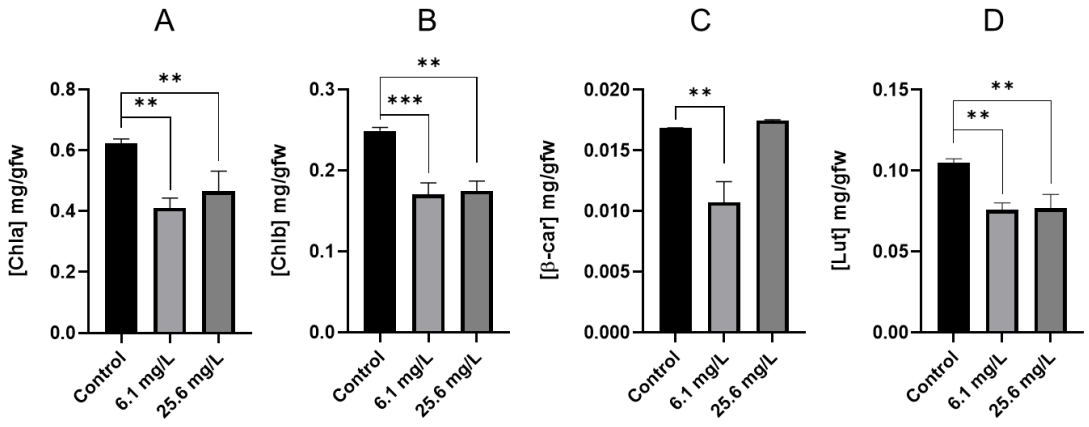

Figure 19| Chlorophyll a (A), Chlorophyll b (B), β – Carotenes (C) and Lutein (D) levels in Shoots of A. thaliana with the increasing concentrations of Ag^{+}: 6.1 and 25.6 mg/L. Values presented are mean ± SD. The "*" on top of the connecting lines represent the significant differences from the control situation. * $p < 0.05$, ** $p < 0.01$, *** $p < 0.001$, **** $p < 0.0001$.

3.6. Iron and silver bioaccumulation

In shoots, Fe accumulation significantly increased in all treatments, although gradually (Figure 20 – A). The highest accumulation registered (67.6%) was detected in the 12.5 mg/L treatment.

The same trend was observed in roots (Figure 20 – B) but in higher levels (approximately 1.2-fold), where a significant increase of 81.2% was registered in the 12.5 mg/L treatment.

Bioaccumulation of Ag in roots also increased significantly with the increase of concentration within each treatment – 52.4% in the 6.1 mg/L Ag and 65.1% in the 25.6 mg/L Ag (Figure 20 – D). However, in shoots, a statistically significant increase was only detected in the higher concentration treatment (65.9%), as shown in Figure 20 – C.

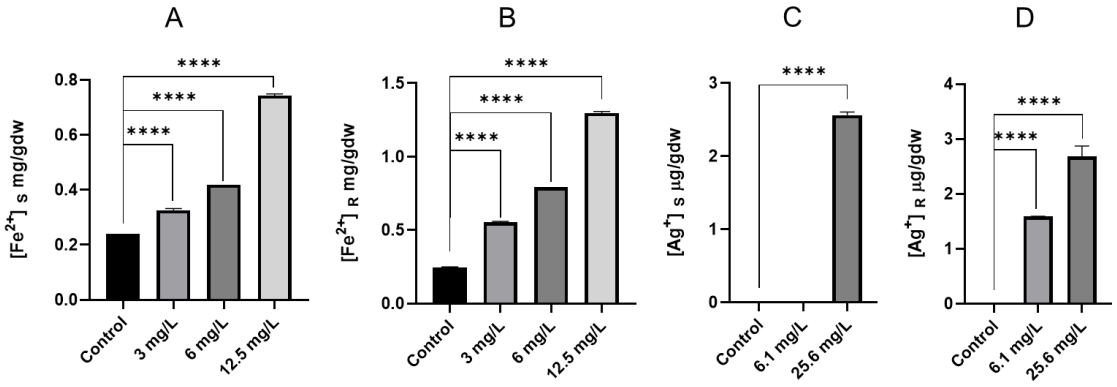

Figure 20| Bioaccumulation of Fe and Ag in Shoots (S) and Roots (R) of *A. thaliana* with the increasing concentrations of Fe^{2+} (A and B): 3, 6 and 12. 5 mg/L; and Ag^{+} (C and D): 6.1 and 25.6 mg/L. Values presented are mean ± SD. The "*" on top of the connecting lines represent the significant differences from the control situation. * $p < 0.05$, ** $p < 0.01$, *** $p < 0.001$, **** $p < 0.0001$.

3.7. *In vivo* assessment of vacuolar targeting of *A. thaliana*'s MTs

3.7.1. Cloning of *AtMT2b* and *AtMT1a* genes.

The first step was to effectively clone the full-length cDNAs of *A. thaliana* MTs chosen for this study: *AtMT1a* and *AtMT2b*.

Because these cDNAs are relatively small (200 bp and 250 bp, respectively), several strategies were attempted to clone these genes in the pSK vector successfully. However, only *AtMT2b* cloning was successful (Figure 21 - A).

In the case of *AtMT1a*, successful integration in the pSK plasmid was never verified, even though different strategies were applied, and several attempts were made. As such, a different approach involving a cloning kit was used for this cDNA: the full-length cDNA was integrated into a pMiniT 2.0 plasmid. This plasmid holds a toxic minigene under the control of a constitutive promoter that triggers in the case of pMiniT2.0 re-circularisation without an insert. This causes a lethal inhibition of protein synthesis, preventing colony growth. In the end, cloning of the *AtMT1a* cDNA was achieved using this vector, as seen in Figure 21 - B. However, due to time constraints and this method being used as a last resort, it was not possible to follow up on the experiments with pMiniT2.0-*AtMT1a* in the framework of this work.

After confirming that both genes were successfully integrated into the respective vector, the constructs were sent to sequencing to ensure no errors were found in the final DNA construction.

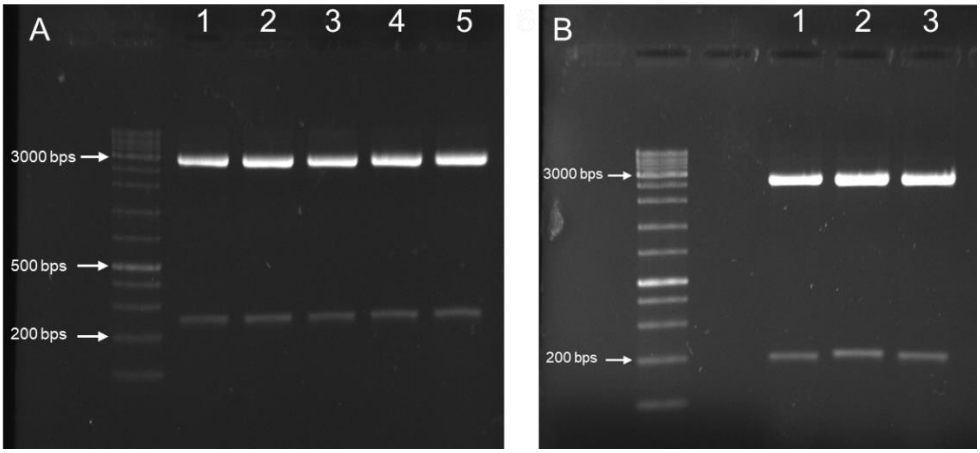

Figure 21| Electrophoresis of the products of the restriction reaction of pSK-MT2bΩ (A) and pMiniT2.0-MT1a (B) with *Xba*I and *Sal*I, in a 1% agarose gel to confirm the correct insertion of the *AtMT2b*Ω, and *AtMT1a* inserts in the respective vector backbone.

3.7.2. Cloning of *AtMT2b* with a vacuolar sorting signal

For this study, the PSI domain of the cardosin A aspartic proteinase, responsible for its targeting to the vacuole, was fused in the middle of the *AtMT2b* gene sequence. This would be necessary to attempt the vacuolar targeting of this *A. thaliana* MT. Moreover, a hexa histidine-tag (also known as 6xHis-Tag) was also added to allow future pull-down assays. A Gibson Assembly was performed to ensure all these sequences were inserted in frame.

After bacterial transformation, a screening for positive colonies was performed by plasmid miniprep restriction (Figure 22), followed by DNA sequencing. One positive clone was then selected for ligation to the pMDC83 plasmid.

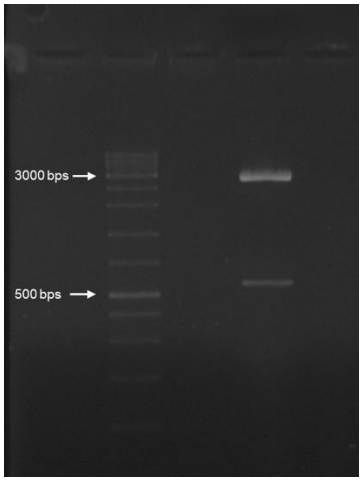

Figure 22| Electrophoresis of the products of the restriction reaction of pSK-MT2bΩ-PSIA-His6x-Tag, with *Xba*I and *Sal*I, restriction enzymes, in a 1% (w/v) agarose gel to confirm the correct insertion of the MT2bΩ-PSIA-His6x-Tag insert in the respective vector backbone.

3.7.3. Construction of plant-expression binary vectors

The final step of this study was to obtain a construct that would allow the visualisation of the AtMT2b in *N. tabacum* cells by its fusion with a fluorescent protein - mNeonGreen.

As such, two constructs were obtained: pMDC83-MT2bΩ-PSIA-6xHis-Tag-mNeonGreen and pMDC83-MT2bΩ-mNeonGreen. Both constructs were inserted in chemically competent TOP10 *E. coli* strain cells. The resulting colonies were screened by enzymatic restriction of purified plasmids with *Xba*I and *Sal*I (Figure 23), and the DNA was sequenced.

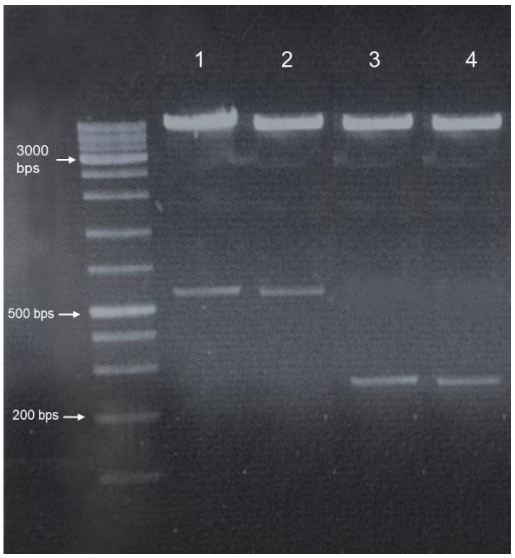

Figure 23| Electrophoresis of the products of the restriction reaction of pMDC83-MT2bΩ-PSIA-His6x-Tag (1 and 2), and pMDC83-MT2bΩ (3 and 4) with *Xba*I and *Sal*I, restriction enzymes, in a 1% (w/v) agarose gel to confirm the correct insertion of the MT2bΩ-PSIA-His6x-Tag insert in the respective vector backbone.

3.7.4. Expression of *AtMT2b* and PSI A-mediated AtMT2b vacuole targeting in *N. tabacum* plants.

Heterologous expression of the PSI A-mediated *AtMT2b* and *AtMT2b* alone, fused with mNeonGreen fluorescence protein, allowed the localisation of these fusion proteins in the cell.

Localisation analysis of the AtMT2b-mNeonGreen was performed first, and results revealed that AtMT2b is present in the cytoplasm (Figure 25). This MT was also found inside the nucleus, confirmed by the clear view of the nucleolus surrounded by green fluorescence (Figure 24 – A, red arrow). Furthermore, some subcellular

accumulations of AtMT2b can also be found in the cell periphery (Figure 24 – B). However, it was not possible to determine the exact nature of these accumulations.

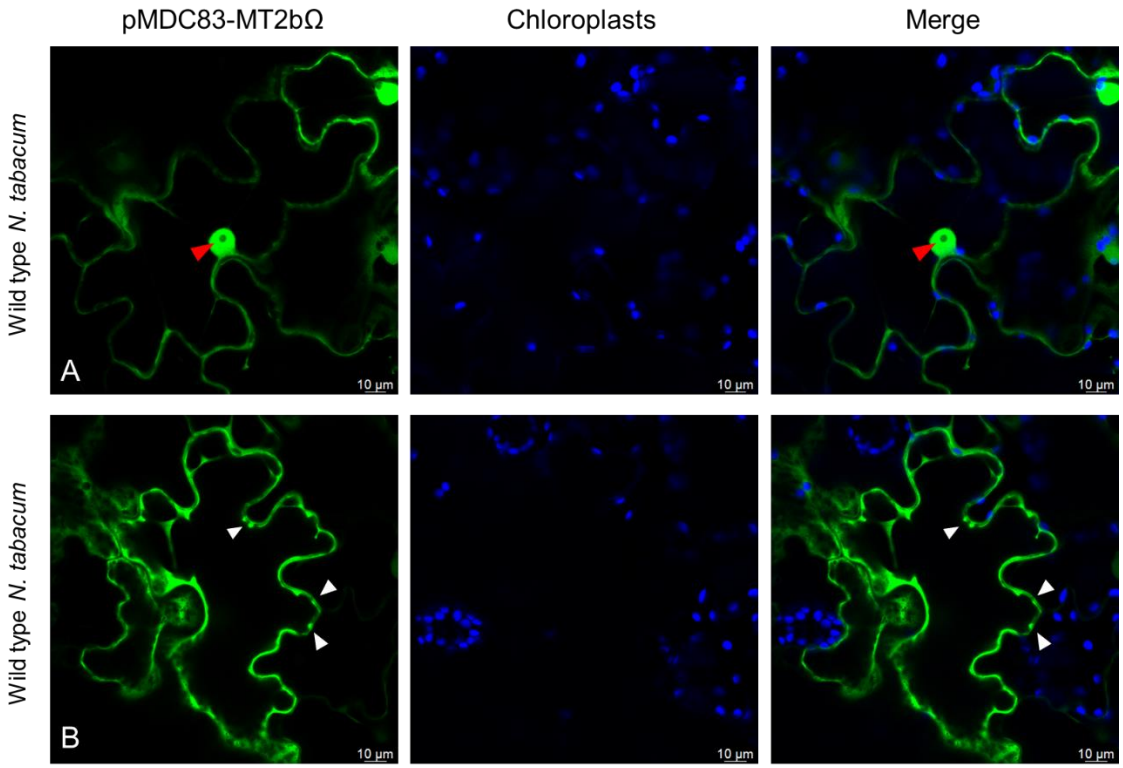

Figure 24| Subcellular localisation of *A. thaliana* type 2 metallothionein (AtMT2b) fused with mNeonGreen in leaves of wild type *N. tabacum*. Both A and B represent examples of the localization of AtMT2b-mNeonGreen found in the same sample. Cytosolic accumulation can be seen in A and B, represented by the green fluorescence lines. The red arrow indicates the accumulation of AtMT2b inside the nucleus; the white arrows indicate the subcellular accumulations. All images were obtained 3 days post-infiltration. The analysis and processing were performed using LAS X (Leica) software. Scale bar: 10 µm.

Regarding the PSI A-AtMT2b, confocal microscopy imaging results showed no accumulation of this MT in the vacuole. Instead, like for the AtMT2b alone, a major cytosolic presence was also found (Figure 25). Protein accumulation in aggregates was also observed (Figure 25, white arrows). The presence of PSI A-AtMT2b inside the nucleus is less evident than AtMT2b alone, but it can still be detected in some cases (Figure 25 – A, red arrow).

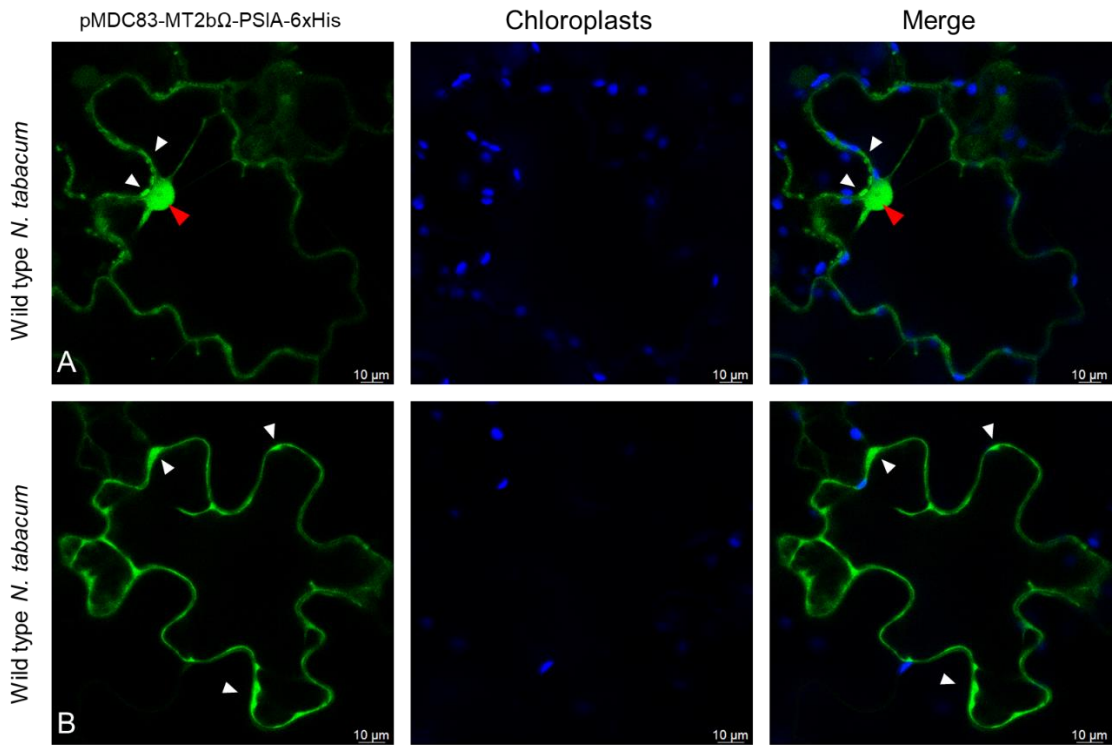

Figure 25| Subcellular localisation of cardosin A PSI + *A. thaliana* type 2 metallothionein (AtMT2b), fused with mNeonGreen in leaves of wild type *N. tabacum*. Both A and B represent examples of the accumulation of PSI A-AtMT2b-mNeonGreen found in the same sample. Cytosolic accumulation can be seen in A and B, represented by the green fluorescence lines. The red arrow indicates the accumulation of PSI A + AtMT2b inside the nucleus; the white arrows indicate the subcellular accumulation. All images were obtained 3 days post-infiltration. The analysis and processing were performed using LAS X (Leica) software. Scale bar: 10 µm.

For both cases, images regarding the chloroplast's autofluorescence and a merged image of both chloroplasts and the mNeonGreen signal were also presented to clearly distinguish subcellular accumulation from a possible chloroplast location.

3.8. *A. thaliana* MT1a and MT2b mutants genotyping

Searching for AtMT1a and AtMT2b mutants was included in this work as a complementary study to understand "how" and "if" the lack of expression of these MTs would affect not only the expression of other metallothionein-encoding genes, but also other physiological adaptations derived from the attempt of the plants to cope with the increasing concentrations of either Fe or Ag.

Several plants were genotyped during this study to isolate homozygous plants for the T-DNA insertion in both MT-type genes. However, despite the efforts, most of the plants (about 2/3) were found to be heterozygous for this insertion, and a small amount

(1/3) wild-type plant. Figures 26 and 27 showcase examples of some genotyping results for *AtMT1a* and *AtMT2b*.

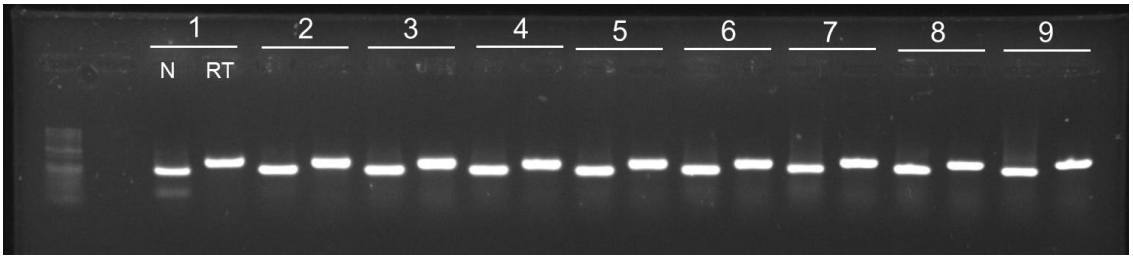

Figure 26| Electrophoresis of the products from *A. thaliana* plants genotyping for the presence of T-DNA mutants in MT type 1a (*AtMT1a*) gene in agarose gel 1% (w/v). Plant samples are represented by 1-9. N – specific pair of primers, forward (Fw) and reverse (Rev), for *AtMT1a*; RT – primer Rev for *AtMT1a* and specific primer for T-DNA. In this case, all plant samples are heterozygous since both wild-type and mutant *AtMT1a* genes are detected.

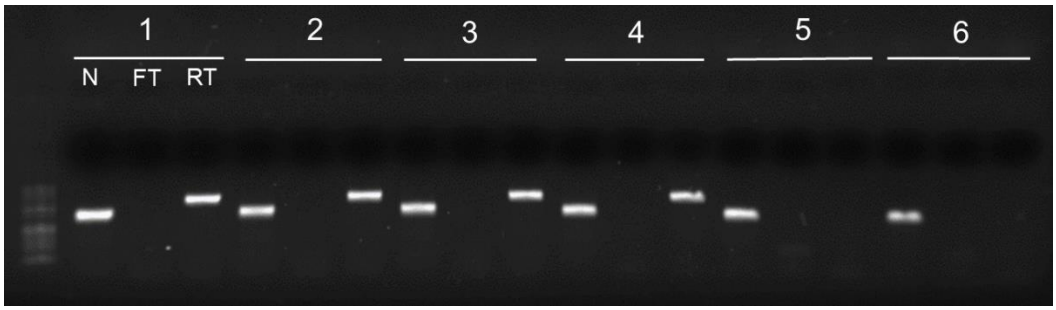

Figure 27| Electrophoresis of the products from *A. thaliana* plants genotyping for the presence of T-DNA mutants in MT type 2b (*AtMT2b*) gene in agarose gel 1% (w/v). Plant samples are represented by 1-6. N – specific pair of primers, forward (Fw) and reverse (Rev), for *AtMT2b*; FT – primer Fw of *AtMT2b* and specific primer for T-Dna; RT – primer Rev for *AtMt2b* and specific primer for T-DNA. 1-4 are heterozygotes since both normal and mutant *AtMT2b* genes are detected. 5 and 6 are wild-type since only the normal *AtMT2b* gene is detected.

4. Discussion

4.1. *A. thaliana* response to Fe and Ag stress

Nowadays, plant's exposure to HMs has become an overwhelming concern. The persistence of these compounds poses a danger at many levels, not only to the environment and the many ecosystems but also to humans and other animals, as their subsequent accumulation throughout the food chain can lead to severe health decreases. Iron (Fe) and Silver (Ag) are among them, and despite their difference in utility for the plant (essential and non-essential, respectively), both are known to induce nefarious effects when in high concentrations. In this study, a biochemical approach was conducted to understand the impacts of these HM in plants to either know how to prevent them or find ways to optimise how plants cope with them. Moreover, an insight into the expression of MT-encoding genes under Fe and Ag exposure was also performed.

For this, *A. thaliana* plants were used as test subjects to assess the effects of increasing concentrations of Fe and Ag in separate treatments, analysing several stress indicators: H_2O_2, malondialdehyde, chlorophylls a and b, ß-carotenes, lutein, reduced glutathione, non-protein and protein thiols and proline. The bioaccumulation of these metals in both roots and shoots was also determined. The concentrations chosen were 3, 6 and 12.5 mg/L for Fe and 6.1 and 25.6 mg/L for Ag.

4.1.1. Bioaccumulation of Fe and Ag

Regarding the bioaccumulation of Fe and Ag in *A. thaliana*'s shoots and roots, results have shown different responses from the plant for both HM.

In the case of Fe, a significant increase in accumulation was found in both organs following the increasing supply of Fe. This would be expected in the roots, as they primarily absorb Fe. In the shoots, the same pattern occurred; however, it is possible to observe that more Fe is accumulated in the roots. According to the literature, in normal conditions, shoots tend to accumulate roughly 80% more Fe than the roots [143]. This is consensual because Fe plays an essential role in the photosynthetic apparatus. Not only is it responsible for pigment metabolism, but it is also necessary for chloroplast ultrastructure [24, 144]. However, because roots are accumulating more Fe than shoots as the experimental concentrations increase, this might be indicative of a protective roll on their part to prevent high levels of Fe toxicity in the remaining parts of the plant.

As for the treatment with Ag, the presence of this HM in both organs occurred differently. Like Fe, the accumulation of Ag by the roots is directly related to its increasing supply, meaning that more Ag is accumulated when its concentration in the nutrient

media increases. Once again, this would be expected in the roots, and it can be verified by the significant rise detected in both Ag concentrations used: 6.1 mg/L and 25.6 mg/L. However, shoots only seem to accumulate significant amounts of Ag with the highest concentration, suggesting that it might be retained in the roots, preventing its translocation to the aerial part of the plant. Like in the case of Fe treatment, roots also seem to act as a protective shield for shoots, however more intensely. The apparent absence of Ag in the shoots in the lowest concentration (6.1 mg/L) and the sudden accumulation increase in the highest Ag concentration used in this study (25.6 mg/L) suggest this. Thus, when Ag concentrations are too high, roots can no longer retain it, and, as a result, Ag is transported to shoots in higher amounts.

4.1.2. Biometric analysis of the effects of Ag and Fe excess

The results revealed that both Fe and Ag significantly reduce not only the size of the root but the leaf area as well. In the case of iron, root size significantly decreases in all experimental situations. As for the shoot area, the most impactful change was detected in the highest concentration of Fe used (12.5 mg/L). In the case of Ag, all experimental situations lead to a significant decrease in root size and shoot area.

Toxicity by HM is known to have severe implications on plant growth and development, mainly due to the oxidative stress they cause [145]. One of the main reasons is that it can disturb the normal function of photosystem II by compromising chlorophyll production by excessive ROS presence [146, 147]. This, in turn, reduces the efficiency of the photosynthetic apparatus – the primary source of carbon fixation – and thus compromises the overall plant's growth. As such, it is plausible to suggest that a disturbance in the photosystem is the motif behind the overall growth impairment observed during Fe and Ag toxicity. Moreover, considering the roots, exposure to HM had additional effects. Previous work performed by Li et al., 2015 in *A. thaliana* showed that ferrous toxicity can inhibit the cell division and elongation of the primary root but, on the contrary, stimulates lateral root formation [148] Similar results were obtained in this study, reinforcing the idea that Fe toxicity not only affects plant growth in general but also has a major impact in root morphology. Excess Ag, on the other hand, did not affect the main root as severely as iron; however, a reduction in its elongation could also be observed. These results are in accordance with those obtained by Haifeng et al., 2013 who also showed that Ag^{+} caused a significant inhibition of root elongation in a dose-dependent manner [51].

4.1.2. Photosynthetic pigments analysis

Photosynthetic pigments, such as chlorophyll and carotenoids, are essential elements of plants, as they are involved in the photosynthetic machinery – an important function that allows plants to produce chemical compounds necessary for their development [149]. Heavy metals are known to disturb the photosynthetic apparatus [19], so the impact of increasing concentrations of Fe and Ag was assessed.

Increasing concentrations of both HMs induced a general decrease in photosynthetic pigments. Regarding Fe, β – carotenes were the most affected, showing a significant reduction in their levels in all Fe concentrations. Additionally, chlorophylls also significantly decreased when exposed to 6 mg/L. Despite this, statistically significant results were only found in the cases mentioned above, where increasing concentrations of Fe caused a general decrease in all photosynthetic pigments analysed. It has been demonstrated previously that chlorophyll concentration is affected by the supply of excess Fe, revealing a reduction in chlorophylls a and b [150]. Some cases include the reduction of chlorophyll content in rice [151] and pea seedlings [152]. Carotenoids, like β – carotenes and lutein, are known to be synthesised in plastids such as chloroplasts [153]. Excess of Fe potentiates the disruption of normal chloroplast function [152] , which blocks carotenoid and chlorophyll production. Comparing these results with the literature, there seems to be a correlation that further suggests the role of Fe toxicity in disrupting the photosynthetic apparatus. In addition, carotenoids are known to be powerful antioxidants, and the significant reduction in their content might correlate with them being used to counteract Fe-induced oxidative stress [153].

As for Ag, chlorophylls a and b and lutein concentrations decreased significantly in all Ag concentrations tested. On the other hand, β – carotenes appear to have only suffered mainly in the 6 mg/L Ag treatment. This indicates that Ag also has a negative impact on the photosynthetic machinery, as is usually the case with HM toxicity.

Moreover, the reduction in these photosynthetic pigments undoubtedly contributed to the overall growth impairment in the plants under Fe or Ag treatment, similar to other case studies [51, 154].

4.1.3. Ag and Fe oxidative stress evaluation

4.1.3.1. H_2O_2

Starting with the levels of H_2O_2, Fe and Ag exposure showed different results. For Fe, no significant results were found for both shoots and roots. However, it is possible to observe a tendency to increase in both organs despite not being significant. From this, it

is possible to see a correlation between these results and those observed in the bioaccumulation of Fe in the plant. Except in the highest concentration treatment (12.5 mg/L), despite not being statistically significant, lower levels of H_2O_2 in the roots were detected when Fe accumulation was at its highest. Fe excess can induce ROS activity, as has been demonstrated by previous studies [23, 155, 156] explaining the increase in H_2O_2 levels. Even so, plants possess several mechanisms to prevent this oxidative stress and maintain Fe homeostasis, such as using proteins with ferroxidase activity, like ferritin [143] and sulphur compounds, like glutathione. Additionally, because Fe is toxic in its bivalent form (Fe^{2+}), it is generally found inside the cell in Fe complex compounds such as Fe-S [23, 157]. Therefore, this might explain why no significant increases in H_2O_2 concentration and its low levels in the 12.5 mg/L Fe treatment were detected.

Regarding Ag, opposite results were found in both organs: H_2O_2 levels significantly increased in the shoots and decreased in the roots. Being an HM, Ag has the potential to induce the formation of ROS when in higher concentrations. Moreover, the results obtained for the shoots are similar to those observed by Li et al. (2018) in their study regarding the use of silver nanoparticles [158]. The present results indicate that in shoots, Ag promotes the formation of H_2O_2 but inhibits its formation in the roots. Additionally, the Ag bioaccumulation results seem to be directly related to the concentration of H_2O_2 in the shoots but are inversely related in the roots. This suggests that Ag is somehow helping the plant cope with the roots' oxidative stress but is causing oxidative stress in the aerial part. The high accumulation of Ag verified in the roots supports this observation. Because Ag can block the receptors for ethylene, a known stress-related hormone [159], it inhibits the ethylene-related stress response pathway, thus resulting in less ROS accumulation.

4.1.3.2. Lipid peroxidation

ROS activity induced by HM toxicity causes oxidative stress in the cell that can lead to severe membrane damage. Most of this damage is the result of lipid peroxidation [87, 160]. The levels of malondialdehyde (MDA), an end-product of polyunsaturated fatty acids peroxidation in the cells, were measured to assess this. The results obtained in the treatment with Fe show a general increase in MDA levels in both shoots and roots. Moreover, MDA concentration has significantly increased in the shoots in the 12.5 mg/L Fe treatment. These results follow the same pattern as the ones obtained for H_2O_2 assessment, demonstrating that the high levels of MDA detected were a direct consequence of ROS activity. On the contrary, MDA concentration in the roots is slightly

lower in the 12.5 mg/L Fe treatment than in the 6 mg/L. The same can be observed in H_2O_2 levels, further supporting the abovementioned observation.

As for the Ag treatment, MDA results also correlate with the ones obtained for H_2O_2. In shoots, a significant increase was detected in the 25.6 mg/L Ag treatment, and in the roots, a significant decrease occurred in both 6.1 mg/L and 25.6 Ag treatments. The same pattern can be observed when assessing the H_2O_2 levels, which means that the increase of lipid peroxidation in the shoots was a direct consequence of the increased ROS activity - also detected in the shoots – and the decreased levels in the roots led to a significant reduction of membrane damage.

4.1.4. *A. thaliana* response to Fe- and Ag-induced oxidative stress

4.1.4.1. Reduced glutathione

As previously discussed, Fe and Ag in excess can induce oxidative stress in the plant. However, several non-enzymatic antioxidant mechanisms were analysed to validate and better understand this response, including the reduced glutathione.

Reduced Glutathione (GSH) is a tripeptide composed of the amino acids L-glutamate, L-cysteine and glycine that possess antioxidant activity, increasing cell resistance to oxidative stress [161]. It also has chelating properties that allow it to interact with HMs and thus reduce their toxicity in the cell [52].

The assessment of GSH levels in both shoots and roots of *A. thaliana* revealed that Fe and Ag generally increased its accumulation in both organs.

Regarding Fe, GSH concentration tended to increase in shoots and roots with every experimental situation, revealing a significant increase in the last one, where 12.5 mg/L of Fe was present in the media. Comparing these results with the ones of H_2O_2 levels, it is notable that as the ROS presence increases, so does the accumulation of GSH. Therefore, this increase in GSH levels may be a reactive response to the accumulation of H_2O_2. Furthermore, the concentration of GSH present in the roots in the 12.5 mg/L Fe treatment showed a slightly higher level than the one detected in the shoots. Looking at the previous results that revealed that both MDA and H_2O_2 levels dropped in the situation with the highest supply of Fe (12.5 mg/L), it might mean that the GSH presence is counteracting the effects of oxidative stress.

With Ag, GSH accumulation also increased in both organs, although significant results were only found in the shoots when the media was supplied with 25.6 mg/L of Ag. Despite this, GSH accumulation in the roots was more prominent than in the shoots, almost 4-fold higher. This might be the result of the more considerable Ag uptake, earlier discussed in the bioaccumulation assessment, that provoked an increasing tendency in

GSH accumulation as a way to mitigate the stress caused by the excess of Ag, either by chelation of Ag or through antioxidant action [159]. This might also explain the significant decrease in MDA and H_2O_2 levels detected in the roots. As for the shoots, despite an increase in GSH accumulation, it might not have been sufficient to protect them from oxidative stress damage. These results are in frame with other studies where GSH acted in response to metal-induced stress [162, 163].

4.1.4.2. Total thiols, non-protein thiols and protein thiols

The involvement of thiol metabolites in response to Fe and Ag oxidative stress was also analysed in this study. Looking at the Fe treatment assays, both shoots and roots significantly increased the total thiol (TT) concentration in the 12.5 mg/L Fe situation, however, for different reasons. Both non-protein thiols (NPT) and protein thiols (PT) generally increased, with statistical significance in the 12.5 mg/L Fe treatment. As such, these results for TT in the shoots were due to the increase of both NPT and PT. In the roots, the same can be observed for the PT. However, NPT decreased compared to the control situation, with statistical significance in both 3 mg/L and 6 mg/L Fe treatments. Therefore, TT accumulation in the roots was mainly due to the increase of PT.

Thiol ligands are known for their ability to interact with HMs, forming complexes and reducing their cell toxicity [164, 165]. As the shoots accumulate more Fe, the risk of oxidative stress increases, thus leading to the necessity of an effective response by the plant. This data revealed that *A. thaliana* plants, especially the aerial part, strongly rely on NPT and PT to address the eminent Fe-induced stress. As discussed earlier, the increased GSH in the shoots might explain this accumulation of NPT since GSH is the most abundant form of NPT [166]. Interestingly, the roots had a higher accumulation of thiols than the shoots despite protein-bound thiols being the primary source of their increase. This is contradictory when looking at the GSH results in this organ since they show an increase in its levels. However, in this case, the increased accumulation of GSH may not be impactful enough to alter the overall level of NPTs. Moreover, GSH is known to be a precursor for phytochelatins (PC) production [52, 167], so it is possible that part of the GSH produced is redirected to PC metabolism. Therefore, in future work, assessing the production of phytochelatins in response to Fe-induced stress would be most relevant.

As for the Ag treatment assays, the TT and PT levels tended to increase in the shoots, with statistical significance in the 25.6 mg/L Ag treatment. However, no changes in the thiol groups occurred in the roots. Like the results obtained for roots in Fe treatments, the increase detected in TT in shoots is associated with the production of

PT. Confronting these results with those of GSH, the same logic can be applied to explain why the increase in this metabolite did not alter the levels of NPTs in both shoots and roots. Nonetheless, it is evident in this study that thiol ligands do not have a prominent role in the detoxification process occurring in the roots, except for GSH. Since the roots accumulate more Ag than the shoots, the detoxification mechanisms are expected to have a higher impact on this organ. However, the results have shown that roots suffer much less oxidative stress than shoots. Therefore, shoots seem to rely on the action of both GSH and PT to respond to the Ag-induced stress. However, other metabolites, such as proline, must be considered.

4.1.4.3. Proline

It has been suggested that proline also acts as a defence mechanism against metal toxicity due to its properties as an osmoprotectant, antioxidant and metal chelator [95]. As such, the proline levels were assessed to address its response in case of HM toxicity. For Fe treatments, proline accumulation had a general decrease in both shoots and roots, with statistical significance in the 6 mg/L Fe and 12.5 mg/L Fe situations in the shoots and all experimental conditions in the roots - despite higher values detected in the 6 mg/L and 12.5 mg/L Fe treatments in comparison to the 3 mg/L Fe treatment. As for Ag, proline levels significantly increased in the shoots in an Ag dose-dependent manner, but no changes were detected in the roots. Several studies have demonstrated that, during HM toxicity, the levels of proline increase. Some examples include nickel (Ni), molybdenum (Mo), zinc (Zn) and lead (Pb) [168-170]. So, confronting those results with the ones obtained for the shoots under Ag stress, it is possible to observe this same tendency.

Additionally, considering what was previously discussed, shoots suffered way more oxidative stress than the roots. Therefore, the detoxification mechanisms were expected to act more intensively in the aerial part rather than in the roots. On the other hand, when looking at plants under Fe treatment, the results seem contradictory.

As mentioned, proline has many functions and being a metal chelator was suggested as one of them. So, the low levels detected can result from this proline being used to chelate free Fe^{2+} ions. However, there have been suggestions that proline might have a more prominent role as an antioxidant than a metal chelator [171]. This is also valid information that can be used to explain the results obtained for the oxidative stress caused by H_2O_2 that, despite being significant in some cases, might not have been strong enough to induce high levels of proline production. However, the decrease in its levels suggests that the plant might be using already present free proline to address the ROS

issue. A similar case was found during Ni toxicity, where proline levels decreased in the lower Ni concentrations tested but increased in the highest Ni concentration [172]. Therefore, testing higher Fe concentrations to determine whether proline levels would rise would be interesting.

4.1.5. Metallothionein expression assessment.

As previously mentioned, MTs have a prominent role as metal chelators when addressing the issue of oxidative stress due to HM toxicity [66]. As such, in this study, the expression of 5 out of the 8 known MTs from *A. thaliana* was analysed through RT-qPCR to assess their role in dealing with Fe and Ag excess in shoots and roots. The MTs selected were *AtMT1a*, *AtMT1c*, *AtMT2a*, *AtMT2b* and *AtMT3*.

Starting with the analysis of the type I MTs (*At*MT1a and *At*MT1c) under Fe treatment, the results showed that both subtypes of this MT family have different expression levels within the different organs. In most cases, this expression did not show any significant results. In shoots, none of the experimental situations showed statistically significant differences for *AtMT1a*. As for *AtMT1c*, there appears to be a downregulation of its expression in the shoots with the increasing Fe supplied, with a significant decrease in the 3 mg/L Fe treatment. However, despite not being significant, the expression of this MT seems to recover in response to higher Fe concentrations. In the roots, the situation changes. Expression variations in both *AtMT1a* and *1c* fluctuate when the concentration of Fe increases, but their values had no significant changes. Regardless, in this organ, the expression of these MTs seems to be downregulated by the presence of Fe, particularly *AtMT1c*. According to the literature, type I MTs are preferably expressed in roots [66, 173]; thus, these results appear contradictory. As such, a preference for expression in a specific organ does not imply exclusiveness.

Previous work in our lab regarding the characterisation of MTs in *A. thaliana* revealed that *AtMT1* was also expressed in the shoots in non-stressed conditions [136]. Moreover, there have been reports in which *AtMT1* expression in the leaves was induced in the presence of Cu [174, 175], suggesting that this increasing tendency in *AtMT1*'s expression in the leaves might be a plausible cause of Fe-induced expression and, in fact, characteristic of *A. thaliana*. However, further studies are required to confirm this hypothesis. Moreover, the non-significance of the results in roots does not imply the certainty of its downregulation.

As for *AtMT2*, the results showed a tendency of Fe stress to upregulate the expression of *AtMT2a* and *AtMT2b* in the shoots and downregulate it in the roots. However, the generality of the results showed no statistical significance, except in the

case of *AtMT2a*, where a significant decrease in expression was detected in the 6 mg/L Fe treatment. It is also noteworthy that the expression of both *AtMT2* in the roots, despite being relatively lower than the control, tends to increase in a Fe dose-dependent manner. *AtMT3* expression also increased in both organs but showed no significant results. In addition, the relative expression obtained for *AtMT3* in roots was higher than in the shoots.

Types II and III MTs can both be expressed in leaves [173, 176]. And, looking at the results obtained, it is possible to verify the same. Despite not being significant, their tendency to increase in expression shows that these MTs are being transcribed in this organ in response to the Fe-induced stress. Considering the expression of these MTs in the roots, the presented results may go against the literature. However, recent reports also observed that *AtMT2* and *AtMT3* are expressed in the roots of *A. thaliana* [136].

Exposure to Ag, on the other hand, showed more significant results. All the MTs analysed in shoots revealed similar expression levels, with a significant increase in the 25.6 mg/L Ag treatment. Coupled with the fact that no significant results were observed for the 6 mg/L Ag situation, this indicates that silver induces MT expression in shoots but only in a stress-inducible concentration. This also suggests that *A. thaliana* leaves might have a certain tolerance to Ag. However, further studies must be performed using concentrations of Ag between 6 and 25.6 mg/L to assert the gene-inducing threshold.

As for roots, both *AtMT1* genes also increase significantly, similar to their increase in the shoots. This is in accordance with the literature, as it was previously said that MT1 is mainly expressed in the roots. However, the increased expression in the leaves is evidence that this MT type is also expressed in the shoots and, in this case, must be acting against Ag-induced toxicity.

AtMT2 genes' expression in roots displayed different behaviours with the HMs used. While *AtMT2a* was tendentially downregulated with the highest concentration of Ag used (25.6 mg/L), *AtMT2b* was tendentially upregulated in all experimental situations. However, in both cases, no significant results were found. This suggests that, in the presence of Ag, roots favour the upregulation of *AtMT2b* rather than *AtMT2a*. It can be assumed that *A. thaliana* might be attempting to mitigate the stress caused by Ag in the roots by increasing MT2-encoding genes' expression. Despite the knowledge that MT2 encoding genes are mainly expressed in the leaves, a study has revealed that *AtMT2b* is involved in root development [177]. Type III MT expression also showed no significant results despite its tendential increase in response to Ag. As roots, in this case, accumulated more Ag than shoots, coupled with oxidative damage in this organ's

significantly lower, the involvement of AtMT2b and AtMT3 might be key elements in ensuring root homeostasis.

Overall, the exposure of Fe and Ag had some impact on all MTs analysed. It is known that MTs act in defence of metal toxicity. Unfortunately, most studies on this subject focus on differential accumulations of HMs when in the presence of MT rather than expression of the latter in response to HMs. Moreover, due to the high risk that some metals pose to health safety, such as Cd, As, Cr and Pb [17, 57, 88], most of the research is directed towards these HM. As such, this work is pivotal to future studies, as it sheds new knowledge on the effects of Fe and Ag in MT expression. However, it is important to notice that the action of MTs can be both species-dependent and metal-dependent [73]. A study by Foley et al. [178], where *AtMT1a*, *AtMT1b* and *AtMT2* were recombinantly expressed in the presence of equimolar quantities of Cd, Cu, Zn and Fe, showed that these MTs had different preferences regarding the type of metal, where Cd was the most preferred and Fe the least. Another study by Lv et al. (2013) [179] showed that MT1 and MT2 from *Brassica campestris* directly responded to Cd, but only MT1 reacted to Cu. On the other hand, MT1a and MT2 from *A. thaliana* increased their expression in response to Cu [175].

In this study, the relation between Fe excess and MT expression may not have been significant in most cases. However, the variations in up and downregulation detected should not be discarded, and it may even help justify other aspects of the oxidative stress study performed. For example, the tendential upregulation of MTs in the leaves may be involved in the significant increase of PT detected in this organ to address the higher accumulation of Fe. In the roots, the significant increase of PT detected can be associated with the tendential rise in expression of *AtMT3* and the recovery observed for both *AtMT2* genes. However, Fe is a micronutrient essential for plants, so the mechanisms regulating its homeostasis are more complex. Thus, the actions of other proteins and metabolites not addressed in this study, such as phytochelatins (PCs) and ferritin, might have a more prominent role rather than MTs.

In the case of Ag, MTs seem to respond to its toxicity actively. Hence, a more direct correlation between MT gene expression increases and other aspects evaluated in the oxidative stress assessment can be made. Due to the overall significant increase detected in the expression of MTs in the shoots for the 25.6 mg/L treatment, it is plausible to assume that these metal-chelator proteins were involved in the protection of this organ as a response to the sudden accumulation of silver, that ultimately caused the increased levels of H_2O_2 and MDA. It may also account for the significant increase in PT levels in the same organ. As for the roots, their capability to withstand large Ag levels and,

simultaneously, to prevent high levels of oxidative stress can be due to the use of MTs, where both MT1 might have had a more prominent role, with the aid from other MTs already discussed. However, this can be one of the reasons why no statistically significant changes occurred in the protein thiols in the roots. The excessive mitigation of Ag that happened with the 25.6 mg/L treatment from roots to shoots might suggest the involvement of MT1 genes in the translocation of silver.

4.2. AtMT2b localisation

4.2.1. Transient expression of *AtMT2b*

HM homeostasis is one of the most important roles in plants, ensuring they acquire and maintain essential nutrients for their development and avoiding characteristic toxicity induced by these same HMs. The use of cytosolic metal transporters and chelators like phytochelatins (PCs) and metallothioneins (MT), as well as plasmatic compartments, like the vacuole, are some examples of the extensive metal sequestration stratagems that plants possess to deal with toxic HM concentrations [180-182]. Type II metallothioneins are known metal chelators mainly found in leaves. Thus, a better understanding of their functions in this organ and their locations and movements around the intracellular space are relevant to further expanding the knowledge regarding this MT family. Therefore, in this study, a construct that would allow the heterologous expression of *A. thaliana's AtMT2b* cDNA, associated with a fluorescence protein in *N. tabacum* leaves, was assembled, and its location in the cell through confocal microscopy was performed.

The results showed that AtMT2b is mainly a cytosolic protein but was also detected inside the nucleus. In plants, HM trafficking can occur via apoplastic or symplastic routes [182], meaning that it can be performed outside and inside the cell, respectively. Some HMs, like Fe, are essential co-factors for intracellular metabolism [7], and therefore, the cytosolic activity of AtMT2b might indicate HM transport inside the cell. This is relevant for other cases with HM trafficking: some metals, like manganese (Mn), which are toxic to the cell, can be transported and accumulated in the vacuole, or even the Golgi complex, to mitigate their harmful effects [181, 183].

Additionally, AtMT2b also seems to form agglomerates near the cell wall. It has been reported that the cell wall also functions as a defence barrier for many compounds, including HM ions [184, 185]. As such, the accumulation of AtMT2b in this region might be due to the transport of HMs to the cell wall or the cell exterior. Nevertheless, the

possibility that it might result from gene overexpression cannot be ruled out. Regardless, the exact nature of this accumulation is still unknown.

Additionally, MTs are also known to participate in antioxidant activities. Leaf cell metabolism, such as photosynthesis, is prone to generating ROS [56]. Henceforth, AtMT2b, accumulated explicitly in the leaves, can have a role in mitigating oxidative stress.

Nevertheless, strong evidence supports this study's findings regarding AtMT2b as a cytosolic protein, reinforcing the idea that MTs play essential physiological roles inside the cell. Moreover, it is a pioneer in the *in vivo* localisation and tracking of AtMT2b.

4.2.2 *At*MT2b PSI A-mediated vacuolar targeting

Over the last years, our laboratory has been particularly interested in studying the aspartic proteinases (APs) cardosin A and B from *C. cardunculus*, specifically their plant-specific insert (PSI A and B) domains [112, 119]. It has been shown that PSIs are involved in the vacuolar targeting of APs, as the presence of PSI A alone allowed the targeting of cardosin A and the mCherry protein to vacuole, evidencing their role as a vacuolar sorting determinant [119].

With this background, an attempt to target AtMT2b to the vacuole was performed with the help of PSI A. *AtMT2b* fused with PSI A was expressed in *N. tabacum* leaf samples, in-frame with a fluorescence protein. The visualisation of the fused protein was once again performed by confocal microscopy.

The results have shown that the fusion of the AtMT2b to the PSI A was insufficient to target AtMT2b to the vacuole, contrary to what was presumed. In fact, the localisation of the fusion protein was very similar to the one verified for the AtMT2b alone. The selection of the PSI A was not an arbitrary decision. Firstly, this peptide domain is specific to cardosin A, which is known to have been successfully expressed in heterologous systems such as *A. thaliana* and *N. tabacum* [120]. Secondly, it was selected because of the study that suggested its involvement in the vacuolar targeting of the same AP.

Sorting proteins to the vacuole requires the presence of a VSD. As mentioned earlier, VSDs can be associated with the C-terminal (Ct-VSDs), sequence-specific (ss-VSDs) or dependent on the physical structure of the protein (ps-VSDs) [104]. According to Pereira et.al. (2013), the suggestion that PSI A behaves as a VSD resulted from the experience where cardosin A, with its Ct-VSD removed but not its PSI A domain, and mCherry fused with PSI A alone were able to reach the vacuole. Because, in the case of this work, PSI A was not able to target the AtMT2b to the vacuole, it suggests that other entities might be at play, such as signal peptides (SP). These short peptides, present at

the N-terminal regions, exist in almost all secretory proteins, including APs. Their main function is to mark those proteins to the secretory pathway and determine their target [186].

MT are not known to be secretory proteins, as confirmed by their cytoplasmic localisation within this study, and do not have an SP. Moreover, it is noteworthy to mention that the mCherry gene fused with PSI A, in Pereira et.al. (2013) had an SP. This suggests that PSI A alone might be able to function as a VSD for secretory proteins that include an SP; however, the same does not happen for cytoplasmic proteins.

Unexpectedly, these results shed new light on understanding the PSI functions, showing that it is far more complex than what was understood until now. The inclusion of an SP in the AtMT2b protein may enable its targeting to the vacuole when mediated by PSI A. This would prove that an SP is required to assert the VSD function of the PSI domain. However, including more genetic information might compromise the normal function of the MT, that otherwise could be used for testing in sequestering metal ions to the vacuole.

4.3. Analysis of T-DNA insertion in *AtMT1a* and *AtMT2b* mutants

Regarding the assessment of *AtMT1a* and *AtMT2b* mutants homozygous for the T-DNA insertion, these were never found, with most being heterozygous and some wild-type. Mendelian law of segregation states that within the offspring of a heterozygous plant: ¼ would be wild-type; ½ heterozygous; ¼ homozygous for the T-DNA insertion. Genotyping results have shown that the number of wild-type and heterozygous mutants was down to 1/3 and 2/3 proportions, respectively, which might indicate lethality for the T-DNA insertion homozygous mutants. Three hypotheses might explain why no homozygous mutant was found: (1) the product of these genes are essential for seed production and plants overall growth and development, which implies no homozygous mutant seeds generated in the mother plant; (2) these genes play an essential role in seed germination, and therefore homozygous mutant seeds never germinated; (3) a combination of (1) and (2). These hypotheses are in accordance with the consistent results obtained during this work. Moreover, similar results were obtained by other colleagues in our laboratory [136].

Also, silencing these genes using constructs with inducible promoters in the wild type could be a future approach to overcome these obstacles. This would allow these genes to be active during seed formation and germination and silenced during posterior studies of metal toxicity assessment.

Plus, a reanalysis made at the end of this work of the primers used revealed that those were not well designed, which may have compromised the obtained results, and, therefore, a similar approach with better-designed primers should be followed in future genotyping assays.

Conclusion

Facing the imminent threat of HM accumulation in soils is of massive importance. Unfortunately, eliminating these pollutants is nearly impossible, and plant crops take the biggest toll. Therefore, the best option is to find alternatives to help plants mitigate HM toxicity, usually by improving their tolerance in HM-contaminated soils. As such, a better understanding of the toxic effects of different HMs and the plant's response is necessary.

In this study, the toxicity effects of growing concentrations of Fe (3 mg/L, 6 mg/L and 12.5 mg/L) and Ag (6.1 mg/L and 25.6 mg/L) were analysed in *A. thaliana* plants 21 days after germination on some of its defence mechanisms. Looking at the several stress indicators assessed, it is possible to observe many significant changes. This means that exposure to high concentrations of Fe and Ag induced oxidative stress – confirmed by the overall reduction in plant size, correlated with the decrease in photosynthetic pigments, and to increasing levels of H_2O_2 and MDA – but it also means that the plants' defensive mechanisms were active. Interestingly, how plants responded to these stresses differed for each HM and organ. *A. thaliana* plants exposed to Fe tended to rely heavily on the use of thiols, such as reduced glutathione, to address the oxidative stress in both shoots and roots. However, while shoots used non-protein and protein thiols, roots preferred the latter. In both organs, the reduction of proline is indicative of its use as an antioxidant. Considering the response to Ag, *A. thaliana* plants preferably stored it in the roots to protect shoots, proceeding to its translocation only in the highest concentration used. Additionally, while shoots relied primarily on proline and protein thiols against ROS accumulation, roots only used reduced glutathione as a non-enzymatic defence mechanism.

Regarding MTs, these results suggest that the *modus operandi* of these metal chelator proteins is highly metal-dependent. Their expression during Fe stress showed almost no significant changes, apart from some significant downregulation in *AtMT1c* and *AtMT2b* in some cases. Nonetheless, the tendencies observed for up and downregulations for all MT-encoding genes might be indicative of their expression but probably not in response to Fe. On the other hand, Ag significantly induced the expression of all MTs in the shoots in the highest Ag concentration treatment, most likely

as a response to the sudden increase of Ag. In the roots, however, only type I MTs' expression significantly increased in high Ag concentrations to enhance the plant's tolerance by accumulating Ag.

The vacuolar targeting of proteins opens new possibilities for biotechnological approaches to increase plant phytoremediation functionalities. This work attempted one of these strategies by combining a type II MT from *A. thaliana* with a PSI A domain and assessing the endorsement to the vacuole in *N. tabacum* leaf cells. However, the results demonstrated that this did not work, as no fluorescence was detected inside the vacuole. As for the heterologous evaluation of AtMT2b, the results show that this protein has a cytosolic activity.

Regarding the mutant plants for T-DNA insertion in *AtMT1a* and *AtMT2b* genes, no homozygous for this mutation were found. This can be associated with the poor design of the primers used which may have compromised the overall results. However, the importance of these genes for seed germination and plant development cannot be discarded as their absence in existing mutants may not have allowed the development of the plant so that sufficient biological material could be collected. Nonetheless, the lack of knockout mutants did not allow their use in the HM stress assays to further understand these MTs' role in HM tolerance and seed germination. Other gene silencing strategies, such as inducible promoters, can address this topic in future works.

To summarise, *A. thaliana* plants are susceptible to toxicity by Fe and Ag, although they employ different strategies to address the HM stress. However, it is important to mention that being an essential or non-essential metal can be a critical factor in determining how the plant responds to its toxicity. MT-encoding genes' responses further sustain this suggestion since they revealed higher activity during Ag contamination than Fe. Other factors, such as the employment of ferritins and PCs and perhaps higher concentrations of Fe, are interesting subjects for further study in this subject. As for the vacuolar targeting of AtMT2b mediated by PSI, the fact that no endorsement in the vacuole was observed can be related to the cytosolic presence of this MT, further demonstrated by the *in vivo* visualisation of this protein. Other strategies, including adding a signal peptide (SP) to the MT, can be tested in future works, as it would be interesting to see a functional construct being accumulated in vacuoles for an increased tolerance and phytoremediation capacity of Ag and other HMs. In addition, the His6x-Tag included in the final construct can be used for future *Pull-down* assays to confirm the vacuole endorsement levels.

References

1. Maja, M.M. and S.F. Ayano, *The Impact of Population Growth on Natural Resources and Farmers' Capacity to Adapt to Climate Change in Low-Income Countries.* Earth Systems and Environment, 2021. **5**(2): p. 271-283.
2. Dodson, J.C., et al., *Population growth and climate change: Addressing the overlooked threat multiplier.* Science of The Total Environment, 2020. **748**: p. 141346.
3. Sillanpää, M. and C. Ncibi, *Bioeconomy: The Path to Sustainability*, in *A Sustainable Bioeconomy: The Green Industrial Revolution*, M. Sillanpää and C. Ncibi, Editors. 2017, Springer International Publishing: Cham. p. 29-53.
4. Alengebawy, A., et al., *Heavy Metals and Pesticides Toxicity in Agricultural Soil and Plants: Ecological Risks and Human Health Implications.* Toxics, 2021. **9**(3): p. 42.
5. Bhunia, P., *Environmental toxicants and hazardous contaminants: Recent advances in technologies for sustainable development.* Journal of Hazardous, Toxic, Radioactive Waste, 2017. **21**(4): p. 02017001.
6. Chin, N.P., *Environmental toxins: physical, social, and emotional.* Breastfeed Med, 2010. **5**(5): p. 223-4.
7. Ahmed, T., et al., *Current trends and future prospective in nanoremediation of heavy metals contaminated soils: A way forward towards sustainable agriculture.* Ecotoxicology and Environmental Safety, 2021. **227**: p. 112888.
8. Ghous, M., et al., *Halophyte quinoa: a potential hyperaccumulator of heavy metals for phytoremediation.* 2022.
9. Mishra, S., et al., *Heavy metal contamination: an alarming threat to environment and human health.* Environmental biotechnology: For sustainable future, 2019: p. 103-125.
10. Adlak, T., et al., *Biotechnology: An Advanced Tool for Crop Improvement.* Current Journal of Applied Science and Technology, 2019. **33**(1): p. 1-11.
11. Kiran, R. Bharti, and R. Sharma, *Effect of heavy metals: An overview.* Materials Today: Proceedings, 2022. **51**: p. 880-885.
12. Leonard, S.S., G.K. Harris, and X. Shi, *Metal-induced oxidative stress and signal transduction.* Free Radical Biology and Medicine, 2004. **37**(12): p. 1921-1942.
13. Samuel, M.S., et al., *A state of the art review on characterization of heavy metal binding metallothioneins proteins and their widespread applications.* Science of The Total Environment, 2021. **775**: p. 145829.
14. Fasae, K.D. and A.O. Abolaji, *Interactions and toxicity of non-essential heavy metals (Cd, Pb and Hg): lessons from Drosophila melanogaster.* Current Opinion in Insect Science, 2022. **51**: p. 100900.
15. Camponeschi, F., L. Banci, and A. Chemistry, *Metal cofactors trafficking and assembly in the cell: a molecular view.* Pure, 2019. **91**(2): p. 231-245.
16. Janssens, T.K., D. Roelofs, and N.M. Van Straalen, *Molecular mechanisms of heavy metal tolerance and evolution in invertebrates.* Insect Science, 2009. **16**(1): p. 3-18.
17. Briffa, J., E. Sinagra, and R. Blundell, *Heavy metal pollution in the environment and their toxicological effects on humans.* Heliyon, 2020. **6**(9).
18. He, Z.L., X.E. Yang, and P.J. Stoffella, *Trace elements in agroecosystems and impacts on the environment.* J Trace Elem Med Biol, 2005. **19**(2-3): p. 125-40.
19. Angon, P.B., et al., *Sources, effects and present perspectives of heavy metals contamination: Soil, plants and human food chain.* Heliyon, 2024. **10**(7).
20. Nazar, R., et al., *Cadmium Toxicity in Plants and Role of Mineral Nutrients in Its Alleviation.* American Journal of Plant Sciences, 2012. **03**(10): p. 1476-1489.

21. Adrees, M., et al., *The effect of excess copper on growth and physiology of important food crops: a review.* Environ Sci Pollut Res Int, 2015. **22**(11): p. 8148-62.
22. Balafrej, H., et al., *Zinc Hyperaccumulation in Plants: A Review.* Plants (Basel), 2020. **9**(5): p. 562.
23. Kobayashi, T., T. Nozoye, and N.K. Nishizawa, *Iron transport and its regulation in plants.* Free Radic Biol Med, 2019. **133**: p. 11-20.
24. Tripathi, D.K., et al., *Acquisition and homeostasis of iron in higher plants and their probable role in abiotic stress tolerance.* Frontiers in Environmental Science, 2018. **5**: p. 86.
25. Kim, S.A. and M.L. Guerinot, *Mining iron: iron uptake and transport in plants.* FEBS Lett, 2007. **581**(12): p. 2273-80.
26. Eide, D., et al., *A novel iron-regulated metal transporter from plants identified by functional expression in yeast.* Proc Natl Acad Sci U S A, 1996. **93**(11): p. 5624-8.
27. Vert, G.g., et al., *IRT1, an Arabidopsis Transporter Essential for Iron Uptake from the Soil and for Plant Growth.* The Plant Cell, 2002. **14**(6): p. 1223-1233.
28. Takagi, S.i., K. Nomoto, and T. Takemoto, *Physiological aspect of mugineic acid, a possible phytosiderophore of graminaceous plants.* Journal of Plant Nutrition, 2008. **7**(1-5): p. 469-477.
29. Curie, C., et al., *Maize yellow stripe1 encodes a membrane protein directly involved in Fe(III) uptake.* Nature, 2001. **409**(6818): p. 346-9.
30. Mahawar, L., et al., *Iron deficiency in plants: an update on homeostasis and its regulation by nitric oxide and phytohormones.* Plant Growth Regulation, 2023. **100**(2): p. 283-299.
31. Sagi-Kazar, M., K. Solymosi, and A. Solti, *Iron in leaves: chemical forms, signalling, and in-cell distribution.* J Exp Bot, 2022. **73**(6): p. 1717-1734.
32. Samborska-Skutnik, I., et al., *Structural and functional response of photosynthetic apparatus of radish plants to iron deficiency.* Photosynthetica, 2020. **58**.
33. Kobayashi, T., et al., *Identification of novel cis-acting elements, IDE1 and IDE2, of the barley IDS2 gene promoter conferring iron-deficiency-inducible, root-specific expression in heterogeneous tobacco plants.* 2003. **36**(6): p. 780-793.
34. Tognetti, V.B., et al., *Enhanced plant tolerance to iron starvation by functional substitution of chloroplast ferredoxin with a bacterial flavodoxin.* Proc Natl Acad Sci U S A, 2007. **104**(27): p. 11495-500.
35. Msilini, N., et al., *Inhibition of photosynthetic oxygen evolution and electron transfer from the quinone acceptor QA- to QB by iron deficiency.* Photosynth Res, 2011. **107**(3): p. 247-56.
36. Nikolic, M. and J. Pavlovic, *Plant responses to iron deficiency and toxicity and iron use efficiency in plants*, in *Plant micronutrient use efficiency*. 2018, Elsevier. p. 55-69.
37. Krohling, C.A., et al., *Ecophysiology of iron homeostasis in plants.* Soil Science and Plant Nutrition, 2016. **62**(1): p. 39-47.
38. Broadley, M., et al., *Function of nutrients: micronutrients*, in *Marschner's mineral nutrition of higher plants*. 2012, Elsevier. p. 191-248.
39. Kaur, G. and B. Asthir, *Molecular responses to drought stress in plants.* Biologia Plantarum, 2017. **61**(2): p. 201-209.
40. Cesco, S., et al. *Uptake of ^{59}Fe from soluble ^{59}Fe-humate complexes by cucumber and barley plants*. in *Plant and Soil*. 2002.
41. Hell, R. and U.W. Stephan, *Iron uptake, trafficking and homeostasis in plants.* Planta, 2003. **216**(4): p. 541-551.

42. Nikolic, M. and V. Römheld, *Nitrate Does Not Result in Iron Inactivation in the Apoplast of Sunflower Leaves.* Plant Physiology, 2003. **132**(3): p. 1303-1314.
43. Kolesnikov, S., et al., *Silver ecotoxicity estimation by the soil state biological indicators.* Applied environmental soil science, 2020. **2020**(1): p. 1207210.
44. Kaveh, R., et al., *Changes in Arabidopsis thaliana gene expression in response to silver nanoparticles and silver ions.* Environ Sci Technol, 2013. **47**(18): p. 10637-44.
45. Tsepina, N., et al., *Soil contamination by silver and assessment of its ecotoxicity.* Reviews in Agricultural Science, 2022. **10**: p. 186-205.
46. Yan, A. and Z. Chen, *Impacts of Silver Nanoparticles on Plants: A Focus on the Phytotoxicity and Underlying Mechanism.* Int J Mol Sci, 2019. **20**(5): p. 1003.
47. Reidy, B., et al., *Mechanisms of Silver Nanoparticle Release, Transformation and Toxicity: A Critical Review of Current Knowledge and Recommendations for Future Studies and Applications.* Materials (Basel), 2013. **6**(6): p. 2295-2350.
48. Sun, C., et al., *Silver nanoparticles induced neurotoxicity through oxidative stress in rat cerebral astrocytes is distinct from the effects of silver ions.* Neurotoxicology, 2016. **52**: p. 210-21.
49. Sharma, V.K., et al., *Organic-coated silver nanoparticles in biological and environmental conditions: fate, stability and toxicity.* Adv Colloid Interface Sci, 2014. **204**: p. 15-34.
50. Guo, X., et al., *Size- and coating-dependent cytotoxicity and genotoxicity of silver nanoparticles evaluated using in vitro standard assays.* Nanotoxicology, 2016. **10**(9): p. 1373-84.
51. Qian, H., et al., *Comparison of the toxicity of silver nanoparticles and silver ions on the growth of terrestrial plant model Arabidopsis thaliana.* J Environ Sci (China), 2013. **25**(9): p. 1947-55.
52. Dutta, S., et al., *Oxidative and genotoxic damages in plants in response to heavy metal stress and maintenance of genome stability.* Plant Signaling & Behavior, 2018. **13**(8): p. e1460048.
53. Solanki, R. and R. Dhankhar, *Biochemical changes and adaptive strategies of plants under heavy metal stress.* Biologia, 2011. **66**(2): p. 195-204.
54. Kotrba, P., et al., *Genetically modified plants in phytoremediation of heavy metal and metalloid soil and sediment pollution.* Biotechnol Adv, 2009. **27**(6): p. 799-810.
55. Sebastian, A., et al., *Chapter 1 - Transgenics in Phytoremediation of Metals and Metalloids: From Laboratory to Field*, in *Transgenic Plant Technology for Remediation of Toxic Metals and Metalloids*, M.N.V. Prasad, Editor. 2019, Academic Press. p. 3-22.
56. Thakur, M., et al., *Metal tolerance in plants: Molecular and physicochemical interface determines the "not so heavy effect" of heavy metals.* Chemosphere, 2022. **287**: p. 131957.
57. Dubey, A.K., et al., *Over-expression of chickpea metallothionein 1 gene confers tolerance against major toxic heavy metal stress in Arabidopsis.* Physiol Mol Biol Plants, 2021. **27**(12): p. 2665-2678.
58. DalCorso, G., et al., *How plants cope with cadmium: staking all on metabolism and gene expression.* Journal of integrative plant biology, 2008. **50**(10): p. 1268-1280.
59. Freisinger, E., *Structural features specific to plant metallothioneins.* J Biol Inorg Chem, 2011. **16**(7): p. 1035-45.
60. Giritch, A., et al., *Structure, expression and chromosomal localisation of the metallothionein-like gene family of tomato.* Plant Mol Biol, 1998. **37**(4): p. 701-14.

61. Xiong, W., et al., *The rice "fruit-weight 2.2-like" gene family member OsFWL4 is involved in the translocation of cadmium from roots to shoots.* Planta, 2018. **247**: p. 1247-1260.
62. Martins, M.L.R., *Metabolic Pinpointing of Solanum Lycopersicum L. Response to High Zn Levels-the Relevance of Metallothioneins, GSH Metabolism and the Antioxidant System*. 2017, Universidade do Porto (Portugal).
63. Sekhar, K., et al., *Metallothionein 1 (CcMT1) of pigeonpea (Cajanus cajan, L.) confers enhanced tolerance to copper and cadmium in Escherichia coli and Arabidopsis thaliana.* Environmental Experimental Botany, 2011. **72**(2): p. 131-139.
64. Jin, S., et al., *Expression of the rgMT gene, encoding for a rice metallothionein-like protein in Saccharomyces cerevisiae and Arabidopsis thaliana.* Journal of genetics, 2014. **93**: p. 709-718.
65. Zhu, W., et al., *Arabidopsis thaliana metallothionein, AtMT2a, mediates ROS balance during oxidative stress.* Journal of Plant Biology, 2009. **52**: p. 585-592.
66. Cobbett, C. and P. Goldsbrough, *PHYTOCHELATINS AND METALLOTHIONEINS: roles in heavy metal detoxification and homeostasis.* Annu Rev Plant Biol, 2002. **53**(Volume 53, 2002): p. 159-82.
67. Yang, Z., et al., *OsMT1a, a type 1 metallothionein, plays the pivotal role in zinc homeostasis and drought tolerance in rice.* Plant Molecular Biology, 2009. **70**(1): p. 219-229.
68. Hassinen, V., et al., *Plant metallothioneins–metal chelators with ROS scavenging activity?* Plant Biology, 2011. **13**(2): p. 225-232.
69. Ren, Y., et al., *Type 4 metallothionein genes are involved in regulating Zn ion accumulation in late embryo and in controlling early seedling growth in Arabidopsis.* Plant Cell Environ, 2012. **35**(4): p. 770-89.
70. Ferraz, P., et al., *Phytostabilization of nickel by the zinc and cadmium hyperaccumulator Solanum nigrum L. Are metallothioneins involved?* Plant Physiol Biochem, 2012. **57**: p. 254-60.
71. Dundar, E., G.D. Sonmez, and T. Unver, *Isolation, molecular characterization and functional analysis of OeMT2, an olive metallothionein with a bioremediation potential.* Mol Genet Genomics, 2015. **290**(1): p. 187-99.
72. Yang, J., et al., *Overexpression of the Tamarix hispida ThMT 3 gene increases copper tolerance and adventitious root induction in Salix matsudana Koidz.* Plant Cell, Tissue Organ Culture, 2015. **121**: p. 469-479.
73. Leszczyszyn, O.I., H.T. Imam, and C.A. Blindauer, *Diversity and distribution of plant metallothioneins: a review of structure, properties and functions.* Metallomics, 2013. **5**(9): p. 1146-69.
74. Zimeri, A.M., et al., *The plant MT1 metallothioneins are stabilized by binding cadmiums and are required for cadmium tolerance and accumulation.* Plant Mol Biol, 2005. **58**(6): p. 839-855.
75. Xia, Y., et al., *Overexpression of Elsholtzia haichowensis metallothionein 1 (EhMT1) in tobacco plants enhances copper tolerance and accumulation in root cytoplasm and decreases hydrogen peroxide production.* J Hazard Mater, 2012. **233-234**: p. 65-71.
76. Guo, W.J., M. Meetam, and P.B. Goldsbrough, *Examining the specific contributions of individual Arabidopsis metallothioneins to copper distribution and metal tolerance.* Plant Physiol, 2008. **146**(4): p. 1697-706.
77. Zhigang, A., et al., *Expression of BjMT2, a metallothionein 2 from Brassica juncea, increases copper and cadmium tolerance in Escherichia coli and Arabidopsis thaliana, but inhibits root elongation in Arabidopsis thaliana seedlings.* J Exp Bot, 2006. **57**(14): p. 3575-82.

78. Zhang, J., et al., *Metallothionein 2 (SaMT2) from Sedum alfredii Hance confers increased Cd tolerance and accumulation in yeast and tobacco.* PLoS One, 2014. **9**(7): p. e102750.
79. Murphy, A. and L. Taiz, *Comparison of Metallothionein Gene Expression and Nonprotein Thiols in Ten Arabidopsis Ecotypes (Correlation with Copper Tolerance).* Plant Physiology, 1995. **109**(3): p. 945-954.
80. Mekawy, A.M.M., D.V.M. Assaha, and A. Ueda, *Constitutive overexpression of rice metallothionein-like gene OsMT-3a enhances growth and tolerance of Arabidopsis plants to a combination of various abiotic stresses.* Journal of Plant Research, 2020. **133**(3): p. 429-440.
81. Mekawy, A.M.M., et al., *Characterization of type 3 metallothionein-like gene (OsMT-3a) from rice, revealed its ability to confer tolerance to salinity and heavy metal stresses.* Environmental and Experimental Botany, 2018. **147**: p. 157-166.
82. Lee, J., et al., *Arabidopsis metallothioneins 2a and 3 enhance resistance to cadmium when expressed in Vicia faba guard cells.* Plant Molecular Biology, 2004. **54**(6): p. 805-815.
83. Imam, H.T. and C.A. Blindauer, *Differential reactivity of closely related zinc (II)-binding metallothioneins from the plant Arabidopsis thaliana.* JBIC Journal of Biological Inorganic Chemistry, 2018. **23**: p. 137-154.
84. Fulda, S., et al., *Cellular stress responses: cell survival and cell death.* Int J Cell Biol, 2010. **2010**(1): p. 214074.
85. Chaki, M., J.C. Begara-Morales, and J.B. Barroso, *Oxidative Stress in Plants.* Antioxidants (Basel), 2020. **9**(6): p. 481.
86. Moller, I.M., P.E. Jensen, and A. Hansson, *Oxidative modifications to cellular components in plants.* Annu Rev Plant Biol, 2007. **58**(Volume 58, 2007): p. 459-81.
87. Mithöfer, A., B. Schulze, and W. Boland, *Biotic and heavy metal stress response in plants: evidence for common signals.* FEBS letters, 2004. **566**(1-3): p. 1-5.
88. Paithankar, J.G., et al., *Heavy metal associated health hazards: An interplay of oxidative stress and signal transduction.* Chemosphere, 2021. **262**: p. 128350.
89. Shahid, M., et al., *Heavy-metal-induced reactive oxygen species: phytotoxicity and physicochemical changes in plants.* Rev Environ Contam Toxicol, 2014. **232**: p. 1-44.
90. García-Caparrós, P., et al., *Oxidative Stress and Antioxidant Metabolism under Adverse Environmental Conditions: a Review.* The Botanical Review, 2020. **87**(4): p. 421-466.
91. Anwar Hossain, M., et al., *Proline Protects Plants Against Abiotic Oxidative Stress*, in *Oxidative Damage to Plants*, P. Ahmad, Editor. 2014, Academic Press: San Diego. p. 477-522.
92. Dar, M.I., et al., *An Introduction to Reactive Oxygen Species Metabolism Under Changing Climate in Plants*, in *Reactive Oxygen Species and Antioxidant Systems in Plants: Role and Regulation under Abiotic Stress*, M.I.R. Khan and N.A. Khan, Editors. 2017, Springer Singapore: Singapore. p. 25-52.
93. Liang, D., et al., *Ascorbic acid metabolism during sweet cherry (Prunus avium) fruit development.* PLOS ONE, 2017. **12**(2): p. e0172818.
94. Roukas, T., *The role of oxidative stress on carotene production by Blakeslea trispora in submerged fermentation.* Crit Rev Biotechnol, 2016. **36**(3): p. 424-33.
95. Spormann, S., et al., *Accumulation of Proline in Plants under Contaminated Soils—Are We on the Same Page?* 2023. **12**(3): p. 666.
96. Jurgens, G., *Membrane trafficking in plants.* Annu Rev Cell Dev Biol, 2004. **20**(Volume 20, 2004): p. 481-504.
97. Bassham, D.C., et al., *The secretory system of Arabidopsis.* Arabidopsis Book, 2008. **6**(6): p. e0116.

98. Marty, F., *Plant vacuoles.* Plant Cell, 1999. **11**(4): p. 587-600.
99. Shimada, T., et al., *Plant Vacuoles.* Annu Rev Plant Biol, 2018. **69**(1): p. 123-145.
100. Martinoia, E., A. Massonneau, and N. Frangne, *Transport processes of solutes across the vacuolar membrane of higher plants.* Plant Cell Physiol, 2000. **41**(11): p. 1175-86.
101. Bethke, P.C. and R.L. Jones, *Vacuoles and prevacuolar compartments.* Curr Opin Plant Biol, 2000. **3**(6): p. 469-75.
102. Hatsugai, N., et al., *A plant vacuolar protease, VPE, mediates virus-induced hypersensitive cell death.* Science, 2004. **305**(5685): p. 855-8.
103. Müntz, K., *Deposition of storage proteins.* Plant Molecular Biology, 1998. **38**(1/2): p. 77-99.
104. Vitale, A. and G. Hinz, *Sorting of proteins to storage vacuoles: how many mechanisms?* Trends in plant science, 2005. **10**(7): p. 316-323.
105. Zouhar, J., A. Munoz, and E. Rojo, *Functional specialization within the vacuolar sorting receptor family: VSR1, VSR3 and VSR4 sort vacuolar storage cargo in seeds and vegetative tissues.* Plant J, 2010. **64**(4): p. 577-88.
106. Rogers, J.C., *Multiple Vacuoles in Plant Cells.* Plant Physiology, 2008. **146**(3): p. 1024-1025.
107. Frigerio, L., G. Hinz, and D.G. Robinson, *Multiple vacuoles in plant cells: rule or exception?* Traffic, 2008. **9**(10): p. 1564-70.
108. Eisenach, C., R. Francisco, and E. Martinoia, *Plant vacuoles.* Curr Biol, 2015. **25**(4): p. R136-7.
109. Xiang, L., E. Etxeberria, and W. Van den Ende, *Vacuolar protein sorting mechanisms in plants.* FEBS J, 2013. **280**(4): p. 979-93.
110. Pereira, C., S. Pereira, and J. Pissarra, *Delivering of proteins to the plant vacuole—An update.* International journal of molecular sciences, 2014. **15**(5): p. 7611-7623.
111. Di Sansebastiano, G.P., et al., *Trafficking routes to the plant vacuole: connecting alternative and classical pathways.* J Exp Bot, 2017. **69**(1): p. 79-90.
112. Vieira, V., et al., *N-Linked Glycosylation Modulates Golgi-Independent Vacuolar Sorting Mediated by the Plant Specific Insert.* Plants (Basel), 2019. **8**(9): p. 312.
113. Cervelli, M., et al., *A novel C-terminal sequence from barley polyamine oxidase is a vacuolar sorting signal.* The Plant Journal, 2004. **40**(3): p. 410-418.
114. Neuhaus, J.-M., et al., *A short C-terminal sequence is necessary and sufficient for the targeting of chitinases to the plant vacuole.* Proceedings of the National Academy of Sciences, 1991. **88**(22): p. 10362-10366.
115. Saalbach, G., et al., *Different legumin protein domains act as vacuolar targeting signals.* The Plant Cell, 1991. **3**(7): p. 695-708.
116. Vieira, M., et al., *Molecular cloning and characterization of cDNA encoding cardosin B, an aspartic proteinase accumulating extracellularly in the transmitting tissue of Cynara cardunculus L.* Plant Mol Biol, 2001. **45**(5): p. 529-39.
117. Pissarra, J., et al., *From Flower to Seed Germination in Cynara cardunculus: A Role for Aspartic Proteinases.* 2007.
118. Pereira, C.S., et al., *Cardosins in postembryonic development of cardoon: towards an elucidation of the biological function of plant aspartic proteinases.* Protoplasma, 2008. **232**(3-4): p. 203-13.
119. Pereira, C., et al., *Cardosin A contains two vacuolar sorting signals using different vacuolar routes in tobacco epidermal cells.* Plant J, 2013. **76**(1): p. 87-100.
120. Duarte, P., J. Pissarra, and I. Moore, *Processing and trafficking of a single isoform of the aspartic proteinase cardosin A on the vacuolar pathway.* Planta, 2008. **227**(6): p. 1255-68.

121. Oliveira, A., et al., *Characterization of aspartic proteinases in C. cardunculus L. callus tissue for its prospective transformation.* Plant Science, 2010. **178**(2): p. 140-146.
122. da Costa, D.S., et al., *Dissecting cardosin B trafficking pathways in heterologous systems.* Planta, 2010. **232**(6): p. 1517-30.
123. da Costa, D.S., S. Pereira, and J. Pissarra, *The heterologous systems in the study of cardosin B trafficking pathways.* Plant Signal Behav, 2011. **6**(6): p. 895-7.
124. Ramalho-Santos, M., et al., *Identification and proteolytic processing of procardosin A.* Eur J Biochem, 1998. **255**(1): p. 133-8.
125. Simoes, I. and C. Faro, *Structure and function of plant aspartic proteinases.* Eur J Biochem, 2004. **271**(11): p. 2067-75.
126. Soares, A., S.M. Ribeiro Carlton, and I. Simoes, *Atypical and nucellin-like aspartic proteases: emerging players in plant developmental processes and stress responses.* J Exp Bot, 2019. **70**(7): p. 2059-2076.
127. Bryksa, B.C., et al., *Structure and mechanism of the saposin-like domain of a plant aspartic protease.* J Biol Chem, 2011. **286**(32): p. 28265-75.
128. Egas, C., et al., *The saposin-like domain of the plant aspartic proteinase precursor is a potent inducer of vesicle leakage.* J Biol Chem, 2000. **275**(49): p. 38190-6.
129. Törmäkangas, K., et al., *A Vacuolar Sorting Domain May Also Influence the Way in Which Proteins Leave the Endoplasmic Reticulum.* The Plant Cell, 2001. **13**(9): p. 2021-2032.
130. Terauchi, K., et al., *Plant-specific insertions in the soybean aspartic proteinases, soyAP1 and soyAP2, perform different functions of vacuolar targeting.* J Plant Physiol, 2006. **163**(8): p. 856-62.
131. Kramer, U., *Planting molecular functions in an ecological context with Arabidopsis thaliana.* Elife, 2015. **4**: p. e06100.
132. Huala, E., et al., *The Arabidopsis Information Resource (TAIR): a comprehensive database and web-based information retrieval, analysis, and visualization system for a model plant.* Nucleic Acids Res, 2001. **29**(1): p. 102-5.
133. Woodward, A.W. and B. Bartel, *Biology in Bloom: A Primer on the Arabidopsis thaliana Model System.* Genetics, 2018. **208**(4): p. 1337-1349.
134. Raza, A., et al., *Arabidopsis thaliana: Model Plant for the Study of Abiotic Stress Responses*, in *The Plant Family Brassicaceae*, M. Hasanuzzaman, Editor. 2020, Springer Singapore: Singapore. p. 129-180.
135. Schneider, C.A., W.S. Rasband, and K.W. Eliceiri, *NIH Image to ImageJ: 25 years of image analysis.* Nat Methods, 2012. **9**(7): p. 671-5.
136. Afonseca, A.F.S., *Characterisation of the Arabidopsis thaliana Metallothionein gene family in response to nickel with the aid of specific mutants.* 2023.
137. Ferreira, M.J., et al., *I Choose You: Selecting Accurate Reference Genes for qPCR Expression Analysis in Reproductive Tissues in Arabidopsis thaliana.* Biomolecules, 2023. **13**(3): p. 463.
138. Czechowski, T., et al., *Genome-wide identification and testing of superior reference genes for transcript normalization in Arabidopsis.* Plant Physiol, 2005. **139**(1): p. 5-17.
139. Heath, R.L. and L. Packer, *Photoperoxidation in isolated chloroplasts. I. Kinetics and stoichiometry of fatty acid peroxidation.* Arch Biochem Biophys, 1968. **125**(1): p. 189-98.
140. de Sousa, A., et al., *Metalaxyl-induced changes in the antioxidant metabolism of Solanum nigrum L. suspension cells.* Pesticide biochemistry physiology, 2013. **107**(2): p. 235-243.

141. Tosin, R., et al., *Assessing predawn leaf water potential based on hyperspectral data and pigment's concentration of Vitis vinifera L. in the Douro Wine Region.* Scientia Horticulturae, 2021. **278**: p. 109860.
142. Gibson, D.G., et al., *Enzymatic assembly of DNA molecules up to several hundred kilobases.* Nature methods, 2009. **6**(5): p. 343-345.
143. Briat, J.-F., F. Cellier, and F. Gaymard, *Ferritins and Iron Accumulation in Plant Tissues*, in *Iron Nutrition in Plants and Rhizospheric Microorganisms*, L.L. Barton and J. Abadia, Editors. 2006, Springer Netherlands: Dordrecht. p. 341-357.
144. Kroh, G.E. and M. Pilon, *Regulation of Iron Homeostasis and Use in Chloroplasts.* Int J Mol Sci, 2020. **21**(9): p. 3395.
145. Ashfaque, F., et al., *Influence of heavy metal toxicity on plant growth, metabolism and its alleviation by phytoremediation-a promising technology.* Journal of Agriculture Ecology Research International, 2016. **6**(2): p. 1-19.
146. Aarti, P., R. Tanaka, and A. Tanaka, *Effects of oxidative stress on chlorophyll biosynthesis in cucumber (Cucumis sativus) cotyledons.* Physiologia Plantarum, 2006. **128**(1): p. 186-197.
147. Kipp, E. and M. Boyle, *The effects of heat stress on reactive oxygen species production and chlorophyll concentration in Arabidopsis Thaliana.* Res Plant Sci, 2013. **1**(2): p. 20-3.
148. Li, G., et al., *Auxin Resistant1 and PIN-FORMED2 Protect Lateral Root Formation in Arabidopsis under Iron Stress* Plant Physiology, 2015. **169**(4): p. 2608-2623.
149. Myśliwa-Kurdziel, B. and K. Strzałka, *Influence of Metals on Biosynthesis of Photosynthetic Pigments*, in *Physiology and Biochemistry of Metal Toxicity and Tolerance in Plants*, M.N.V. Prasad and K. Strzałka, Editors. 2002, Springer Netherlands: Dordrecht. p. 201-227.
150. Lapaz, A.d.M., et al., *Iron toxicity: effects on the plants and detoxification strategies.* Acta Botanica Brasilica, 2022. **36**.
151. Pinto, S.d.S., et al., *Oxidative damage and photosynthetic impairment in tropical rice cultivars upon exposure to excess iron.* Scientia Agricola, 2016. **73**.
152. Xu, S., et al., *Excess iron alters the fatty acid composition of chloroplast membrane and decreases the photosynthesis rate: a study in hydroponic pea seedlings.* Acta Physiologiae Plantarum, 2015. **37**(10): p. 212.
153. Nisar, N., et al., *Carotenoid metabolism in plants.* Mol Plant, 2015. **8**(1): p. 68-82.
154. Rout, G.R. and S. Sahoo, *Role of iron in plant growth and metabolism.* Reviews in Agricultural Science, 2015. **3**: p. 1-24.
155. Caro, A. and S. Puntarulo, *Effect of in vivo iron supplementation on oxygen radical production by soybean roots.* Biochim Biophys Acta, 1996. **1291**(3): p. 245-51.
156. Pekker, I., E. Tel-Or, and R.J.P.M.B. Mittler, *Reactive oxygen intermediates and glutathione regulate the expression of cytosolic ascorbate peroxidase during iron-mediated oxidative stress in bean.* 2002. **49**: p. 429-438.
157. Takahashi, M., et al., *Role of nicotianamine in the intracellular delivery of metals and plant reproductive development.* Plant Cell, 2003. **15**(6): p. 1263-80.
158. Li, X., et al., *The interactive effects of diclofop-methyl and silver nanoparticles on Arabidopsis thaliana: Growth, photosynthesis and antioxidant system.* Environ Pollut, 2018. **232**: p. 212-219.
159. LAZAR, T., *Taiz, L. and Zeiger, E. Plant physiology. 3rd edn*. 2003, Oxford University Press.
160. Wojtaszek, P., *Oxidative burst: an early plant response to pathogen infection.* Biochem J, 1997. **322 (Pt 3)**(Pt 3): p. 681-92.

161. García-Caparrós, P., et al., *Oxidative Stress and Antioxidant Metabolism under Adverse Environmental Conditions: a Review.* The Botanical Review, 2021. **87**(4): p. 421-466.
162. Hultberg, B., A. Andersson, and A. Isaksson, *Copper ions differ from other thiol reactive metal ions in their effects on the concentration and redox status of thiols in HeLa cell cultures.* Toxicology, 1997. **117**(2-3): p. 89-97.
163. Ilyas, S. and A. Rehman, *Oxidative stress, glutathione level and antioxidant response to heavy metals in multi-resistant pathogen, Candida tropicalis.* Environ Monit Assess, 2015. **187**(1): p. 4115.
164. Bjørklund, G., et al., *A review on coordination properties of thiol-containing chelating agents towards mercury, cadmium, and lead.* Molecules, 2019. **24**(18): p. 3247.
165. Ajsuvakova, O.P., et al., *Sulfhydryl groups as targets of mercury toxicity.* Coordination chemistry reviews, 2020. **417**: p. 213343.
166. Noctor, G., et al., *Glutathione in plants: an integrated overview.* Plant Cell Environ, 2012. **35**(2): p. 454-84.
167. Vatamaniuk, O.K., et al., *A New Pathway for Heavy Metal Detoxification in Animals: Phytochelatin Synthase Is Required for Cadmium Tolerance in Caenorhabditis Elegans.* Journal of Biological Chemistry, 2001. **276**(24): p. 20817-20820.
168. Gajewska, E. and M. Skłodowska, *Differential biochemical responses of wheat shoots and roots to nickel stress: antioxidative reactions and proline accumulation.* Plant Growth Regulation, 2008. **54**: p. 179-188.
169. Hadi, F., N. Ali, and M.P. Fuller, *Molybdenum (Mo) increases endogenous phenolics, proline and photosynthetic pigments and the phytoremediation potential of the industrially important plant Ricinus communis L. for removal of cadmium from contaminated soil.* Environ Sci Pollut Res Int, 2016. **23**(20): p. 20408-20430.
170. Chaturvedi, R., et al., *EDTA-Assisted Metal Uptake in Raphanus sativus L. and Brassica oleracea L.: Assessment of Toxicity and Food Safety.* Bull Environ Contam Toxicol, 2019. **103**(3): p. 490-495.
171. Tripathi, B.N. and J.P. Gaur, *Relationship between copper- and zinc-induced oxidative stress and proline accumulation in Scenedesmus sp.* Planta, 2004. **219**(3): p. 397-404.
172. Hemadri Reddy, S., et al., *Proline and other physiological changes as an indicator of abiotic stress caused by heavy metal contamination.* Journal of King Saud University - Science, 2024. **36**(8): p. 103313.
173. Zhou, J. and P.B. Goldsbrough, *Structure, organization and expression of the metallothionein gene family in Arabidopsis.* Mol Gen Genet, 1995. **248**(3): p. 318-28.
174. Zhou, J. and P.B. Goldsbrough, *Functional homologs of fungal metallothionein genes from Arabidopsis.* Plant Cell, 1994. **6**(6): p. 875-84.
175. Khandekar, S. and S. Leisner, *Soluble silicon modulates expression of Arabidopsis thaliana genes involved in copper stress.* J Plant Physiol, 2011. **168**(7): p. 699-705.
176. Guo, W.J., W. Bundithya, and P.B. Goldsbrough, *Characterization of the Arabidopsis metallothionein gene family: tissue-specific expression and induction during senescence and in response to copper.* New Phytol, 2003. **159**(2): p. 369-381.
177. Yuan, J., et al., *Characteristic and expression analysis of a metallothionein gene, OsMT2b, down-regulated by cytokinin suggests functions in root development and seed embryo germination of rice.* Plant Physiol, 2008. **146**(4): p. 1637-50.

178. Foley, R.C., Z.M. Liang, and K.B. Singh, *Analysis of type 1 metallothionein cDNAs in Vicia faba.* Plant Mol Biol, 1997. **33**(4): p. 583-91.
179. Lv, Y., et al., *Metallothioneins BcMT1 and BcMT2 from Brassica campestris enhance tolerance to cadmium and copper and decrease production of reactive oxygen species in Arabidopsis thaliana.* Plant and Soil, 2012. **367**(1-2): p. 507-519.
180. Clemens, S., *Molecular mechanisms of plant metal tolerance and homeostasis.* Planta, 2001. **212**(4): p. 475-86.
181. Sharma, S.S., K.J. Dietz, and T. Mimura, *Vacuolar compartmentalization as indispensable component of heavy metal detoxification in plants.* Plant Cell Environ, 2016. **39**(5): p. 1112-26.
182. Shi, W., et al., *Physiological and molecular mechanisms of heavy metal accumulation in nonmycorrhizal versus mycorrhizal plants.* Plant Cell Environ, 2019. **42**(4): p. 1087-1103.
183. Peiter, E., et al., *A secretory pathway-localized cation diffusion facilitator confers plant manganese tolerance.* Proc Natl Acad Sci U S A, 2007. **104**(20): p. 8532-7.
184. Chen, G., et al., *Cadmium adsorption by willow root: the role of cell walls and their subfractions.* Environmental Science Pollution Research, 2013. **20**: p. 5665-5672.
185. Parrotta, L., et al., *Target or barrier? The cell wall of early- and later-diverging plants vs cadmium toxicity: differences in the response mechanisms.* Front Plant Sci, 2015. **6**: p. 133.
186. Owji, H., et al., *A comprehensive review of signal peptides: Structure, roles, and applications.* Eur J Cell Biol, 2018. **97**(6): p. 422-441.

Appendix

Supplementary Table 11| Purity assessment and quantification of RNA samples for the Fe treatment. Shoots: S01 to S03 – control; S11 to S13 – 3 mg/L: S21 to S23 – 6 mg/L; S31 to S33 – 12.5 mg/L. Roots: R01 to R03 – control; R11 to R13 – 3 mg/L; R21 to R23 – 6 mg/L; R31 to R33 – 12.5 mg/L.

Fe					
Shoots			**Roots**		
Sample Name	Concentration (ng/µL)	A(260)/A(280)	**Sample Name**	Concentration (ng/µL)	A(260)/A(280)
S01	66.454	1.98	**R01**	331.633	1.96
S02	72.404	1.96	**R02**	113.378	1.86
S03	159.363	1.73	**R03**	142.445	1.90
S11	57.274	1.93	**R11**	325.378	1.92
S12	71.419	1.93	**R12**	218.257	1.91
S13	278.098	1.99	**R13**	116.794	1.92
S21	104.601	1.73	**R21**	197.505	1.86
S22	128.69	1.95	**R22**	158.251	1.86
S23	89.174	1.86	**R23**	194.582	1.91
S31	115.199	2.04	**R31**	417.043	1.92
S32	181.637	1.94	**R32**	266.897	1.94
S33	209.468	1.98	**R33**	249.644	1.81

Supplementary table 12| Purity assessment and quantification of RNA samples for the Ag treatment. Shoots: S01 to S03 – control; S11 to S13 – 6.1 mg/L: S21 to S23 – 25.6 mg/L. Roots: R01 to R03 – control; R11 to R13 – 6.1 mg/L; R21 to R23 – 25.6 mg/L.

Ag					
Shoots			**Roots**		
Sample Name	Concentration (ng/µL)	A(260)/A(280)	**Sample Name**	Concentration (ng/µL)	A(260)/A(280)
S01	120.995	2.01	**R01**	189.541	1.61
S02	1363.072	1.97	**R02**	165.332	1.96
S03	101.894	1.87	**R03**	91.398	1.92

S11	76.892	1.99	**R11**	94.504	1.87
S12	59.133	1.97	**R12**	110.931	1.89
S13	76.555	1.99	**R13**	34.439	1.90
S21	95.893	1.97	**R21**	99.219	1.90
S22	15.787	1.88	**R22**	86.471	1.93
S23	120.823	1.96	**R23**	159.245	1.88

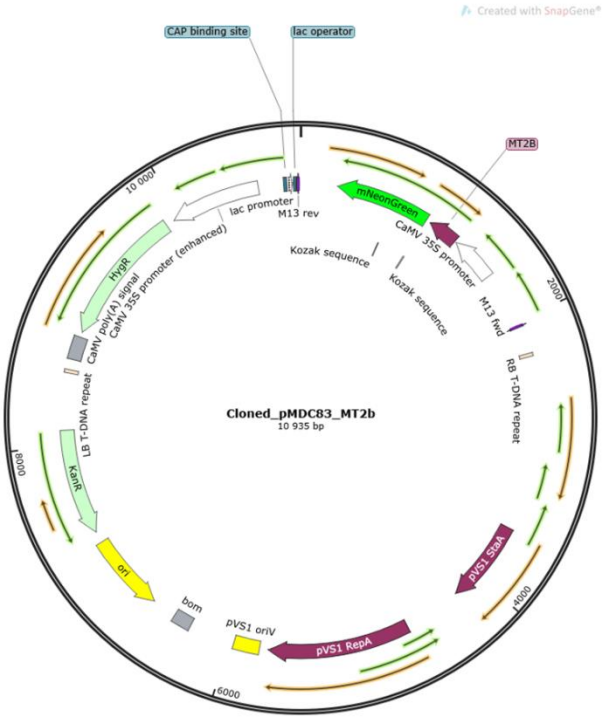

Supplementary Figure 28| pMDC83 map used to assemble the pMDC83-MT2bΩs construct.

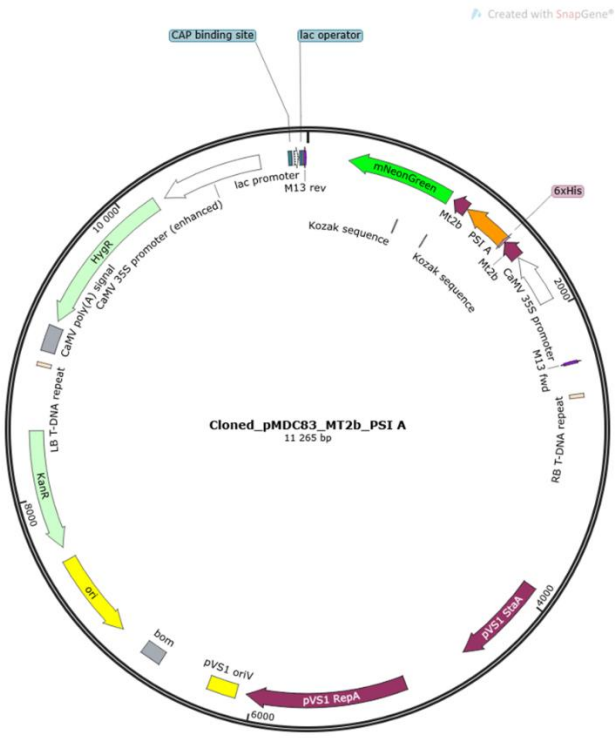

Figure 29| pMDC83 map used to assemble the pMDC83-MT2bΩs-PSIA-His6x-Tag construct.